UNIVERSITÀ DEGLI STUDI DI TRIESTE

DIPARTIMENTO DI FISICA, SEZIONE DI ASTRONOMIA

XXII CICLO DEL
DOTTORATO DI RICERCA IN
FISICA

The Effects of Galactic Fountains on the Chemical evolution of Galaxies

SETTORE SCIENTIFICO-DISCIPLINARE FIS/05

DOTTORANDO: **EMANUELE SPITONI**

RESPONSABILE DOTTORATO DI RICERCA
PROF. GAETANO SENATORE – UNIVERSITÀ DI TRIESTE

RELATORE/SUPERVISORE
PROF. FRANCESCA MATTEUCCI – UNIVERSITÀ DI TRIESTE

ANNO ACCADEMICO 2008/2009

To Elisa

Abstract

In this thesis we study the effect of galactic fountains, namely gas and flows from the disk of galaxies produced by multiple supernova explosions, on the chemical evolution of galaxies. Sequential supernova explosions create a superbubble, whereas the swept up interstellar medium is concentrated in a supershell which can break out a stratified medium, producing bipolar outflows. The gas of the supershells can fragment into clouds which eventually fall toward the disk producing so-called galactic fountains.

Many works in literature have dealt with superbubble expansion in stratified media. However, very few papers in the past have taken into account the chemical evolution of the superbubble and how the supershell get polluted from the metals produced by supernova explosions. With this thesis for the first time the effect of galactic fountains we consider in a detailed chemical evolution model for the Milky Way.

In the first part of our work we study the expansion law and chemical enrichment of a supershell powered by the energetic feedback of a typical Galactic OB association at various galactocentric radii. We follow the orbits of the fragments created when the supershell breaks out and we compare their kinetic and chemical properties with the available observations of high - and intermediate - velocity clouds. We use the Kompaneets (1960) approximation for the evolution of the superbubble driven by sequential supernova explosions and we compute the abundances of oxygen and iron residing in the thin cold supershell. Due to Rayleigh-Taylor instabilities we assume that supershells are fragmented and we follow the orbit of the clouds either ballistically or by means of a hybrid model considering viscous interaction between the clouds and the extra-planar gas. We find that if the initial metallicity is solar, the pollution from the dying stars of the OB association has a negligible effect on the chemical composition of the clouds. The maximum height reached by the clouds above the plane seldom exceeds 2 kpc and when averaging over different throwing angles, the landing coordinate differs from the throwing coordinate by only 1 kpc. Therefore, it is unlikely that galactic fountains can affect abundance gradients on large scales. The range of heights and $[O/Fe]$ ratios spanned by our clouds suggest that the high velocity clouds cannot have a Galactic origin, whereas intermediate velocity clouds have kinematic properties similar to our predicted clouds but have observed overabundances of the $[O/Fe]$ ratios that can be reproduced only with initial metallicities which are too low compared to those of the Galaxy disk.

Even if it is unlikely that galactic fountains can affect abundance gradients on large scales, they can still affect the chemical enrichment of the interstellar medium (ISM) because of the time-delay due to the non-negligible time taken by fountains to orbit around and fall back into the Galaxy. This implies a delay in the mixing of metals in ISM which conflicts with the instantaneous mixing approximation (IMA) usually assumed in all models in literature. We test whether relaxing this approximation in a detailed chemical evolution model can improve or worsen the agreement with observations. To do that, we investigate two possible causes for relaxing of the instantaneous mixing: i) the "galactic fountain time delay effect" and ii) the "metal cooling time delay effect". We find that the effect of galactic fountains is negligible if an average time delay of 0.1 Gyr, as suggested by our model, is assumed. Longer time delays produce differences in the results but they are not realistic. The metal cooling time delays produce strong effects on the evolution of the chemical abundances only if we adopt stellar yields depending on metallicity. If, instead, the yields computed for the solar chemical composition are adopted, negligible effects are produced, as in the case of the galactic fountain delay. The relaxation of the IMA by means of the galactic fountain model, where the delay is considered only for massive stars and only in the disk, does not affect the chemical evolution results. The combination of metal dependent yields and time delay in the chemical enrichment from all stars starting from the halo phase, instead, produces results at variance with observations.

Contents

Introduction

Galactic fountains are created by multiple supernova (SN) explosions in the disk of galaxies and consist of gas flows from the disk (Bregman 1980): these gas flows reach a certain height above the galactic plane and then fall back.

In this thesis we study the physical mechanism producing such fountains in the Milky Way (hereafter MW) and external galaxies and its effects on the chemical enrichment. To do that we need to introduce some basic concepts such as stellar populations of the MW, SNe (II,I) and OB associations.

0.1 Stellar populations of the Milky Way

Following the Hubble classification, the morphological type of the MW is the Sbc one, namely it is a barred spiral galaxy with relatively loosely-wound arms. The MW and the Andromeda Galaxy are a binary system of giant spiral galaxies belonging to a group of $\sim$ 50 closely bound galaxies known as the Local Group, itself being part of the Virgo Supercluster.

The MW can be described as a centrally flattened disk of gas and stars with a stellar bulge and a bar in the center, surrounded by a spherical halo of stars and globular cluster (see Fig. 1). The MW possesses also an extended and massive halo of dark matter. We can distinguish at least four distinct stellar population in the Galaxy (Matteucci et al. 2001):

- *Halo population*: star with metallicities $[Fe/H] < -1.0$ dex, height above the galactic plane larger than $\sim$ 900 pc , galacticentric distances up to $\sim$ 100 kpc and eccentric and elongated orbits. They are among the oldest stars in the Galaxy.

- *Bulge population*: stars with metallicities in the range $-1.5 < [Fe/H] < +1.0$ dex and kinematics like the halo stellar population but concentrated in the innermost $\sim$ 3 kpc of the Galaxy. They are also old stars as the halo stars.

- *Thick-disk population*: stars with metallicities in the range $-1.0 < [Fe/H] < -0.6$ dex, height above the the galactic plane between $\sim$ 250 and $\sim$ 900 pc and kinematics intermediate between the halo and the thin disk stars. They are probably younger than the halo stars.

- *Thin-disk population*: stars with metallicities $[Fe/H] > -0.6$ dex, height above the the galactic plane inside ~ 250 and circular orbits. Their ages span a large range from $\sim 9 - 10$ Gyr to few million years.

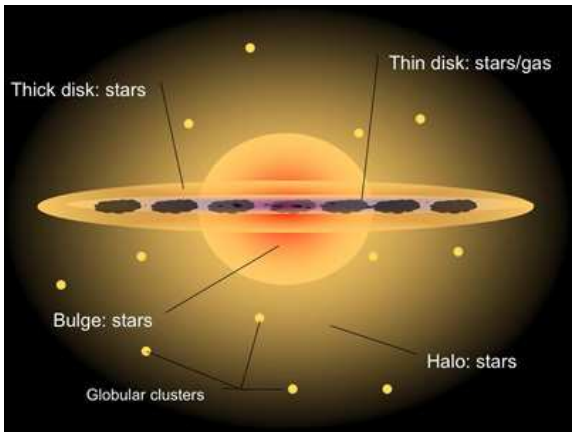

Figure 1: An image of the MW stellar populations in an artist's rendering. (Swinburne Astronomy Online)

0.2 Supernovae

SNe are exploding stars. They represent the very final stages of evolution for some stars or systems of stars (binaries). The remains of the matter which is ejected away from the star is known as a supernova remnant. SNe were first studied in 1934 by the astronomers Fritz Zwicky and Walter Baade.

0.2.1 Supernova taxonomy

SNe are classified according to the absorption lines of different chemical elements that appear in their early spectra (see e.g. Filippenko 1997 for a review). One of the primary reasons for subdividing SNe into well-defined Types according to their observed characteristics is that careful classification often constitutes the foundation for a more complete physical description of the phenomena.
Minkowskii (1941) was the first who noticed that there are at least two different Types of SNe: **Type II** and **Type I** SNe according to the fact that they show hydrogen lines in their spectra or not, respectively. Among those Types, there are finer subdivisions according to the presence of lines from other elements and the shape of the light curve[1].

A SN with no H lines is defined as Type I. Furthermore, if it shows a strong SiII absorption line at about 6150 $\mathring{A}$ is designed as **Type Ia** (see e.g. Leibundgut 2000

[1]Supernova's apparent magnitude (or luminosity) versus time

for a review). This Type of SNe is discovered in all morphological types of galaxies (Barbon et al. 1999) and is not associated with arms of spirals as strongly as other SN Types (e.g. Trimble 1982; Wheeler 1982). The early spectra are characterized by strong Fe lines plus lines of intermediate mass elements (Ca, O, Si and S). In the '80s, it was recognized (e.g. Panagia 1985) that a number of peculiar Type I SN , missing in the spectrum near maximum the typical Si feature at $\sim 6510\mathring{A}$, had a completely different nebular spectrum dominated by forbidden Ca and O emissions instead of Fe lines. Examining more carefully the near maximum spectra it was noticed that these Type I SNe come in at least two flavors: those showing strong He lines, first observed by Bertola in 1964, were labeled **Ib** (Elias et al. 1981; Harkness et al 1987), the others **Ic**. These two Types of SNe appear only in spirals (Barbon et al. 1999; Porter & Filippenko 1987) and have been associated with a parent population of massive stars (e.g. Van Dyk et al 1999). After maximum, SNe Ia show strong emissions of FeII and FeIII, while SNe Ib/c are dominated by CaII and OI.

The SN taxonomy based on spectra near maximum may be somewhat confusing when one tries to build a coherent progenitor scenario. The fact that the nebular spectrum of Type Ib/c SNe is similar to that of SNe II, but for the H emission, suggests a similar explosion mechanism. Instead, the weakness of intermediate element emissions, in particular O, in the nebular spectrum of SNe Ia suggests that the progenitors of SNe Ia are not massive stars. Indeed a more physical classification could be based on the distinction between SNe arising from the collapse of massive stars, the so called **Core-Collapse SNe** (SNe II and SNe Ib/c) and those due to thermonuclear explosions of low mass stars (Type Ia SNe) (see Fig. 2). The detailed classification of SNe requires not only the identification of specific features in the early spectra, but also the analysis of the line profiles, luminosity and spectral evolutions.

The differences between the various Types of SNe (in both spectra and light curves) are basically due to the different nature of the stellar progenitors, ending their lives on different timescales and by different explosion mechanisms.

0.2.2 Type II Supernovae

Type II SNe are probably produced by the core collapse of massive stars, namely stars more massive than $8M_{\odot}$ (e.g. Iben & Renzini 1983; Woosley & Weaver 1986) and less massive than $40M_{\odot}$ (e.g. Maeder 1984). The mass range is consistent with the observation that SNe II can be found only in galaxies that have efficient, ongoing star formation, such as spiral and irregular galaxies (preferentially occurring in spiral arms; e.g. Maza & van den Bergh 1976). Thus, the lifetime of a SN II progenitor is shorter than about 30 million years (and can be as short as a few million years). The details of the explosion mechanism of a star as a SN II are well explained by several authors, for example Miyaji et al. (1980), Nomoto (1981), Woosley & Weaver (1986, 1995). In synthesis, a massive star, once its central hydrogen fuel is exhausted, can

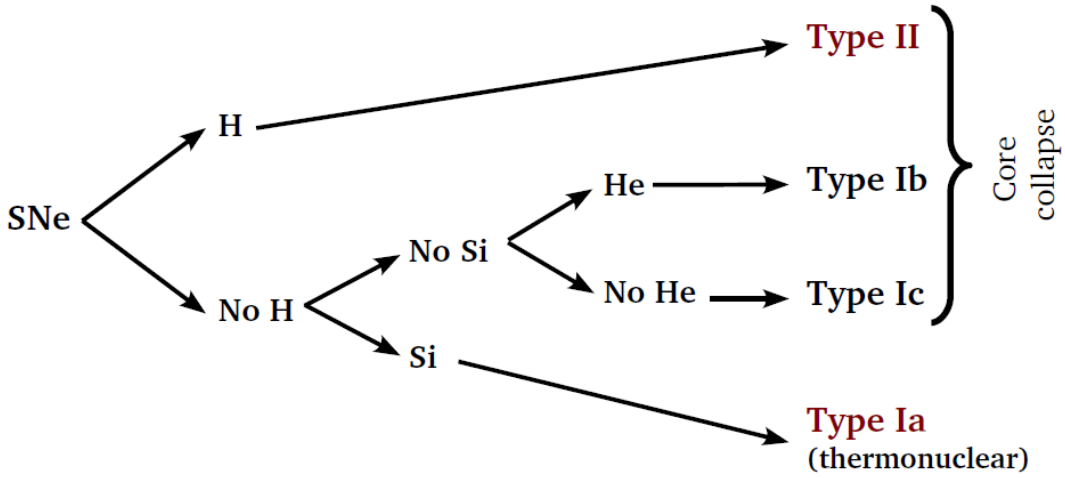

Figure 2: The classification scheme of SNe. Type Ia SNe are associated with the thermonuclear explosion of accreting white dwarfs. Other SN types are associated with the core collapse of massive stars.

ignite helium in its core and then, subsequently, heavier elements up to iron and nickel. In fact, the binding energy per nucleon has a peak in correspondence with these elements and the fusion of heavier elements does not produce energy. This iron-nickel core photo-dissociates into helium nuclei and free protons and collapses until reaching densities similar to the density of the nuclei of the atoms ($\sim 10^{14}$ g cm^{-3}). At this point the strong force prevents further collapse and the surrounding layers of the stars bounce back, creating a shock wave able to expel all the external mantel of the star (only the collapsed core remains).

From a chemical point of view, Type II SNe are responsible for producing the bulk of heavy elements, in particular the elements such as ^{16}O,^{20}Ne,^{24}Mg, ^{28}Si,^{32}S,^{40}Ca (so called α elements) and r-process elements.

0.2.3 Type Ib/c Supernovae

Type Ib and Ic SNe are actually similar to Type II, because they, too, are thought to be Core-Collapse SNe, namely, as for Type II SNe, the explosion is triggered by the collapse of their Fe core. The Type II and Ib/c SNe occur only in regions in which the star formation is still ongoing (near HII regions and in Late Type galaxies), which confirms their association with massive stars. The only difference with Type II SNe should be therefore that the progenitors of SNeIb and SNeIc have lost, before the explosion, all their H envelope (SNeIb) and eventually also the He

envelope (SNeIc). For this reason, Type Ib SNe have strong He lines, whereas Type Ic SNe have weak or no He lines in their spectra. The most likely progenitors of these Type of SNe are the Wolf-Rayet stars (with masses $40 \leq M_*/M_\odot \leq 100$) which eject their H envelope (and possibly He envelope) by means of intense stellar winds. These stars can in fact produce the observed amount of ^{56}Ni (e.g. Filippenko & Sargent 1986). Other possible progenitors could be close binary systems composed by a He star and a white dwarf (WD; e.g. Baron 1992; Pols 1997). Recently, other candidates such as massive stars ($M > 10M_\odot$) in close binary systems have been proposed as progenitors of Type Ib SNe.

From a chemical point of view, after the explosion Type Ib and Ic SNe produce the same chemical species that Type II SNe produce. If the progenitors of these SNe are Wolf-Rayet stars, then the stellar winds of these objects produce also substantial amounts of He, C, Ne and N.

0.2.4 Type Ia Supernovae

Type Ia SNe have become very popular in the last decade because of their role in determining the geometry of the Universe. In fact, the similarities of absolute magnitude peaks make them very good standard candles, which, due to their intrinsic high luminosities, can be observed also in very distant galaxies. Although it is now clear that differences of more than one order of magnitude in the peak luminosity can be observed between different SNeIa, these objects can be still used efficiently as standard candles by means of a proper calibration. In fact, it has been shown that the peak luminosity strongly correlates with the rate of decline in magnitude in the 15 days after the maximum light.

As already mentioned, Type Ia SNe are discovered in all types of galaxies, also in ellipticals (Barbon et al. 1995), and are not associated with the arms of spirals as strongly as other SN types (McMillan & Ciardullo 1996; Van Dyk et al. 1999), therefore their progenitors should have a broad range of masses (and, consequently, lifetimes). The spectra are characterized by strong Fe lines plus lines of intermediate mass elements such as calcium, oxygen, silicon and sulfur during the peak phase and by the absence of H at any time. The contribution of the Fe lines increases with time and several months past the maximum the spectra are dominated by [Fe II] and [Fe III] lines. The overall homogeneous spectroscopic and photometric behavior has led to a general consensus that they are associated with the thermonuclear explosion of a white dwarf in a binary system. In fact, in this case the WD can accrete material from the companion star, either because the envelope of the companion (for instance during the red giant phase) overcomes its Roche lobe and enters in the Roche lobe of the WD, or because the companion becomes a WD itself and the two WDs lose energy via gravitational wave radiation until merging. In both cases, an explosion is expected when the mass of the WD approaches the Chandrasekhar limit of ~ 1.38 $M_\odot$, namely the mass above which the pressure of degenerate electrons (as the ones in the WD) cannot balance anymore the gravity and the WD explodes. In this way, the explosion always occurs in a WD of similar mass and similar structure, hence

the SNeIa parameters (light curves, peaks of brightness, spectra) are similar among different SNeIa.

We recall here the most common models for the progenitors of Type Ia SNe proposed insofar:

- The merging of two C-O WDs, due to gravitational wave radiation, which reach the Chandrasekhar mass and explode by C-deflagration (Iben & Tutukov 1984). This is known as double-degenerate (DD) scenario.
- The C-deflagration of a Chandrasekhar mass C-O WD after accretion from a non-degenerate companion (Whelan & Iben 1973; Munari & Renzini 1992; Kenyon et al. 1993). This model is known as the single-degenerate (SD) one.
- A sub-Chandrasekhar C-O WD exploding by He-detonation induced by accretion of He-rich material from a He star companion (Tornambé & Matteucci 1987; Limongi & Tornambé 1991).

From a chemical point of view, SNeIa produce the bulk of iron-peak elements plus traces of other light elements.

0.3 OB associations

Brown et al. (2001) defined OB associations as young ($\lesssim$50 Myr) stellar groupings of low density, such that they are likely to be unbound, containing a significant population of B stars. Their observed dimensions range from $\sim$10 to $\sim$100 pc.

The nearby OB associations offer an uniquely detailed view of the relation between early-type stars and the interstellar medium, hereafter ISM (Brown et al. 2001) which helps us to understand the impact of associations on the interstellar matter throughout the Galaxy. Much work has been done, concentrating especially on the ISM around Ori OB1. The characteristics of the ISM related to Sco OB2 were summarized in Blaauw (1991) and de Geuss (1992).

Analyzing the distribution of HI around Orion over the velocity range -1 to $+8$ km s^{-1}, one can clearly distinguish a cavity surrounded by a shell of HI, the Orion-Eridanus bubble, and the whole of the cavity is filled with very hot gas, $\sim 10^6$ K, emitting in X-rays (Burrows 1993, Brown 1995, Snowden et al. 1995). The shell has a measured expansion velocity of about 40 km s^{-1} and a mass of $2.3 \pm 0.7 \times 10^5$ M$_\odot$. Taking into account the initial mass function (IMF) and the ages of the subgroups, the mechanical energy output in the form of stellar winds and supernovae over the lifetime of the association was estimated to be $\sim 10^{52}$ ergs (Brown et al. 1994). Using semi-analytic models of wind-blown bubbles which take the density stratification of the Galactic HI layer into account (Koo & McKee 1990), it was shown that this energy is indeed enough to account for the size as well as for the expansion velocity of the HI shell (Brown 1995).

Early-type stars also have a large effect on the ISM through their ionizing radiation, producing both localized HII regions and diffuse ionized gas. Based on the

distribution of OB associations in the Galaxy, it was shown that their luminosity function can be fit with a truncated power law, and that there probably is a physical limit to the maximum size of HII regions in the Galaxy (McKee & Williams 1997). A comparison with the distribution of giant molecular clouds (Williams & McKee 1997) showed that a 10^6 $M_\odot$ cloud is expected to survive about 30 Myr, and that on average 10 per cent of its mass is converted into stars by the time it is destroyed. The overall distribution of associations is also important for understanding the hot-gas filling factor of the ISM (Ferriere 1995, Ferriere 1998).

A comprehensive census of the stellar content of the OB associations within 1 kpc from the Sun is presented in de Zeeuw et al. (1999). The census is based on Hipparcos positions, proper motions, and parallaxes. It is a key part of a long-term project to study the formation, structure, and evolution of nearby young stellar groups and related starforming regions. The Galactic OB stars studied are the three subgroups Upper Scorpius, Upper Centaurus Lupus, and Lower Centaurus Crux of Sco OB2, as well as Vel OB2, Tr 10, Col 121, Per OB2, a Persei (Per OB3), Cas Tau, Lac OB1, Cep OB2, and a new group in Cepheus, designated as Cep OB6. In Table 2.7 we report the number of Wolf-Rayet stars (WR), O, B and A stars for each OB association.

0.4 The Galactic fountains

In the galactic fountain model (Shapiro & Field 1976; Houck & Bregman 1990), hot gas is ejected out of the Galactic disk by SN explosions, and part of this gas falls back in the form of condensed neutral clouds. Sequential explosions of SNe from an OB association in a stratified medium create a superbubble: a large thin shell of cold gas surrounding a hot pressurized interior. Theoretical models of superbubble expansion in a stratified medium come in many varieties (see Chapter 1). Kompaneets (1960) found a semi-analytic solution for the expansion of a blast wave in an exponential atmosphere and an analytic expression for the shape of the superbubble during its expansion. The time-evolution of the supershell can be found by numerical integration. The supershell can eventually blowout at the transition from deceleration to acceleration upwards. After some time, a region of the supershell can fragment due to the occurrence of Rayleigh-Taylor instabilities (hereafter RTIs). Therefore, condensed neutral gas clouds can form and fall back into the galactic disk forming so called galactic fountains. An artist's rendering of the Galactic fountain process is reported in Fig. 3. From a sequential explosion of Type II SNe in a OB association (blue dots), the superbubble rises up (pink region). After the blow-up and fragmentation phases, clouds of HI could be formed (light-blue circles). These clouds leave the stellar disk, orbit around and fall back to the disk.

Numerous non-homogenous filamentary structures observed in the extra-planar thick HI disk in edge-on galaxies like NGC 5775 (Collins et al. 2000) and NGC 891 (Fraternali et al. 2004) suggest that the kinematics of these halos could be interpreted with ballistic models. Ballistic models describe the gas as an inhomogeneous collection of clouds, subject only to the gravitational potential of the galaxy: for

example, in the galactic fountain model the ejected gas from SN events falls back ballistically (Bregman 1980). These models are able to explain the vertical motion of the cold and warm gas components observed in several spiral galaxies (e.g. Fraternali et al. 2004; Boomsma et al. 2005). In the MW, the evidence has mainly been in the form of fragments and vertical structures in the large scale maps of the ISM. A multi-wavelength survey of the halos of several star forming galaxies (e.g., Dettmar 2005) has revealed a correlation of these halos with the rates of star formation and the energy input rates by SNe, suggesting that gaseous halos are associated to star formation processes in the disk.

Shapiro & Field (1976) first proposed the idea that galactic fountain induced by SN explosions would cause gas circulation between the disk and the halo. This scenario was afterwards explored analytically in detail by Bregman (1980) and Kahn (1981).

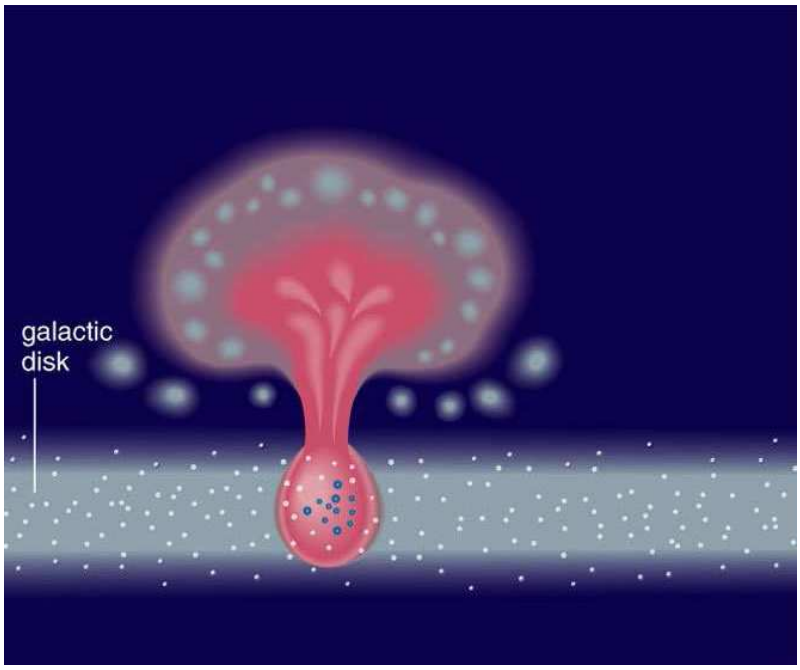

Figure 3: An artist's rendering of the Galactic fountain driven by a sequential explosion of Type II SNe in a OB association (Pearson Education, Inc., publishing as Addisono Wesley, 2006).

Extensive work on the formation of galactic fountains in the MW has been carried out over the last decades; e.g., de Avillez (2000) showed results of a three-dimensional model for disk-halo interaction. The model considers explicitly the input of energy and mass by isolated and correlated SNe in the disk. The approach adopted assumes that the Galactic fountains are intimately related to the vertical structure of the thick gas disk and to the rate occurrence of SNe per unit area in the disk.

An observed feature which seems to be correlated to gas circulation in galactic fountains are the so-called intermediate and high-velocity-clouds (IVCs and HVCs,

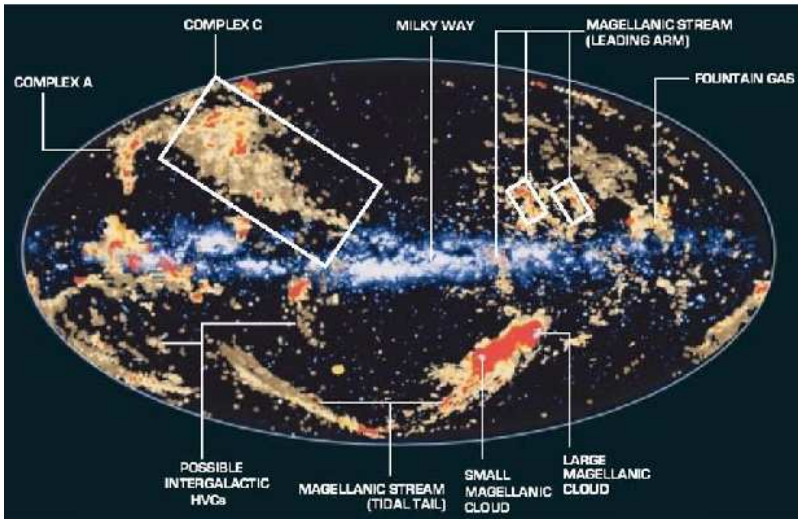

Figure 4: Map of the galactic gas and its environment: it combines radio observations of neutral hydrogen (HI) of the environment with a visible light image of the MW (the galactic disk in the middle). The high and intermediate-velocity clouds of hydrogen, such as complexes A and C, are located above and below the disk. A galactic fountain is also identified in the map.(Figure taken by de Gouveia Dal Pino et al 2008).

respectively).

These are mainly neutral hydrogen (HI) clouds observed in the halo of the MW and in other star forming galaxies. The distinction between HVCs and IVCs is loosely based on the observed radial velocities of the clouds; IVCs have radial velocities with respect to the Local Standard of Rest (LSR) of 30 km s $^{-1} \leq |V_{LSR}| \leq$ 90 km s^{-1} while HVCs have typical velocities $|V_{LSR}| > 90$ km s^{-1}.

Although significant progress has been made in the last few years in exploring the distribution and chemical composition of IVCs and HVCs in the halo of the MW (see Fig 4), an overall unified model for their formation is still lacking. These gas clouds have radial velocities which are not consistent with a simple model of differential galactic rotation (Richter et al. 2001). Several studies (Lu et al. 1998; Wakker et al. 1999; Murphy et al. 2000; Bluhm et al. 2001; Sembach et al. 2001) reveal different chemical compositions for several of these clouds in different directions in the sky. Oort (1970) proposed that these clouds represent condensed gaseous relics from the formation of the MW. This idea was later revived by Blitz et al. (1999), who suggested that HVCs represent the building blocks of galaxies in a hierarchical galaxy formation scenario. Since the Galaxy is surrounded by smaller satellite galaxies (e.g., the Magellanic Clouds), another explanation is that IVCs and HVCs are gaseous streams related to the merging and accretion of these satellites by the MW. In this picture, HVCs would be the gaseous counterparts of the MW circumgalactic stellar streams, which are believed to represent the relics of dwarf galaxies that have been accreted by the MW (e.g., Ibata 1994). While all

these models assume that HVCs are truly extragalactic objects which are about to merge with the Galaxy from outside, there are other scenarios that see the IVCs and HVCs as "galactic fountains". Whatever the origin of the MW IVCs and HVCs is, it has become clear that they must play an important role in the evolution of our Galaxy. Two extremely important parameters to distinguish between the Galactic and extragalactic models of IVCs and HVCs are the *distance* and the *chemical composition* of these clouds. In the case of the Galactic model, the clouds ejected by SN explosions must have a velocity high enough to explain the observed distances and their chemical composition must be correlated with the abundances of the gas in the disk

0.5 Plan of the thesis

Here we intend to study the galactic fountains and their effect on the chemical enrichment of the Galactic disk. In Chapter 1 we present an overview of theoretical models concerning the evolution of a superbubble. First of all we present the well known analytical results concerning superbubble with spherically symmetric shocks. Then we show some results in the case of superbubbles in a stratified medium, and we focus on the study of an exponential atmosphere. We compare the analytic results, obtained with the Kompaneets (1960) approximation, with the "thin shell" and hydrodynamical results.

In Chapter 2 we calculate the expansion law and chemical enrichment of a supershell powered by the energetic feedback of a typical Galactic OB association at various galactocentric radii. We study the orbits of the fragments created when the supershell breaks out and we compare their kinetic and chemical properties with the available observations of HVCs and IVCs. We present precise calculations about the physical and chemical properties of the swept up gas by sequential SN events. We use the Kompaneets (1960) approximation for the evolution of the superbubble driven by sequential SN explosions and we compute the abundances of oxygen and iron residing in the thin cold supershell. We assume that supershells are fragmented by RTIs and we follow the orbits of the clouds either ballistically or by means of a hybrid model considering viscous interaction between the clouds and the extra-planar gas and we compare our result with the observed features of HVC and IVC.

In Chapter 3 we describe the chemical evolution models in which we include galactic fountains. First of all we present the "simple models", namely we make simplifying assumptions about the lifetimes of stars and the mixing of freshly produced metals, This allows us to solve analytically the equations for the evolution of gas masses and metallicities. We focus on models in which the outflow is differential, namely in which the heavy elements (or some of the heavy elements) can leave the parent galaxy more easily than the whole gas. In this context, we present new analytical solutions in the case of the simple model in presence of galactic fountains. Finally, we present the detailed chemical evolution model for the MW that we used to test the effects of galactic fountains.

In Chapter 4 we explore the effect of galactic fountains on the chemical evolution of galaxies. It is the first time that such dynamical effect is taken into account in this kind of models. First of all, we implement the galactic fountain effect on the detailed chemical evolution model of François et al. (2004). Galactic fountains can affect the chemical enrichment because of the time-delay due to the non-negligible time taken by fountains to orbit around and fall back into the Galaxy. This implies a delay in the mixing of metals with the ISM, which conflicts with the instantaneous mixing approximation (IMA) usually assumed in all chemical models. This assumption is probably not realistic, as indicated by the existence of chemical inhomogeneities, although current chemical evolution models of the MW can reproduce the majority of the observational constraints under the IMA. We test whether relaxing this approximation in a detailed chemical evolution model can improve or worsen the agreement with observations. To do that, we investigate two possible causes for relaxing the instantaneous mixing: i) the "galactic fountain time delay effect" and ii) the "metal cooling time delay effect".

Finally, in Chapter 5 we also investigate how different hypotheses about Type Ia SN progenitors can affect the chemical evolution model for the Galaxy. Type Ia SNe, in fact, are believed to be the main producers of Fe and the timescale with which Fe is restored into the ISM depends on the assumed SN progenitor model. We included different Type Ia SN progenitor models, identified by their distribution of time delays (DTDs), in a very detailed chemical evolution model for the MW which follows the evolution of several chemical species.

In Chapter 6 some conclusions are drawn.

Chapter 1

The Superbubble evolution

1.1 Superbubbles with spherically symmetric shocks

Strong stellar winds with thermal velocities of about 1000 km/s from stars of early spectral type were discovered by Morton (1967). Such winds cause the ejection of gas with a large amount of kinetic energy into the ISM. Since the velocity of these winds is highly supersonic (the typical sound speed of the ISM being 10 km/s), a shock wave forms and propagates through the surrounding ISM. Also SN explosions produce spherical blast waves that propagate through the ISM at very large velocities (typically 10^4 km/s), shocking and compressing the surrounding gas into a spherically symmetric shell. SN 1987A provides an example of such a process (see the reviews of Imshennik & Nadyozhin 1989 and McCray 1993).

To describe the evolution of a shock wave after a SN explosion, a well known solution is the self similar one of Sedov (1946) and Taylor (1950) for an adiabatic blast wave caused by a point explosion in a cold, homogenous, uniform medium. The hypothesis of an adiabatic expansion is reasonable as long as radiative losses are negligible compared with the initial explosion energy.

There are only two parameters with independent dimension in this problem: the energy explosion E_0 and the density of the ambient gas ρ_0. Using the π theorem of the theory of dimensions (Sedov 1958, Korobeinikov 1985), it is possible to obtain the radius of the shock front R_s as a function of time:

$$R_s = \left(\frac{\xi_0 E_0}{\rho_0}\right)^{1/5} t^{2/5}, \tag{1.1}$$

where $\xi_0 = 2.02597$ (for a ratio of specific heats $\gamma = 5/3$) is a constant which follows from the energy integral and the solution of the self-similar equations (Sedov, 1958). This result is also known as *Sedov-Taylor solution*. This solution also shows that $\sim 72\%$ of E_0 becomes thermal energy, while the remaining $\sim 28\%$ is organized as direct kinetic energy. The velocity of a strong spherical shock is then given by:

$$v_s = \frac{dR_s}{dt} = \frac{2}{5}\frac{R_s}{t}. \tag{1.2}$$

The Sedov-Taylor solution is valid until the time t_c in which $\int_0^{t_c} L(t)dt = bE_0$, where $L(t)$ is the instantaneous power radiated by the shell. Namely, we can assume the adiabatic Sedov-Taylor solution only if the total energy lost by the shell is a fraction b (typically $\sim 30\%$) of the initial explosion energy E_0. Detailed calculations show that t_c is of the order of a few 10^4 yr (see e.g. Cioffi et al. 1988). After this time, the shell becomes cool and very thin and its further expansion is driven by the pressure of the very hot gas inside the cavity. The expansion of the shell slows down from $R_s \sim t^{2/5}$ to $R_s \sim t^{2/7}$. It can also happen that the cavity, too, radiates away a significant fraction of energy. If this happens, the expansion of the shell is no more sustained by the thermal pressure of the cavity, but is driven by the conservation of momentum, hence by the kinetic pressure. In this case it is $R_s \sim t^{1/4}$. The expansion of the shell terminates when the expansion velocity becomes comparable with the local sound speed (typically after a few Myr).

The evolution of a wind-driven bubble (the bubble produced by a stellar wind) is not very different from the evolution of the remnant of a SN explosion, the main difference being that SNe release their energy (almost) instantaneously, whereas stellar winds continuously pump energy into the ISM. The principal model for the interaction of a stellar wind with the circumstellar gas medium has been described by Pikel'ner (1968), Pikel'ner & Shcheglov (1968), and Dyson (1973). Similarly to what happens with SN remnant evolution, there is an adiabatic phase, and a radiative or snow-plow phase when, due to the increasing importance of radiative cooling, the swept-up gas collapses into a thin cold shell. A comprehensive model for the evolution of a wind-driven interstellar superbubble has been advanced by Castor et al. (1975) and Weaver et al. (1977). A schematic view of the radiative

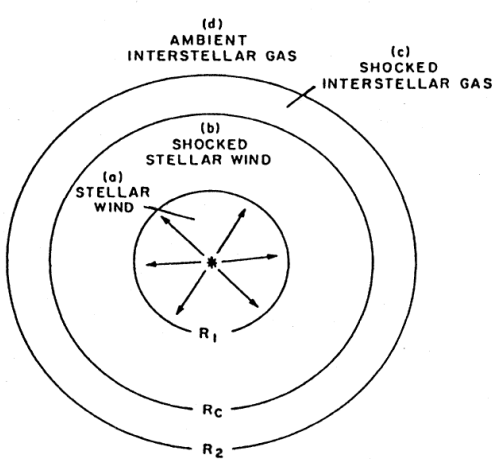

Figure 1.1: Structure of a wind-blown bubble (From Weaver et al. 1977).

wind bubble is shown in Fig. 1.1 taken by Weaver et al. (1977). The bubble has a four-zone structure: (a) a free-expansion stellar wind zone with a constant expansion velocity v_w which is surrounded by the inner shock surface; (b) a hot, almost isobaric

region occupied by the shocked interstellar gas evaporated from the dense shell and stellar wind gas; (c) a dense, cold shell containing most of the swept-up interstellar gas separated from region (b) by a contact discontinuity; and (d) an undisturbed interstellar gas region separated from region (c) by the outer shock-wave.

The motion of the bubble shell follows from the equation of mass, momentum and energy conservation (see Castor et al. 1975), namely:

$$M = \frac{4}{3}\pi\rho_0 R_s^3, \tag{1.3}$$

$$\frac{d}{dt}(Mu_s)4\pi = R_s^2 P_b, \tag{1.4}$$

$$\frac{dE_b}{dt} = L_0 - 4\pi R_s^2 P_b u_s, \tag{1.5}$$

$$\frac{dR_s}{dt} = u_s, \tag{1.6}$$

$$P_b = (\gamma - 1)\frac{3E_b}{4\pi R_s^3}. \tag{1.7}$$

Here ρ_0 is the density of the ambient gas, R_s and u_s are the radius and velocity of the shell, M is the mass of the swept-up interstellar gas, $L_0 = \frac{1}{2}\dot{M}V^2$ is the wind energy supply rate, P_b is the pressure of the hot interior gas and E_b is the total thermal energy of the gas. The substitution of M and u_s from eqs. (1.3) and (1.6) into eqs. (1.4) and (1.5), then P_b from eq.(1.4) into (1.7) and E_b from eq. (1.7) into (1.5) yields to the differential equation:

$$\frac{d^2}{dt^2}(R^3\dot{R}) + (3\gamma - 2)R^{-1}\dot{R}\frac{d}{dt}(R^3\dot{R}) = \frac{9(\gamma - 1)L_0}{4\pi\rho_0}\frac{1}{R}. \tag{1.8}$$

It is easy to see by simple substitution that this equation has a power-law solution (Castor et. al., 1975; Avedisova, 1971):

$$R_s = \left[\frac{375(\gamma - 1)L_0}{28(9\gamma - 4)\pi\rho_0}\right]^{1/5} t^{3/5} \tag{1.9}$$

$$u_s = \frac{3}{5}\frac{R_s}{t}, \tag{1.10}$$

$$P_b = 7\rho_0\left[\frac{3(\gamma - 1)L_0}{700(9\gamma - 4)\pi\rho_0}\right]^{2/5} t^{-4/5}. \tag{1.11}$$

As we can see, the wind-blown bubble expands as $R_s \sim t^{3/5}$, in this case the time dependence is stronger than the expansion rate of SN remnants (eq. 1.1).

Within OB associations, the main source of energy is given by Type II SN explosions. By assuming for simplicity that all the stars with masses larger than 8 $M_\odot$

end their life as Type II SNe, the SNII rate is given by the death rate of massive stars, namely:

$$r_{\rm SNII} = \frac{dN_*}{dt} = \frac{dN_*}{dM}\frac{dM}{dt}.$$

Here is dN_*/dM the number of stars per mass bin, namely the IMF, whereas dM/dt is derived from the lifetime function of massive stars as a function of mass $t = t(M)$. The IMF is typically described by a single-slope power law $dN_*/dM \sim M^{-(1+x)}$ and also the lifetime of massive stars can be well approximated by a function of the form $t(M) \sim M^{-b}$. If we combine these two functions, we obtain $r_{\rm SN} = (dN_*/dM)(dM/dt) \sim t^d$, where $d = x/b - 1$. It is usually $x \simeq b$ and therefore $d \simeq 0$. This means that, if we assume that each SN releases the same amount of energy E_0 into the ISM, an OB association produces an almost constant luminosity $L = r_{\rm SN}E_0$, at least until the last Type II SN explodes. A typical period of activity of an OB association is ~ 30 Myr since this is the lifetime of a 8 $M_\odot$ star. This rough estimate of a constant luminosity in a OB association is confirmed by detailed starburst models (Leitherer et al. 1999).

On the other hand, Mac Low & McCray (1988) (hereafter, MM88) have shown that, once a cold dense shell with isobaric interior has formed, the temperature of the interior becomes high enough for a single SN remnant to be subsonic before collision with the common huge shell (the so called supershell). Thus, the hot interior gas buffers the discrete SN explosions, allowing us to treat them as a continuous energy input after the first 5-10 SNe have occurred. We can therefore consider the superbubble (the bubble formed by the cumulative effect of several SN explosions) as the scaled-up version of the wind-blown bubble and we can describe it with the same equations we have described so far. This has been done for instance by McCray & Kafatos (1987), who assumed that most massive stars are born in compact groups containing some dozens of hundreds stars. The combined action of these stars will create an expanding superbubble with radius given by eq. (1.9), which may be rewritten in astrophysical units as:

$$R_s = 267(L_{38}/n_0)^{1/5}{t_7}^{3/5}\ {\rm pc}, \tag{1.12}$$

where L_{38} is the energy input rate L_{SN} in 10^{38} erg/s units, t_7 is the time in units of 10^7 yr, and n_0 is the particle number density of the ambient gas.

1.2 Superbubbles in stratified media

1.2.1 Superbubbles with variable luminosity and density

Under normal circumstances, the ISM surrounding a superbubble does not have a constant density, neither is the luminosity constant with time. Koo & McKee (1992) found solutions of superbubbles extended to the case of of power-law energy injection,

$$L(t) = L_0 t^{\eta_{in}-1}, \tag{1.13}$$

in a medium with a power-law density distribution

$$\rho = \rho_0 r^{-k_\rho}. \tag{1.14}$$

The self similar solution for the evolution of the superbubble with a variable luminosity and density is:

$$R_s = \left[\frac{(3-k_\rho)\Gamma_{rad}\xi L_0}{3\eta_{in}\rho_0}\right]^{1/(5-k_\rho)} t^\eta \tag{1.15}$$

where $\eta = \frac{2+\eta_{in}}{5-k_\rho}$, ξ is a numerical constant of order unity, and Γ_{rad} is the fraction of the injected energy E_{in} in the superbubble at time t , allowing for possible radiative losses from the shocked ambient medium. $\eta_{in} = 1$ corresponds to the normal wind-blown bubble at constant luminosity, whereas for $\eta_{in} \to 0$ we approach the blast wave solution of Sedov-Taylor for point explosions expressed in eq. (1.1).

It is important to notice here that a critical slope of the density distribution k_ρ exists, above which η is larger than 1. This critical value is given by $3-\eta_{in}$ (2 in the case of a constant luminosity). If $\eta > 1$, $v_s = dR_s/dt$ increases with time (in other words, the shock accelerates). Although very useful in some circumstances, the utility of this solution is limited by the fact that it assumes a spherically symmetric distribution of gas surrounding the source of energy (the OB association in the case of the superbubble), although with a non-constant density. It is therefore a one-dimensional solution, whereas in many astrophysical problems we need (at least) a two-dimensional solution. A typical example is a disk galaxy, where the density is (almost) constant along the disk but the distribution of gas is stratified along the polar direction. In order to describe the superbubble evolution in a disk galaxy (or in general in a stratified atmosphere) we need more sophisticated mathematical tools. The Kompaneets approximation is one of those.

1.2.2 The Kompaneets approximation: an analytical model

A general result of superbubble expansion in a disk galaxy is that, if the scale height of the disk is very large (or if the luminosity driving the superbubble is moderate), the pressure of the ISM in the disk can be enough to counter-balance the expansion of the supershell, which therefore stalls and remains confined in the disk. If instead the luminosity of the superbubble is very large or the disk scale-height is small, then the superbubble overcomes soon in the vertical direction the scale height. After having reached a particular height above the disk (typically 3 times the scale height of the disk; see below), it starts accelerating. This phase (usually called *blow-out*) is very important because the acceleration makes the supershell Rayleigh-Taylor unstable and leads to its fragmentation.

The first analytic discussion of two-dimensional shock waves was presented by Kompaneets (1960), who developed a model that can fairly well describe the evolution of a shock in a stratified medium (like the one of a disk galaxy). The Kom-

paneets approximation assumes the following: uniform pressure within the superbubble, superbubble expansion in a direction normal to the local surface and an expansion speed implied by a strong shock (i.e., the internal pressure dominates the external pressure).

The Kompaneets model considers the propagation of an adiabatic shock wave from a point explosion located at $z = 0$ in a plane-stratified exponential atmosphere with the gas density distribution

$$\rho(z) = \rho_0 \, \exp(-z/H), \tag{1.16}$$

where H is the scale height. In the work of Kompaneets it was assumed that for $z < 0$ the ISM was denser than the gas residing above the disk. Therefore, in this approximation, the superbubble has an asymmetric evolution with respect to the plane of the galaxy. There are three independent dimensional parameters in the problem: the mid-plane density ρ_0, the characteristic scale height of the gas density H, and the thermal energy of the explosion $E_{\rm th}$. Thus it is not possible to extend the self-similar method to describe shock-wave propagation in this case. The main idea of the Kompaneets approach is to calculate the smoothed, averaged parameters of the hot gas within the remnant only, without considering possible space variations of the thermodynamical variables. It is assumed that the pressure in the shocked gas is uniform and equal to:

$$P = (\gamma - 1) \, \frac{E_{\rm th}}{\Omega}, \tag{1.17}$$

where γ is the ratio of specific heats, $E_{\rm th}$ is the thermal energy of the superbubble, and the volume Ω of the remnant is defined in cylindrical symmetric coordinates (r, z) by the integral:

$$\Omega = \pi \int_{z_2}^{z_1} r^2(z,t) \, dz, \tag{1.18}$$

in which z_1 and $z_2 \, (< 0)$ are the top and bottom of the remnant, respectively.

The physical reasons for this simplification are the high temperature and great sound speed in the shocked gas, which permit redistribution of the internal energy to a nearly isobaric state before the shock front moves an appreciable distance. As already said, the Kompaneets approximation assumes that the shock is strong, i.e., the ambient gas pressure is negligible. Since the internal pressure dominates the external pressure, Hugoniot conditions determine the normal component of the expansion velocity at any point in the shock front as function of time:

$$v_n = \sqrt{\frac{\gamma + 1}{2} \, \frac{P(t)}{\rho(z)}}. \tag{1.19}$$

where $\rho(z)$ is the density of the ambient interstellar gas. We can define the surface of the shock front as $f(r, z, t)$=0. The time derivative of this function is

$$\frac{df}{dt} = \frac{\partial f}{\partial t} + \frac{\partial f}{\partial z} v_z + \frac{\partial f}{\partial r} v_r = 0. \tag{1.20}$$

The component of the arbitrary vector $\mathbf{v}$, which is normal to the surface, may be expressed as:

$$v_n = n_z v_z + n_r v_r = \frac{1}{|\nabla f|}\left(\frac{\partial f}{\partial z}v_z + \frac{\partial f}{\partial r}v_r\right). \tag{1.21}$$

Using Eqs. (1.20) and (1.21) we have an expression for the shock-wave velocity in the form (see also Shapiro,1979):

$$v_n = -\frac{\partial f/\partial t}{|\nabla f|}. \tag{1.22}$$

Assuming that the equation of the shock surface may be written in the evident form $r = r(z,t)$ and equating (1.22) to (1.19), we get an equation for the evolution of the shock front, (see also Bisnovatyi-Kogan & Silich 1995):

$$\left(\frac{\partial r}{\partial y}\right)^2 - \frac{\rho(z)}{\rho_0}\left[\left(\frac{\partial r}{\partial z}\right)^2 + 1\right] = 0. \tag{1.23}$$

In equation (1.23), y is a transformed variable (with units of length) defined by:

$$y = \int_0^t \sqrt{\frac{\gamma^2-1}{2}\frac{E_{\rm th}}{\rho_0\Omega}}\,dt. \tag{1.24}$$

Kompaneets (1960) showed that equation (1.23) could be solved analytically by separation of variables, yielding the relation:

$$r(z,y) = 2H\,\arccos\left[\frac{1}{2}e^{z/2H}\left(1 - \frac{y^2}{4H^2} + e^{-z/H}\right)\right]. \tag{1.25}$$

Equation (1.25) describes a sequence of shapes for the shock front, which change as the parameter y varies from 0 to $2H$, at which time the top of the remnant formally reaches infinity.

The top and bottom of the remnant, where $r = 0$, are located at:

$$z_{L,H} = -2H\,\ln\left(1 \mp \frac{y}{2H}\right). \tag{1.26}$$

A solution of eq. (1.26) exists for $0 \le y < 2H$. When y approaches $2H$ and the physical time t also remains finite, the top of the remnant reaches infinity. Physically this means infinite shock acceleration in the z direction due to the strong density gradient. In other words, the supershell experiences blowout. The bottom of the shock wave:

$$z_H = -2H\ln 2, \tag{1.27}$$

does not penetrate downward more than ~ 1.4 scale heights in this model, as a consequence of the the assumption of uniform pressure within the cavity (see Laumbach & Probstein, 1969). When the shock wave blows out, the remnant volume

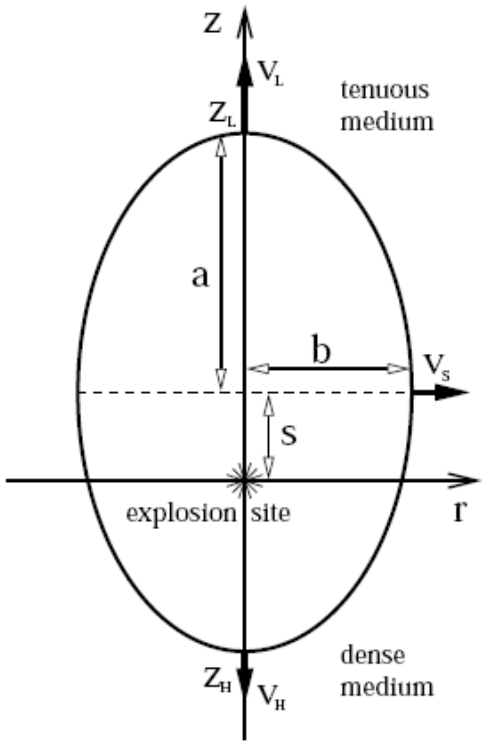

Figure 1.2: The superbubble shape (see Kompaneets 1960) under the assumption that the density below the plane is constant (see text). Some physical quantities are reported: the height of the superbubble in the exponential atmosphere (z_L) and below the plane (z_H), and the semi-minor axis (b). Figure taken from Kompaneets (1960).

goes to infinity, while internal gas pressure and downstream velocity drop to zero. The maximum cylindrical radius of the blastwave can be obtained from eq. (1.25), where $\partial r/\partial z = 0$:

$$b = 2H \arcsin\left(\frac{y}{2H}\right). \tag{1.28}$$

The radius cannot exceed the critical value $r_c = \pi H$ for any explosion energy, because a larger fraction of the explosion energy is escaping away from the plane of the explosion $z = 0$ in the direction of the steepest density gradient.

Eq. (1.25) illustrates an important property of the Kompaneets model; the spa-

tial solution is independent of the time evolution. The shock front evolves through the sequence of shapes given by eq. (1.25) which is a consequence only of the atmospheric structure. However, the *rate* at which it evolves does depend on the details of the energy input into the superbubble, i.e., whether the energy is input at one instant or in a continuous fashion, and at what rate. In fact, for a SN explosion (as considered originally by Kompaneets) the term $E_{\rm th}$ to insert in eq. (1.17) is just the explosion energy of the SN and does not depend on time. If we instead want to apply the Kompaneets approximation to a superbubble model, we just have to replace $E_{\rm th}$ with $\int_0^t L(\tau)d\tau$ (Lt if we consider a constant luminosity). Hence, the shape of an observed bubble can supply information about the ambient atmosphere independent of any knowledge of the energetics of the driving source.

The Kompaneets solution has been used and adapted for application to various astrophysical phenomena, including relativistic blast waves (Shapiro 1979), active galaxy winds (Schiano 1985), and impacts within the deep gaseous envelopes of giant planets (Korycansky 1992). By "Kompaneets approximation" we denote the method in which i) the shock velocity at each point is directed normal to the layer, ii) the energy density behind the shock is taken as a constant part of the average total energy of the bubble. A further improvement of this method, in which dynamic equation for thin-layer motion are solved directly and simplifications i) and ii) are not used they are called "the thin layer approximation" or "thin shell approximation". We stress this difference here, because both methods are sometimes referred to in the literature by the same name, "Kompaneets approximation" (MM88)

1.2.3 Superbubble blowout dynamics

The "thin shell approximation"

More sophisticated models of superbubble expansion include the thin shell approximation (MM88, Bisnovatyi-Kogan et al. 1989). The thin shell approximation is based on two simplifying assumptions: *i*) all swept-up intercloud gas accumulates into an infinitesimally thin shell just behind the shock front and moves with the post-shock velocity; *ii*) the pressure inside the cavity is uniform and therefore depends only on time. By means of this approximation it is possible to calculate the dynamics of the superbubble either by means of analytical or semi-analytical calculations, or through direct numerical integration of the momentum equation for various segments of the thin shell of swept-up gas.

As we have already mentioned, in a disk galaxy superbubbles suffer two possible fates. Either they blow out through one or both sides of the H I disk, producing a "worm" (Heiles 1979, 1984) or "chimney" (Tomisaka & Ikeuchi 1986), or they begin to collapse in on them. Following the definition used by MM88, by "blow-out" we indicate the superbubble begining to accelerate upward. In both cases, Rayleigh-Taylor (hereafter R-T) instabilities will eventually break up the supershell, either when it begins to accelerate into the halo, or when it begins to collapse inward under the influence of the ISM pressure and the galactic gravitational field.

It is possible to understand this behavior qualitatively from a dimensional analy-

sis. Since radiative cooling of the interior is usually negligible before the superbubble becomes dynamically unstable (MM88), we neglect it in the following analysis. An appropriate time scale is the dynamical time defined by equation:

$$t_D \approx H^{5/3}(\rho_0/L_{SN})^{1/3}, \tag{1.29}$$

where H is the density stratification scale height, $L_{SN} = N_* E_{SN}/t_{OB}$ with N_* is the number of stars which will become SNe over the lifetime, t_{OB}, of the OB association, and E_{SN} is the average energy per SN. The scale length is H, the mass scale is $\rho_0 H^3$, and thermal energy scale is $P_e H^3$, where P_e is the pressure of the external ISM. Thus the luminosity scale may be defined by:

$$\mathcal{L} = P_e H^3/t_D = P_e H^{4/3}\rho^{-1/3}L_{SN}^{1/3}. \tag{1.30}$$

The dimensional constants may be combined into the dimensionless dynamics parameter:

$$D = (L_{SN}/\mathcal{L})^{3/2}$$
$$\approx 940 L_{38}\left(\frac{H}{100\,\mathrm{pc}}\right)^{-2}\left(\frac{P_e}{10^4 k\,\mathrm{d}yne\,\mathrm{cm}^{-2}}\right)^{-3/2}\left(\frac{\rho_0}{\mu m_H}\right)^{1/2}, \tag{1.31}$$

where μ is the mean molecular weight and m_H is the proton mass. For $D \approx 1$, the expansion speed of the supershell at one scale height is equal to the effective sound speed of the disk gas. Thus the parameter D determines whether the supershell will collapse or blow out, as long as radiative losses from the interior may be neglected.

MM88 discussed expansion into an exponential atmosphere:

$$n(z) = n_0 \exp(-|z|/H), \tag{1.32}$$

and into the more realistic hybrid model atmosphere described by Lockman et al. (1986). The latter has a Gaussian cloud layer with scale height $H_c = 135$ pc, and an exponential H I layer with scale height $H_s = 500$ pc, giving a density dependence such as:

$$n(z) = n_s \exp(-|z|/H_s) + n_c \exp(-z^2/H_c^2), \tag{1.33}$$

where $n_0 = n_s + 4.2 n_c$. This atmosphere was derived from combined 21 cm and UV observations of OB stars at high galactic latitudes. For both these atmospheres they ran models with different values of the dynamical parameter, D, and different heights above the plane of the galaxy. Here we report only results referred to the exponential atmosphere. In Fig. 1.3 we report MM88 results concerning a superbubble with $D = 1000$, with the OB association either in the plane of the galaxy or 70 pc above it. The scale height of the exponential atmosphere is $H = 100$ pc, the density at the plane of the galaxy is $n_0 = 1$ cm^{-3}, the ISM temperature is 10^4 K, and the luminosity is L_{38}=1.1 (L_{38} is the luminosity in 10^{38} erg/s). For the symmetric model in Fig.1.3, blowout (the transition from deceleration to acceleration upwards) occurs at 5 t_D corresponding to $\sim$ 6 Myr, when the superbubble has a radius in the plane of just

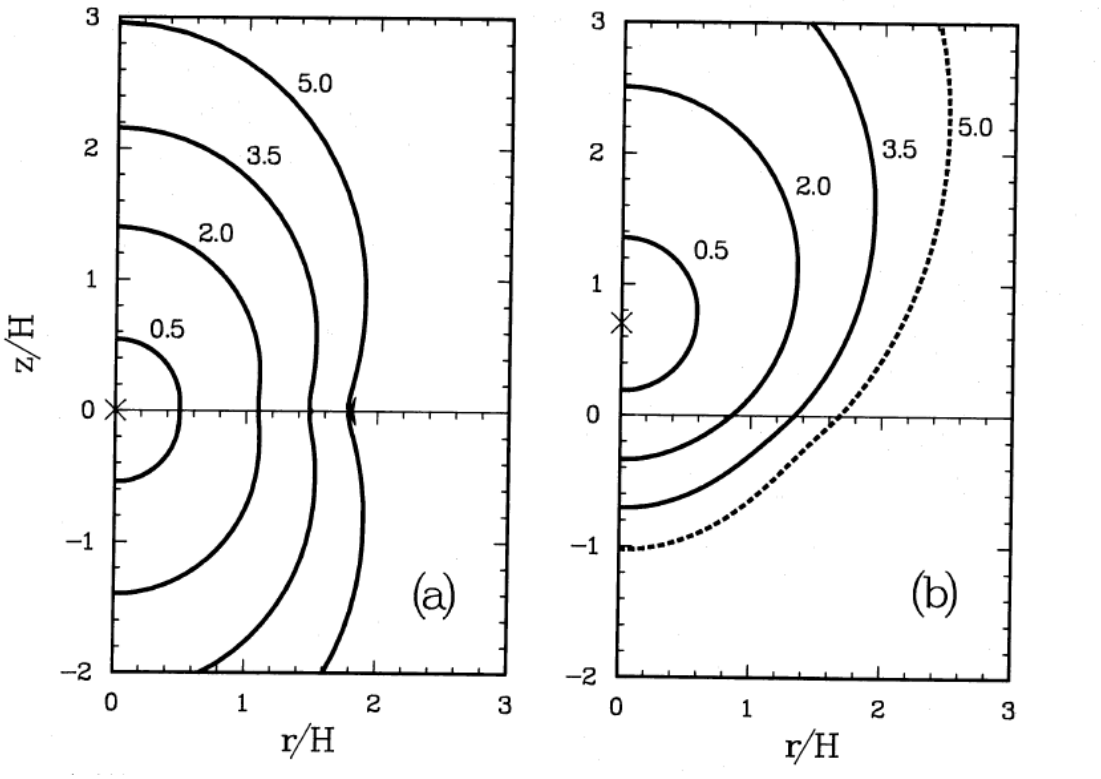

Figure 1.3: $(a-b)$ Shape of a superbubble with $D = 1000$ in an exponential atmosphere with $H = 100$, L_{38}=1.1, $P_e = 10^4$ k dynes cm^{-2}, and $n_0 = 1$ cm^{-3}, implying t_d=1.21 Myr. The off-center model is at 0.7 H (70 pc), as marked by the cross. Note that the cusp at the plane si caused by the double-sided exponential atmosphere. Figure taken by MM88.

$2H$, and a height of $\sim 3H$. The cusp at the equator is caused by the discontinuity in the density gradient across the plane of the galaxy in a symmetric exponential atmosphere. The asymmetric model is high enough above the disk to blow out only on one side. In MM88 the criterion for one-sided blowouts is that, when the top starts to accelerate, the bottom part will be decelerating more strongly than a spherical superbubble would. Using this criterion, they find that superbubbles will blow out only one side if their centers are above ~ 0.6 H in an exponential atmosphere.

In order to show the effects of different values of D on superbubble growth, they showed the radius and height of such supershells as report in Fig. 1.4. Under the influence of gravity, low D superbubbles become slightly oblate collapsing in at the poles, as is illustrated by the $D = 10$ case (curve B). For a density $n_0 = 1$ cm^{-3}, the lowest two curves correspond to unrealistically low SN rates; indeed, a strong stellar wind with L_{38}=0.01 will have $D \sim 10$. We can appreciate also in this figure that the acceleration of the supershell occurs always at ~ 3 H, irrespective of D. Namely, the height above the plane at which the supershell accelerates depends only on the

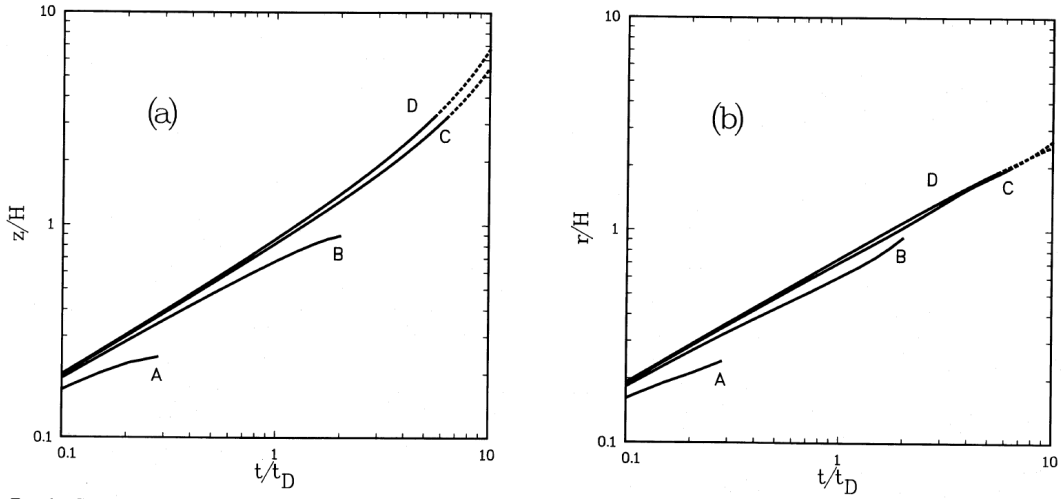

Figure 1.4: Growth of superbubbles in an exponential atmosphere with the same parameters as Fig. 1.3. The dimensionless luminosities vary as follows: (curve A) $D = 1$ ($L_{38} = 1.1 \times 10^{-3}$, $t_D = 12$ Myr). (Curve B) $D = 10$ ($L_{38} = 0.011$, $t_D = 5.6$ Myr), (curve C) $D = 100$ ($L_{38} = 0.11$, $t_D = 2.6$ Myr), (curve D) $D = 1000$ ($L_{38} = 1.1$, $t_D = 1.2$ Myr). Size as a function of time is shown for (a) height above the plane of the galaxy and (b) radius in the plane. The curves are dashed when the superbubbles begin to accelerate and become unstable.(From MM88)

gas stratification; only the time needed to reach it changes with the luminosity. The same result has been obtained with the Kompaneets approximation.

Finally, full numerical integration of the hydrodynamic equations (e.g., Tomisaka & Ikeuchi 1986; MacLow et al. 1989 (hereafter MMN89); Tenorio-Tagle et al. 1990) and magnetohydrodynamic equations (Tomisaka 1992, 1998) yield the most complete solutions to date. These models do not make any simplifying assumption about the thickness of the supershell and the pressure distribution inside the cavity, at variance with the thin shell approximation. For a review of models of bubble expansion in the ISM, see Bisnovatyi-Kogan & Silich (1995).

Hydrodynamical models vs "thin-shell approximation"

The best way to check the validity of the thin shell approximation is to refer to the work of MMN89, who used a two-dimensional hydrodynamics code to model the blowout of a superbubble from exponential and Gaussian models for the vertical density stratification, comparing the results to those from the Kompaneets ("thin-shell") approximation. They found that this approximation works very well. In Fig. 1.5 we report the MMN89 model results concerning the blowout of a superbubble, with mechanical luminosity $L_{SN} = 1.1 \times 10^{38}$ erg s^{-1}, in the same exponential ISM disk used in MM88 (eq. 1.32) and with $T = 10^4$ K throughout.

The energy source is 70 pc above the plane of the disk, namely this models must

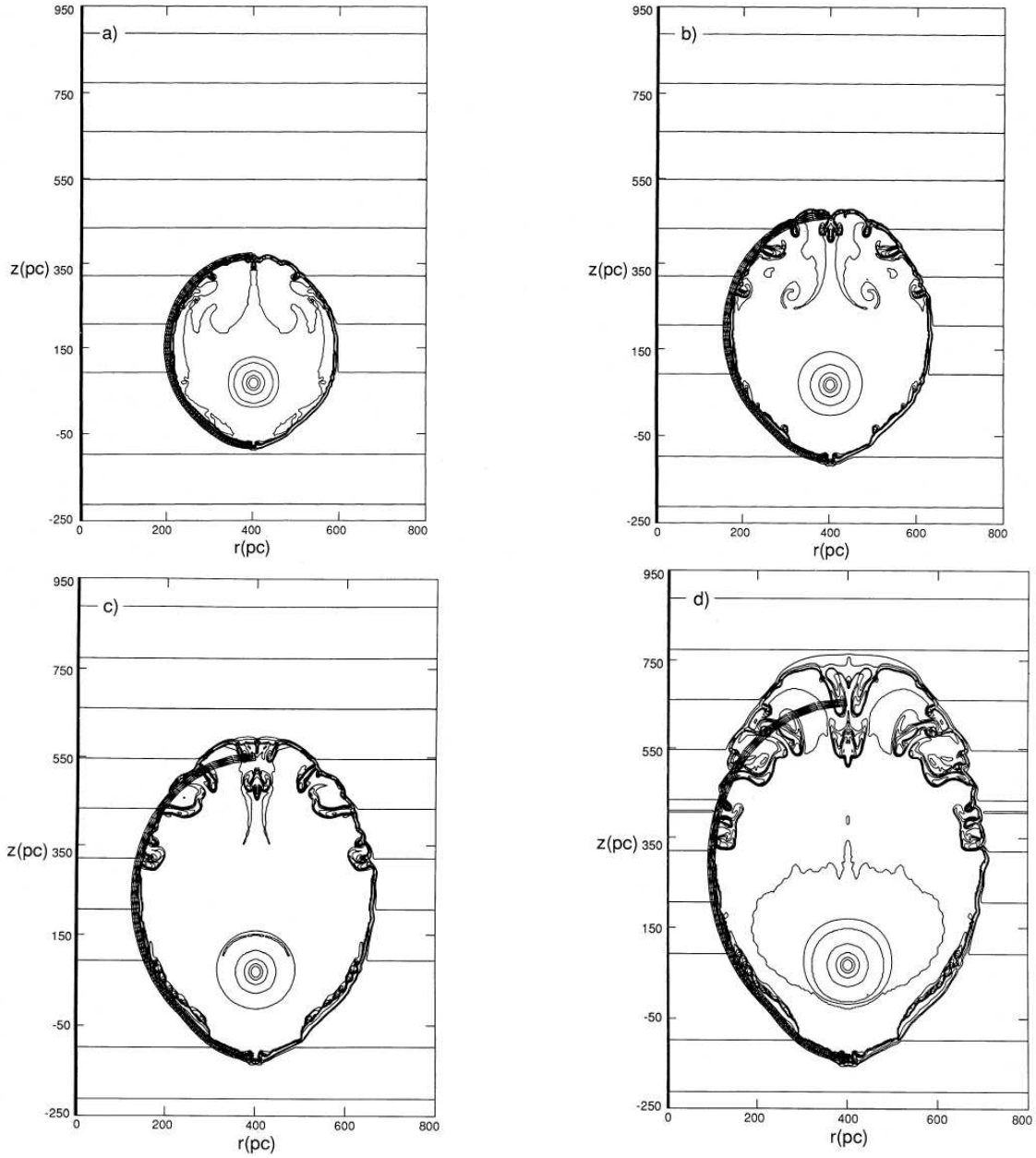

Figure 1.5: Blowout of a superbubble for the hydrodynamical model, The shape of the supershell for the Kompaneets approximation model is shown by the inner boundary of the thick hatched curve. The models are shown at times: 3.83 Myr (panel *a*), 5.02 Myr (panel *b*), 5.89 Myr (panel *c*), and 6.87 Myr (panel *d*) (From MM89).

be compared with the thin shell model shown in Fig. 1.3 (b). In the figure the contours of density are shown for the hydrodynamical model, with logarithmic spacing of 0.5 dex from $\rho = 10^{-28}$ g cm $^{-3}$. The shape of the supershell for the Kompaneets approximation model is shown by the inner boundary of the thick hatched curve.

The models are shown at times: 3.83 Myr (panel *a*), 5.02 Myr (panel *b*), 5.89 Myr (panel *c*), and 6.87 Myr (panel *d*). In MM88 they could follow the growth of the superbubble with confidence only until R-T instabilities set in. In MMN89, using a hydrodynamical code, they could follow the superbubble growth as the cold, dense shell fragments, and realizes the hot cavity gas into the rarefied galactic corona. Blowout of the exponential model, occurs at a time 3.3 t_D, when the top has grown to 2.9 H above the plane (in perfect agreement with the value 3 H found with the thin shell approximation). The breakup of the supershell follows the classic R-T spike-and-bubble form. They found that the the cold supershell first begins to accelerate and breaks up at the polar caps, where the external stratified atmosphere has the lowest density and pressure.

Many more papers in the last decades have dealt with superbubble expansion in stratified media; we cited only some of the most significant ones. However, in spite of all the work done on this subject, very few papers in the past have taken into account the chemical evolution of the superbubble and how the supershell (and the fragments of the supershell, after it becomes R-T unstable) get polluted from the metals produced by the OB stars. Moreover, with this thesis for the first time we consider in a detailed chemical evolution code and in analytical models the effect of galactic fountains.

Chapter 2

Galactic fountains and their connection with HVCs and IVCs

2.1 Description of the model

Type II SNe usually occur in OB associations containing several dozen massive stars. Sequential SN explosions create a superbubble, whereas the swept up gas is concentrated in a thin cold shell called a supershell. The superbubble expansion in a stratified medium does not follow a spherical evolution and the Kompaneets (1960) approximation well describes the way in which the superbubble grows in the meridional Galaxy plane. After some time, a region of the supershell can fragment due to the occurrence of RTIs, therefore clouds of gas can form. Once it has left the stellar disk, the orbit of each cloud can be followed either ballistically or with a hybrid model considering viscous interaction between the cloud and the extra-planar gas.

2.1.1 The Kompaneets approximation in our model

In the work of Kompaneets (1960) described in Chapter 1, it was assumed that for $z < 0$ the ISM was denser than the gas residing above the disk. Therefore, in this approximation, the superbubble has an asymmetric evolution as shown in Fig.2.1 with respect to the plane of the galaxy. In our work for the ISM z-profile we assume the following exponential law

$$\rho(z) = \rho_0 \, \exp(-|z|/H). \tag{2.1}$$

Hence the superbubble driven by sequential explosion of SNe in the galactic plane, i.e.$z = 0$, evolves symmetrically with respect to the galactic plane resulting in a peanut-like shape, as suggested by MM88 and by Tenorio-Tagle et al. (1999). The volume of the superbubble can be estimated as:

$$\Omega = 2 \cdot \frac{4}{3}\pi a^2 b - \frac{4}{3}\pi |z_H|^3 \tag{2.2}$$

where z_L and z_H are obtained from eq.(1.26), $a = (z_L + |z_H|)/2$ is the semi-major axis.

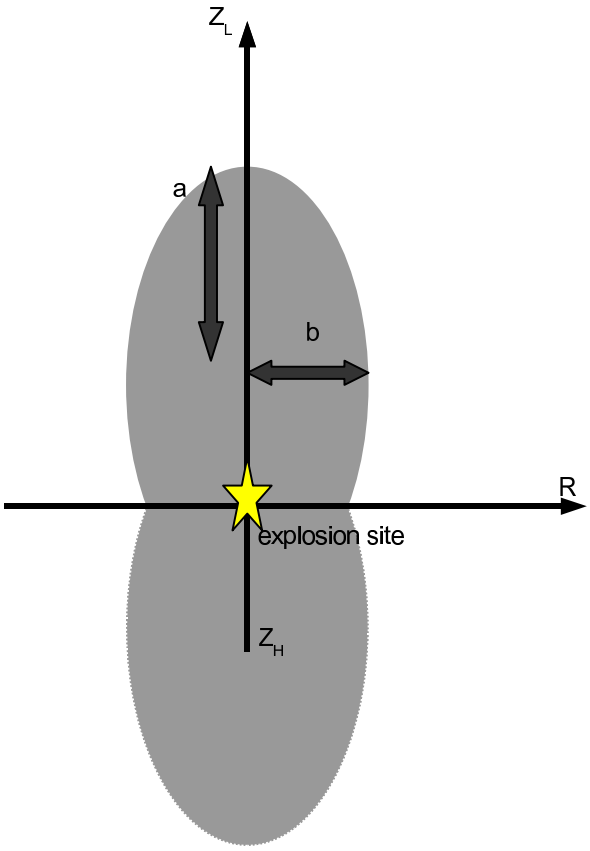

Figure 2.1: The superbubble shape (see Kompaneets 1960) under the assumption that the density follow the eq. (2.1).

The thermal energy is calculated from the differential equation:

$$\frac{dE_{th}}{dt} = L_0 - P\frac{d\Omega}{dt}, \tag{2.3}$$

where L_0 is the wind luminosity.

This equation differs from that used in the blast wave formulation and in the Kompaneets (1960) approximation reported of the in Chapter 1, in which $E_{\rm th}$ is a constant fraction of the energy deposited in an initial blastwave. Equation (2.3) assumes that the wind luminosity is thermalized at the inner shock front, and that the only energy loss is due to the work done against the thin shell. The effect of radiative and evaporative cooling of the bubble interior can also be added here if desired.

A numerical integration of eqs. (1.24) and (2.3), with the help of eqs. (1.17) and (2.2), yields $y(t)$ and E_{th} which implicitly give the time evolution of the superbubble. The solution depends on only three parameters: the scale height H, the density near the source ρ_0, and the wind luminosity L_0. Hence the problem is solved most naturally in a system of units determined by these three parameters. The unit of length is then H_0, the unit of mass is $\rho_0 H^3$, and the unit of time is $(\rho_0 H^5/L_0)^{1/3}$ (see Table 2.1). We obtain the dimensionless solution by integrating the dimensionless form of eqs. (1.24) and (2.3). In Figs. 2.2 and 2.3 we report the dimensionless evolution of y and the velocity dz_L/dt. The dimensionless analysis predicts that the superbubble begins to accelerate at (see Fig. 2.3):

$$\tilde{t_a} = \frac{t_a}{(\rho_0 H^5/L_0)^{1/3}} = 1.72, \tag{2.4}$$

namely when dz_L/dt is at a minimum.

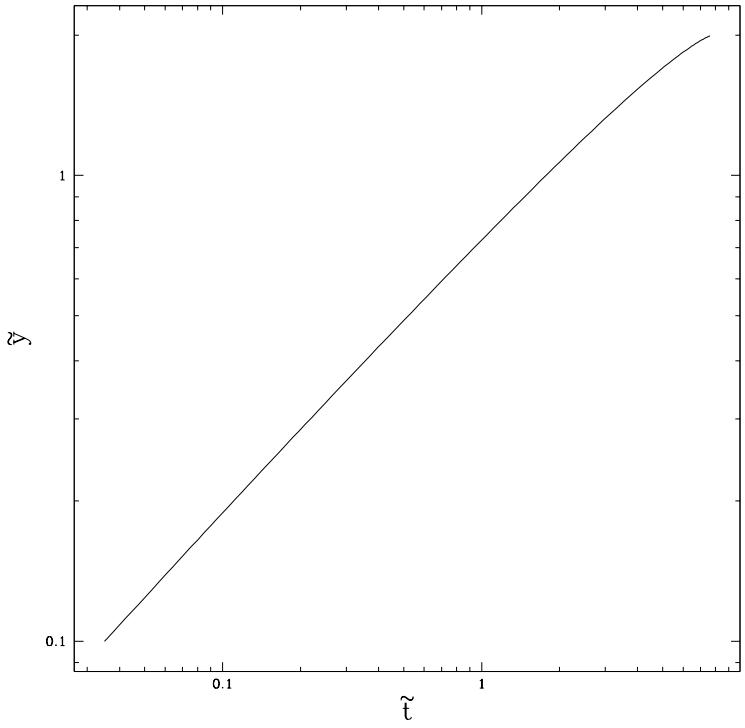

Figure 2.2: Evolution in dimensionless space of the quantity $\tilde{y}$ (eq. 1.24) as a function of $\tilde{t}$. $\tilde{y}$ is related to the top of the superbubble (Z_L) evolution from eq. (1.26). The dimensional time t is given by: $t = \tilde{t} \times (\rho_0 H^5/L_0)^{1/3}$

The simulated superbubbles, characterized by different values of ρ_0, H, L_0, reach the accelerated phase at different times, as shown in eq. (2.4), but they have the same shape and volume. This is a direct consequence of the self-similar nature of

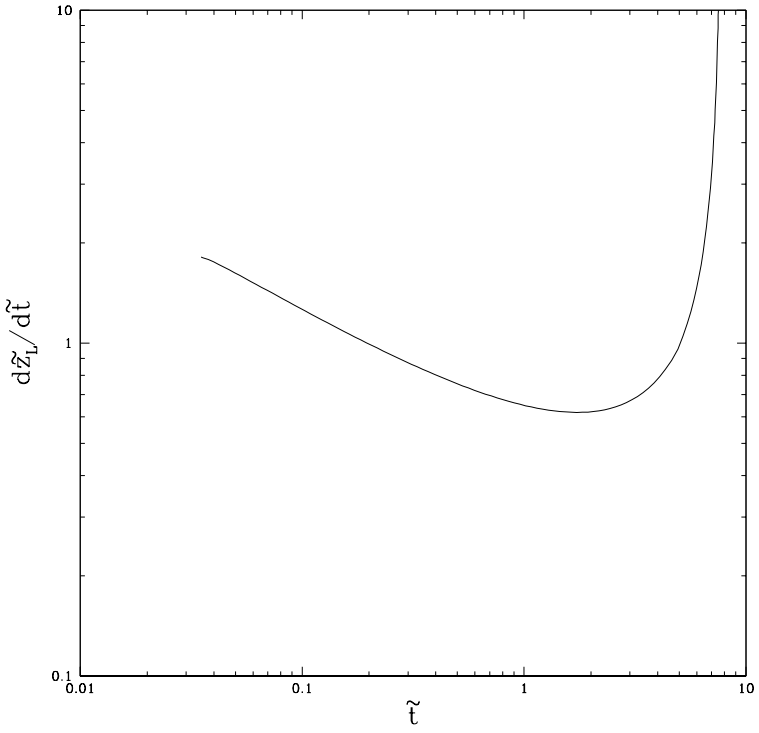

Figure 2.3: Evolution in dimensionless space of the velocity $d\tilde{z_L}/d\tilde{t}$ as function of $\tilde{t}$. The shell starts accelerating at $\tilde{t_a} = 1.72$.

the Kompaneets solutions. Using the scale height H=141 pc (see Section 2.1.3) we obtain for the height of the supershell and for the minor semiaxis the values $z_L = 191$ pc and $b = 145$ pc. From Fig. 2.3 we note that, after the beginning of the accelerated phase, the velocity remains roughly constant for $\sim 2\ \tilde{t}$ $\left(\tilde{t} = (\rho_0 H^5/L_0)^{1/3}\right)$. In this interval of time, the acceleration is negligible. Therefore, we assume that the RTIs begin to grow when the velocity is increased by a factor of 10%, because from that moment on we can assume that the acceleration is not negligible. The choice of this percentage is arbitrary but in this way our results are consistent with the work of MM88. We have also tested velocity variations of 5% and 20% and the results are not very different from the ones presented in this work. In our model, we assume that due to the RTIs, the supershell fragments and we consider each fragment as a cloud with an initial velocity given by the supershell velocity at the moment of the fragmentation. RTIs arise when the supershell accelerates since at that moment, the effective gravity of the supershell exceeds that of the tenuous superbubble. From Tenorio-Tagle et al. (1987) we can derive an estimate of the time of growth of these highly irregular structures:

$$t_{R-T} = 10^5 R_{40}^2 \sqrt{\frac{\lambda_{10}}{E_{51}(t_a + t_{\Delta v})} n_0} \ \text{ yr}, \tag{2.5}$$

Table 2.1: Units of physical quantities

Physical Quantity	Unit
Length	H
Time	$(\rho_0 H^5/L_0)^{1/3}$
Velocity	$(L_0/\rho_0 H^2)^{1/3}$
Acceleration	$(L_0^2/\rho_0^2 H^7)^{1/3}$
Mass	$\rho_0 H^3$
Energy	$(\rho_0 L_0^2 H^5)^{1/3}$
Pressure	$(\rho_0 L_0^2/H^4)^{1/3}$

where λ_{10} is the perturbation wavelength in units of 10 pc and R_{40} the remnant radius measured in units of 40 pc, E_{51} is the thermal energy measured in units of 10^{51} erg at the time $t_a + t_{\Delta v}$, where $t_{\Delta v}$ is the time necessary to reach an appreciable acceleration. We are aware that Tenorio-Tagle et al. (1987) studied the specific the case of the RTIs driven by the acceleration of sequential explosion of supernovae in a constant ISM, but here we are only interested in a rough estimate of the time scale processes and we think that the eq. (2.5) is useful for our aims. At the time when RTIs start growing, the supershell has reached z_L=312 and b=228. For simplicity we consider the formation of a single cloud. For the calculation we consider the maximum perturbation wavelength for the thin shell, roughly given by the supershell thickness. In the case of adiabatic expansion of a spherical thin shell, the thickness δ is given by $\delta = R/12$, where R is the radius of the shell. We assume that δ is the maximum perturbation wavelength and we make the approximation that $R = z_L$, therefore, $\delta = \lambda = 26$ pc. If we define $\tilde{t}_{R-T}$ as:

$$\tilde{t}_{R-T} = \frac{t_{R-T}}{(\rho_0 H^5/L_0)^{1/3}} \tag{2.6}$$

we obtain the total adimensional time necessary for the growth of instabilities and for the fragmentation of the bubble:

$$\tilde{t}_{final} = \tilde{t_a} + \tilde{t}_{\Delta v} + \tilde{t}_{R-T} = 4.37, \tag{2.7}$$

Considering different values of the parameters ρ_0, H, L_0, we obtain different times at which the cloud could leave the disk:

$$t_{final} = 4.37(\rho_0 H^5/L_0)^{1/3}. \tag{2.8}$$

Since the internal pressure dominates the external pressure, the expansion speed is that given by the Hugoniot condition for a strong shock:

$$v_n = \sqrt{\frac{\gamma+1}{2}\frac{P(t)}{\rho(z)}}. \tag{2.9}$$

2.1.2 Abundances of Fe and O in the superbubble

In this section we compute the total amounts of O and Fe which reside in the supershell at the time t_{final} (see eq.2.8), time at which we suppose the fragmented shell can leave the stellar disk of the Galaxy. We assume that all the stars with masses larger than 8 $M_{\odot}$ explode as Type II SNe and we adopt the following main sequence lifetimes (Matteucci & Greggio 1986):

$$\tau_m = 1.2m^{-1.85} + 0.003\mathrm{Gyr}. \tag{2.10}$$

In our model, the upper mass limit of the OB association is assumed to be $40M_{\odot}$. The lifetime of a $40M_{\odot}$ star is, from eq. (2.10), $\tau_{40} \simeq 4.30 \times 10^6$ yr.

For any parameter choice, at the time at which the shell fragments and leaves the disk, the smaller mass stars in the OB association are still active. Using eq. (2.10) we are able to estimate the lower mass limit for a SN event corresponding to the time at which the cloud forms. The time at which the cloud is formed is given by t_{final} plus the lifetime of the largest considered mass, namely:

$$\tau_{lim} = t_{final} + \tau_{40}. \tag{2.11}$$

The mass of metals (in our model we consider only O and Fe) ejected by the SNe considered here is given by:

$$M_{el_\star} = \int_{M_{inf}}^{40} m_{el}(m)\phi(m)dm, \tag{2.12}$$

where $\phi(m)$ is the IMF assumed to be the Salpeter (1955) one, namely: $\phi(m) = Am^{-(2.35)}$. A is the normalization constant, given by:

$$\int_8^{40} \phi(m)dm = A\int_8^{40} m^{-2.35}dm = SNe, \tag{2.13}$$

where SNe is the assumed number of SNe in the OB association. In eq. (2.12) the term $m_{el}(m)$ is the ejected mass of the element considered (O or Fe) by the star of initial mass m (Woosley & Weaver 1995). We consider the stellar yields at four different metallicities: solar metallicity $Z_{\odot}$, 0.1 $Z_{\odot}$, 0.01 $Z_{\odot}$, $10^{-4}Z_{\odot}$. We assume that the ISM in the disk has the same metallicity as the OB association. For the solar abundances (by mass) we use the Anders & Grevesse (1989) values:

$$O_{16_{\odot}} = 9.59 \times 10^{-3}\ ,\ \ Fe_{56_{\odot}} = 1.17 \times 10^{-3}. \tag{2.14}$$

We use this set of solar abundances to be consistent with the yields of Woosley & Weaver (1995) which refer to Anders & Grevesse (1989) abundances. However Asplund et al. (2005) recomputed the O solar abundance and deduced a $\log(O/Fe)_{\odot}$ lower by ~ 0.24 dex than the Anders & Grevesse (1989) one. The total amount $M_{shell-el}$ of the mass of the element which resides in the thin shell of the superbubble is given by the eq.:

$$M_{shell-el} = M_{shell} \cdot Z + M_{el_\star}, \tag{2.15}$$

where Z is the initial metallicity of the OB association (and consequently of the disk ISM). We adopt the extreme approximation that the total amount of the ejected metals from SNe ends up in the shell. M_{shell} is the mass of the ISM swept up into the thin shell and is given by:

$$M_{shell}(z > 0) = \pi \rho_0 b^2 \int_0^{z_L} e^{-z/H} \left(1 - \left(\frac{z - a + |z_H|}{a}\right)^2\right) dz. \tag{2.16}$$

We underline that for the Fe we use only solar yields for the whole range of metallicities (Chiappini et al. 2001).

2.1.3 Galaxy model

The potential well of the Galaxy is assumed to be the sum of three components: a dark matter halo, a bulge and a disk. The dark matter halo gravitational potential is assumed to follow the Navarro et al.(1996) profile:

$$\Phi_{dm}(r) = -4\pi r_{dm,0}^2 \, \rho_{dm,0} \frac{\ln(1+x)}{x}, \tag{2.17}$$

where $\rho_{dm,0}$ is a reference density, $r_{dm,0}$ is the scale radius, $x = r/r_{dm,0}$ and r is the spherical radius. The halo is truncated at a radius $r_{dm,t}$ beyond which its potential follows the 1/r profile. The bulge gravitational potential is given by (Hernquist 1990):

$$\Phi_b(r) = -\frac{GM_b}{r_{b,0} + r} \tag{2.18}$$

where $r_{b,0}$ is the scale radius and M_b is the bulge mass. For the disk potential we have chosen the axisymmetrical Miyamoto & Nagai (1975) model, which in cylindrical coordinates (R, z) can be written as:

$$\Phi_M(R, z) = -\frac{GM_d}{\sqrt{R^2 + \left(a + \sqrt{z^2 + b^2}\right)^2}}. \tag{2.19}$$

Table (2.2) gives the values of all the parameters concerning the Galaxy model. For the ISM z-density profile we used eq. (2.1) where: $\rho_0 = n_0 \mu m_p$ is the density in the disk plane; m_p is the proton mass and μ is mean molecular weight for the disk (assumed to be 0.61). For the value of H we adopted the vertical distributions of the various interstellar components (molecular, cold HI, warm HIa, warm HIb, HII regions, and diffuse HII) in the solar neighborhood as reported by Cox (2005). We obtained:

$$H = \frac{1}{\rho_0} \int_0^\infty \sum_{i=1}^{6} \rho_i(z) dz \simeq 141\text{pc}. \tag{2.20}$$

The ISM density profile along the radius R of the Galaxy is taken from Wolfire et al. (2003). In our model we consider the presence of an extra-planar gas halo. This halo can be described by means of the perfect gas law:

$$P = \frac{\rho k T}{\mu m_p}. \tag{2.21}$$

For simplicity we assume an isothermal and self-graviting distribution, hence introducing the parameter:

$$\beta_0 = \frac{k T_0}{\mu m_p}, \tag{2.22}$$

by means of which eq. (2.21) can be written as:

$$P = \beta_o \rho. \tag{2.23}$$

Using the hydrostatic equilibrium equation with the assumption of a static halo of gas we have:

$$\rho(R, z) = \rho_{0,h} e^{(-\Phi_{tot}+\Phi_0)/\beta_0}, \tag{2.24}$$

where $\Phi_{tot} = \Phi_{dm} + \Phi_b + \Phi_M$ and Φ_0 is the value of Φ_{tot} computed at the galactic center. The temperature T_o has been chosen following the relation:

$$\frac{3}{2} k T_o = \frac{3 m_p \mu v_{c8}^2}{2}, \tag{2.25}$$

where v_{c8} is the circular velocity in the plane of Galaxy in the solar neighborhood and we obtain that:

$$T_0 = 3.7 \times 10^6 \mathrm{K} \tag{2.26}$$

for the chosen parameters.

Table 2.2: Galactic parameters.

$\rho_{dm,0}$ 10^{-24} g cm $^{-3}$	M_b $10^{10} M_\odot$	M_d $10^{10} M_\odot$	$r_{dm,0}$ kpc	$r_{dm,t}$ kpc	$r_{b,0}$ kpc	a kpc	b kpc
0.29	3.5	7.69	30.8	347.7	0.8	8.45	0.26

2.1.4 Galactic fountains in a ballistic model

Once the top of the supershell reaches the height above the galactic plane related to the time t_{final} (see eq. 2.8), the thin shell can leave the stellar disk and move towards the extra-planar gas. Ballistic models describe the gas as an inhomogeneous collection of clouds, subject only to the gravitational potential of the Galaxy. The

fragments of the shell have different initial velocity modulus $\| \mathbf{v}_o \| = v_n$ (v_n is the velocity of the top site z_L of the supershell) and masses depending on the the number of SNe in the OB association and the initial throwing radial coordinate. We have chosen for our simulation Cartesian coordinates with versor $(\hat{\mathbf{e}}_x, \hat{\mathbf{e}}_y, \hat{\mathbf{e}}_z)$. Given a generic point in this space (x, y, z), it corresponds in the meridional plane of the Galaxy to $(R, z) = (\sqrt{x^2 + y^2}, z)$, where R is the radial coordinate. Since the $\| \mathbf{v}_o \|$ velocities are relative to the local standard of rest for the throwing radial coordinate R_0, in the inertial reference frame of the simulation in Cartesian coordinates:

$$\mathbf{v}_{initial}(R_0) = \mathbf{v}_o + v_c(R_o, 0)\hat{\mathbf{e}}_y. \tag{2.27}$$

We take into account the fact that once the cloud is formed, the direction of throwing cannot be known a priori (even if the most likely one is the perpendicular to the Galactic plane); therefore, for each choice of $\| \mathbf{v}_o \|$ we consider different direction of throwing. Given a throwing direction, a generic vector $\mathbf{v}_0$ has components along $\hat{\mathbf{e}}_x$, $\hat{\mathbf{e}}_z$ e $\hat{\mathbf{e}}_y$ with respect to our inertial frame:

$$\begin{cases} v_{z_{init}} = v_n \cos\gamma \\ \\ v_{x_{init}} = v_n \sin\gamma \cos\beta \\ \\ v_{y_{init}} = v_n \sin\gamma \sin\beta + v_c(R_0, 0) \end{cases} . \tag{2.28}$$

The parameters γ e β vary in order to recreate, in the local standard of rest, a symmetrical fountain of clouds:

$$\beta_i = \frac{i\pi}{4} \text{ with } i = 0, 1, ..7 \tag{2.29}$$

and

$$\gamma_j = \frac{\pi}{2} - \frac{\pi}{1+j} \text{ with } j = 2, 3, ..5. \tag{2.30}$$

We consider also the case in which $\mathbf{v}_0$ has only a component along $\hat{\mathbf{e}}_z$. Thus, for each velocity modulus v_n we calculate a fountain composed of the 33 different directions for the ejected cloud.

2.1.5 Beyond the ballistic model: hybrid ballistic-fluid stationary model

In this work we want to provide some hydrodynamical modifications of previous ballistic models. In the equations of motion for a single cloud we insert a Stokes term in order to consider also the viscous interactions between cloud and extra-planar gas. We introduce the drag time t_{drag}, i.e the time after which the relative circular motion between the cloud and halo becomes equal to zero (Barnabè et al. 2005):

$$t_{drag} = \frac{8}{3C_D} \frac{r_c}{v_{rel}} \chi, \tag{2.31}$$

where $C_D \simeq 1$ is a numerical coefficient, r_c is the radius of a typical H I cloud, v_{rel} is the modulus of the relative velocity between the cloud and the homogeneous extra-planar gas, and $\chi \equiv \rho_c/\rho$ is the ratio between the cloud and the medium densities. t_{drag} was estimated assuming pressure equilibrium between cold and hot components, from which $\chi = T/T_c \approx 3000$. A fiducial value of the relative velocity is obtained by assuming $v_{rel} \approx 2 \times 10^7$ cm s^{-1}, while the cloud radius r_c is estimated as:

$$4\pi {r_c}^3 \rho_c/3 = 10^5 M_\odot \tilde{M}_5, \tag{2.32}$$

where $\tilde{M}_5$ is the cloud mass in units of 10^5 $M_\odot$, thus following the work of Barnabè et al. (2005) one obtains:

$$t_{\rm drag} \approx 2.7 \times 10^8 \left(\frac{\tilde{M}_5}{n_{\rm p}} \right)^{1/3} \ {\rm yr}, \tag{2.33}$$

where n_p is the numerical density of the extra-planar gas with the density profile described by eq. (2.24). We note that a viscosity term could not be directly inserted in a Lagrangian formulation, thus we must write the explicit *drag* term to add in the motion equations. The *drag* term can be derived from the brake force as:

$$\mathbf{a}_{drag} \equiv -\frac{\mathbf{v} - \mathbf{v}_g}{t_{drag}}, \tag{2.34}$$

where $\mathbf{v}$ is the velocity of the cloud, and $\mathbf{v}_g$ is the velocity for the extra-planar gas that we assumed equal to zero.

2.2 Our results

2.2.1 Chemical composition of the clouds

In our models we vary the number of SNeII in the OB association (N SNe) and the throwing radial coordinate (R_0). We consider four possible OB associations containing 10, 50, 100, 500 SNe, respectively. Assuming an explosion energy of 10^{51} erg, the luminosities L_0 of these OB associations are 10^{37}, 5×10^{37}, 10^{38} and 5×10^{38} ergs^{-1} respectively. These numbers of massive stars in OB associations are consistent with observations (de Zeeuw et al. 1999). We simulate galactic fountains with 3 different throwing radial coordinates R_0: 4, 8, 12 kpc. Given the assumed Galaxy model, R_0 defines the disk density ρ_0, whereas the scale height is constant (see Sect 2.1.3). In Tabs. 2.3, 2.4, 2.5 we summarize the results for fragmentation times and the velocities of the superbubbles in the direction perpendicular to the galactic plane at those times for 4 kpc, 8 kpc and 12 kpc.

For all the values of N SNe and R_0 considered at the time t_{final} at which clouds are thrown out of the disk, the supershell presents: $z_L = 448$ pc and $b = 259$ pc. Our results are in agreement with the work of MM88: instabilities, for roughly the same luminosity range, become important at $3H$ height scale. The total mass of gas swept up by the SN shock wave for positive z-coordinates is given by eq. (2.16).

Table 2.3: Cloud formation times and cloud velocities for $R_0 = 4$ kpc.

N SNe	t_{final} [yr]	v_n [kms^{-1}]
10	2.29×10^7	23
50	1.34×10^7	39
100	1.06×10^7	49
500	6.21×10^6	83

Table 2.4: Same as Table 2.3 but for $R_0 = 8$ kpc.

N SNe	t_{final} [yr]	v_n [kms^{-1}]
10	1.90×10^7	27
50	1.11×10^7	46
100	8.84×10^6	58
500	5.17×10^6	100

Table 2.5: Same as Table 2.3 but for $R_0 = 12$ kpc.

N SNe	t_{final} [yr]	v_n [kms^{-1}]
10	1.67×10^7	31
50	9.77×10^6	53
100	7.74×10^6	67
500	4.53×10^6	114

Thus, we obtain that the masses of the ISM swept up into the thin shell for R_0= 4, 8, 12 kpc, respectively are:

$$M_4(z>0) = 10.07 \times 10^5 M_\odot, \tag{2.35}$$

$$M_8(z>0) = 5.79 \times 10^5 M_\odot, \tag{2.36}$$

$$M_{12}(z>0) = 3.89 \times 10^5 M_\odot. \tag{2.37}$$

All the results of the O and Fe abundances in the clouds ejected by sequential SN explosions as functions of the total number of SNe (N SNe) and R_0 are reported in the Appendix A. $M_{*Fe_{56}}$ and $M_{*O_{16}}$ are the total amounts of Fe_{56} and O_{16} in units of $M_\odot$, whereas $M_{\star ej}$ is the total mass ejected by the OB association:

$$M_{\star ej} = \int_{M_{inf}}^{40} m_{tot}(m)\phi(m)dm, \tag{2.38}$$

where $m_{tot}(m)$ is the total mass ejected by a SN as a function of its initial mass and metallicity. M_{tot}, $X_{*Fe_{56}}$, $X_{*O_{16}}$ and $[O/Fe]$ are:

$$M_{tot} = M_{shell} + M_{\star ej}, \tag{2.39}$$

$$X_{*Fe_{56}} = \frac{M_{ShellFe_{56}}}{M_{tot}} \ , \ X_{*O_{16}} = \frac{M_{ShellO_{16}}}{M_{tot}}. \tag{2.40}$$

$$[O/Fe] = \log\left(\frac{M_{ShellO_{16}}}{M_{ShellFe_{56}}}\right) - \log\left(\frac{O_{16_\odot}}{Fe_{56_\odot}}\right). \tag{2.41}$$

In Fig 2.4 we show the predicted $[O/Fe]$ ratio as a function of the number of SNe and of the initial metallicity in the solar vicinity. In the meridional plane of the Galaxy the initial conditions are (R, z)=(8 kpc, 448 pc). We note that significant over-abundances of O relative to Fe are found only in the case of a large number of SNe and low initial metallicity. In Fig. 2.5 we report the same quantities but using stellar yields given by Kobayashi et al. (2006). In Fig. 2.6 we show $[O/Fe]$ ratios as functions of the number of SNe assuming solar metallicity but varying the initial throwing coordinate R_o. We note that larger radial coordinates yield a larger $[O/Fe]$, because the amount of swept-up pristine gas is smaller (see eq. 2.37) and therefore the new α elements ejected by SNe are less diluted. In Fig. 2.7 we report the $[O/Fe]$ ratios by varying the initial throwing coordinate R_0 and taking for the initial ISM metallicities the average observed values obtained by Andrievsky et al. (2002a,c, 2004) and Luck et al. (2003), as functions of the galactocentric distance, by analyzing Galactic Cepheids (see Cescutti at al. 2006). Referring to Tab. 4 of the work of Cescutti et al. (2006), we find: $Z = 1.65 \times Z_\odot$ for $R_0 = 4$ kpc and $Z = 0.74 \times Z_\odot$ for $R_0 = 12$ kpc.

2.2.2 Dynamics of the galactic fountains

Our analysis focuses first on the study of solar neighborhood galactic fountains (i.e. with $R_0 = 8$ kpc). In Fig. 2.8 we show our results concerning the orbits of the shell fragments once they leave the stellar disk in the purely ballistic model. The trajectories of the orbits of each galactic fountain are plotted in the meridional plane of the Galaxy (R, z). Spatial initial conditions are the same for all the considered cases: $R_0 = 8$ kpc and $z_0 = 448$ pc, whereas the initial velocities depend on the number of SNe considered (Tab. 2.4). In Fig. 2.8, we also show the average falling radial coordinate in the Galaxy plane. As we can see, the clouds are preferentially thrown outwards, but their final average landing coordinates differ by 1 kpc at most from the throwing coordinate. This result is consistent with the works of Bregman (1980), Fraternali & Binney (2008) and Melioli et al. (2008a). Melioli et al. (2009) presented results for a multiple fountain model produced by randomly clustered explosions of SNe originating in stellar associations spread over a disk area of 8 kpc [2]. As in the case of a single fountain, the spreading of the SN ejecta back into the disk is not very large. Most of the gas lifted up by fountains falls back within a distance ΔR=$\pm$0.5 kpc. On the other hand, in their hydro-simulations for the MW disk, Booth & Theuns (2007) found that clouds ejected from galactic fountains return to the disk at average galactocentric distances several times larger than the galactocentric distance of the fountain. However, their mass resolution (particle mass $\simeq 1.5 \times 10^5 M_\odot$ in the highest resolution simulation) makes their results more suitable for understanding the global behavior of the HI in the Galaxy rather than the evolution of a single superbubble/supershell. In Tab. 2.6 we report the main radial velocity for each fountain given by:

$$< v_R >= \frac{< \Delta R >}{< \Delta t >}, \tag{2.42}$$

where $\Delta R = R_{final} - R_0$ and $\Delta t = t_{orbit}$; the time t_{orbit} is the time required for the cloud to return to the galactic disk once it leaves the supershell. Several chemical evolution studies have suggested that the metallicity gradient disappears if the velocity of the radial flow is $|v_f| > 2$ km s^{-1} (see Matteucci 2001).

Table 2.6: Radial flow velocities (in km s^{-1}) in the solar neighborhood (model without drag) as a function of the radial throwing coordinate.

	4 kpc	8 kpc	12 kpc
10 SNe	0.6	0.6	1.1
50 SNe	1.6	2.3	4.2
100 SNe	2.6	4.1	6.6
500 SNe	4.5	13.2	14.4

For the model with viscous interactions we must know also the mass of the cloud because the drag terms depend on this quantity (see eq. 2.33). Referring to Fig.

2.1 we assume that the part of the shell which could fragment and move upwards is the mass included above the s height where $\frac{dR}{dz} = 0$. Above this height each point of the shell has a positive velocity component along the z axis. Therefore, we estimate that the masses of a gas cloud ejected by sequential SN events in the extra-planar halo are of the order of:

$$M_{cloud_{R_0=4}} = 2.17 \times 10^5 M_\odot, \tag{2.43}$$

$$M_{cloud_{R_0=8}} = 1.24 \times 10^5 M_\odot, \tag{2.44}$$

$$M_{cloud_{R_0=12}} = 0.84 \times 10^5 M_\odot. \tag{2.45}$$

We note that the masses of the clouds are roughly 20% of the initial supershell mass, therefore the total amount of the ejected metals in clouds is roughly 20 % of the metals produced by the OB association, in agreement with the recent Melioli et al. (2008) hydrodynamical simulation results.

In Fig. 2.9 we show that for the range of initial velocities considered here, the effect of a viscous term in the motion equations is weak. The most evident effect is reported in Fig. 2.10 where the hybrid model is compared with the purely ballistic one in the case of 500 sequential SN explosions at R_0= 12 kpc. The natural effect of a viscous interaction between the cloud and the extra-planar gas is to brake the motion of the clouds. Therefore, the average radial of the coordinate falling on the disk for the model with drag $< R_{final} >$= 12.37 kpc is much smaller than the one obtained with the purely ballistic model ($< R_{final} >$= 14.38 kpc)

As shown in Tab. 2.7, it is likely that the most realistic number of massive stars in OB associations in our Galaxy is about 100. In Fig. 2.11 we have shown various fountains for the model without drag obtained with 100 sequential SN explosions respectively at 12, 8, 4 Kpc as radial coordinates. As shown before, different radial initial conditions imply different ejection velocities for the clouds. In particular, the throwing coordinate R_0=12 kpc is surrounded by a more tenuous disk, therefore the velocity is larger and the orbits wider. The highest z coordinate that a cloud could reach in this case is about z= 2.3 kpc.

2.3 Comparison with HVC and IVC observations

In this section we compare our models with observational data concerning distance and chemical composition of some clouds in our Galaxy. We consider two cloud systems: Complex C (HVCs) and IV Arch (IVC).

2.3.1 Complex C

In the work of Wakker et al. (2007) the first successful detection of interstellar $Ca\,\textsc{ii}$ H and K absorption from HVC complex C was reported. They concluded that complex C is located at Galactocentric radius <14 kpc, and lies high above the Galactic plane (z=3–9 kpc).

Table 2.7: Massive stars in OB associations from de Zeeuw et al. (1998)

OB association	WR	O	B	A	Total
Upper Scorpius			49	34	83
Upper Centaurus Lupus			66	68	134
Lower Centaurus Crux			42	55	97
Vela OB2	1		81	5	87
Trumpler 10			22	1	23
Collinder 121	1	1	85	8	95
Perseus OB2			17	16	33
α Perseus OB2			33	30	63
Lacerta OB1		1	35	46	82
Cepheus OB2		1	56	10	67

Integrating the H I column density across the cloud, $M(\ H\,\mathrm{I})$ was estimated to be 0.7-6.0 $\times 10^6 M_\odot$. As we show in eqs. (2.43), (2.44), (2.45), the sizes of our ejected clouds are considerably smaller. Even if we consider the case of the superbubble given by 500 SN explosions with R_0=12 kpc, the highest z we can reach is about $z \simeq 4.4$ kpc and at this height our cloud velocities are roughly zero. In the Tab. 1 of Wakker et al. (2007) the velocities (relative to the LSR) of complex C are reported in the direction of different lines of sight, and on average the complex C velocity is -114 km/s. Therefore, the kinematical data of Complex C are inconsistent with our results.

A key point for understanding the origin of this HVC is to consider its chemical composition. Because oxygen is not significantly depleted onto dust grains (Meyer et al. 1998) and the $O\,\mathrm{I}/H\,\mathrm{I}$ ratio is not altered by ionization effects, we have that $(O\mathrm{I}/H\mathrm{I}) \approx (O/H)$. In the work of Richter et al. (2001) the solar values for the abundances are given by Anders & Grevesse (1989) and Grevesse & Noels (1993). For oxygen they obtained:

$$[O/H] \simeq [O\ \mathrm{I}/H\,\mathrm{I}] = -1.03^{+0.37}_{-0.31}. \tag{2.46}$$

For the iron abundance in the Complex C:

$$[Fe/H] \simeq [(Fe\,\mathrm{II} + Fe\,\mathrm{III})/H\,\mathrm{I}]. = -1.15. \tag{2.47}$$

Based on the data from Fe II they obtained $[Fe/H] = -1.27^{+0.20}_{-0.14}$. Therefore a low iron abundance in Complex C could be a result of depletion of iron onto Fe rich dust (Savage & Sembach 1996). A more careful discussion about the possible effects of dust is given in Sect. 4.3. Hence the relative abundance is $[O/Fe] = 0.12$. In our model a similar result is obtained in the case of 500 SNe with the initial radial throwing coordinate fixed at $R_0 = 12$ kpc and, the disk initial gas metallicity $Z = 0.1 \times Z_\odot$. As we have seen, the most likely metallicity of the disk at R_0= 12

kpc at the present time is 0.74 $Z_\odot$, which is not consistent with the total metallicity of Complex C (eqs. 2.46 and 2.47). With our model we obtain $[O/Fe] = 0.03$ dex only in the case of 500 SNe with a throwing coordinate $R_0 = 12$ kpc and metallicity fixed at 0.74 $Z_\odot$ (see Fig. 2.7) and such a large number of SNe is unlikely. Given the inconsistency of the kinematical data with our predictions, we can rule out a Galactic origin for the Complex C HVC.

2.3.2 IV ARCH

Richter et al. (2001) suggested that IV Arch, given its nearly solar abundance and its z-height of 0.8-1.5 kpc, has its origin in the MW disk, probably as part of a Galactic fountain. These heights are consistent with our results, and also the velocities of IVCs are easily understandable in the framework of galactic fountains. The abundances measured by Richter et al. (2001) are: $[O/H] = -0.01^{+0.35}_{-0.27}$ and $[Fe/H] = -0.26^{+0.19}_{-0.15}$, therefore:

$$[O/Fe] = [O/H] - [Fe/H] = 0.25\,\mathrm{dex}. \tag{2.48}$$

If we assume a Galactic fountain origin, our model yields $[O/Fe] = 0.24$ dex in the case of 500 SN explosions, R_0= 8 kpc and metallicity $Z = 0.01 \times Z_\odot$, and $[O/Fe] = 0.26$ dex in the case of 100 SN explosions, R_0= 12 kpc and metallicity $Z = 0.01 \times Z_\odot$. As we have seen, it is quite unlikely that the initial metallicity of an OB association is nowadays as low as 0.01 $Z_\odot$ and this low initial metallicity would be inconsistent with the nearly solar abundance measured in IV Arch. Therefore, although the kinematic properties of IV Arch are in agreement with our results, its large $[O/Fe]$ casts some doubt about the Galactic origin of this IVC.

2.3.3 The effect of dust

The work of Lu et al. (1998) showed how important is the depletion of metals (in particular Fe) into dust in the ISM. Since this can affect out results about $[O/Fe]$ ratios, here we estimate the time scales of the destruction and accretion of dust in a superbubble. Referring to the work of Calura et al. (2008) we define, for a given element i the destruction time-scale τ_{destr} for the dust in the superbubble due to SN shocks as:

$$\tau_{destr,i} = (\epsilon M_{SNR})^{-1} \cdot \frac{\sigma_{ISM}}{R_{SN}}, \tag{2.49}$$

where R_{SN} is the total SN rate, M_{SNR} is the mass of the interstellar gas swept up by the SN remnant and ϵ is the destruction efficiency in a three-phase medium. We consider for σ_{ISM}, the surface gas density of the ISM, the value of $10 M_\odot$ pc^{-2} and $\epsilon M_{SNR} \simeq 10^5 M_\odot$. For the SN rate we consider the typical case of the OB association with 100 SNe. We assume as the radius of the OB association the conservative value of 100 pc. We obtain that $\tau_{destr,i} \simeq 0.7$ Myr. This timescale is considerably shorter than the time necessary for the formation of a RT instable supershell in our model (See sect. 2.2.1). If the number of SN is smaller, τ_{destr} is larger but it remains

considerably smaller than t_{final}. Given the complexity of the interaction between SN shocks and dust (Draine & Salpeter 1979; Jones et al. 1996) this estimate is necessarily simplified but it leads to the suggestion that only a small amount of dust can survive in the supershell swept up by the OB association, therefore only a small fraction of metals in the clouds driven by the galactic fountains is locked into dust grains. Can this amount significantly increase by dust accretion during the journey of the cloud? To answer this question we have to compare the dynamical timescale of our clouds with the typical dust accretion timescale.

Following again the work of Calura et al. (2008), let X_d be the abundance by mass of the dust and σ the ISM fraction at time t, the quantity $\sigma_{dust} = X_d \cdot \sigma$ represents the normalized mass density of the dust at the time t.

The accretion timescale τ_{accr} is given by:

$$\tau_{accr} = \tau_0/(1 - X_d), \tag{2.50}$$

for τ_0 typical values range between 50 Myr and 200 Myr (see Dwek 1998). The integration of the equation for the temporal evolution of X_d with the initial condition $X_{d,0} \simeq 0$ and $X_d \ll 1$ gives:

$$t \simeq \tau_{0,i} \left[\ln(X_d/X_{d,0}) - \ln(1)\right]. \tag{2.51}$$

Now we can compute the time that it takes to increase the initially small amount of dust up to a non-negligible value. If we calculate for instance the time necessary to accrete 10 times the initial dust fraction (e.g. $X_d/X_{d,0} = 10$), we get:

$$t \simeq 2.3\tau_{0,i}. \tag{2.52}$$

This time is larger than the average time of the cloud orbits (see Table 4.1) , therefore we can conclude that the depletion of metals into dust does not play a important role in the supershell evolution.

2.4 Summary

We have studied the evolution of a supershell powered by the energetic feedback of a typical Galactic OB association at various Galactocentric radii. Based on the Kompaneets (1960) approximation, we have found analytical solutions for the temporal evolution of the supershell and we have established criteria for its fragmentation, which can create clouds that are thrown out of the disk. Given the self-similar behavior of the Kompaneets solutions, the clouds are formed at the same scale height ($\sim$ 450 pc), irrespective of the number of SNe in the OB association or of the Galactocentric radius at which the OB association lies. Assuming that the ejecta of the dying stars of the OB association instantaneously mix with the supershell, we are able to calculate the chemical composition of the clouds and in particular their $[O/Fe]$.

We have considered four different OB associations (containing 10, 50, 100 and 500 SNe, respectively) and three different initial throwing coordinates (4, 8 and 12

Kpc, respectively). Once the clouds are formed and can leave the disk, we follow their orbits either assuming a purely ballistic model, or introducing a viscous force acting between the cloud and the surrounding hot halo gas. Our main conclusions can be summarized as follows:

- If the initial metallicity of the OB association is solar, the pollution from the dying stars has a negligible effect on the chemical composition of the clouds. In particular, the $[O/Fe]$ abundance ratio reaches at most ~ 0.025 in a model in which the throwing coordinate is $R_0 = 12$ kpc. Only starting from very low metallicities (less than 1/100 $Z_\odot$) it is possible to produce a significant enrichment of α-elements relative to Fe.

- Both in the ballistic and in the viscous interaction models the maximum height reached by the clouds is not very large. Only for OB associations composed of 500 SNe is it possible to eject clouds up to heights larger than 2 kpc above the plane of the Galaxy.

- The range of the cloud orbits is also quite small. The clouds are generally directed outwards but the average landing coordinates differ from the throwing coordinates by ~ 1 kpc at most. Only for a throwing coordinate of 12 kpc and an OB association made of 500 SNe does the ballistic model predict a landing coordinate ~ 2 kpc larger than the throwing one.

- Models including a viscous interaction between clouds and the extra-planar gas predict smaller ranges of the cloud orbits. Indeed, the drag experienced by the cloud brakes it and therefore it shortens its journey above the Galactic plane.

- The HVC Complex C has a mass, velocity and inferred height above the plane inconsistent with the results of our models. Its oxygen overabundance ($[O/Fe]$=0.12 dex) can be reproduced only if we assume a large OB association with metallicity 0.1 $Z_\odot$ or smaller, therefore its Galactic origin cannot be completely ruled out on the basis of its chemical composition alone, but the kinematical data suggest a different formation mechanism. The IVC Arch IV instead has velocities and heights above the plane that are easily reproduced by our models, but its $[O/Fe]$ =0.25 dex is much larger than the one of Complex C and it can be explained only by assuming initial metallicities smaller than 1/100 $Z_\odot$, which are unlikely at the present time for the Galactic disk. Therefore, it is unlikely that the two studied clouds originated in a Galactic fountain motion.

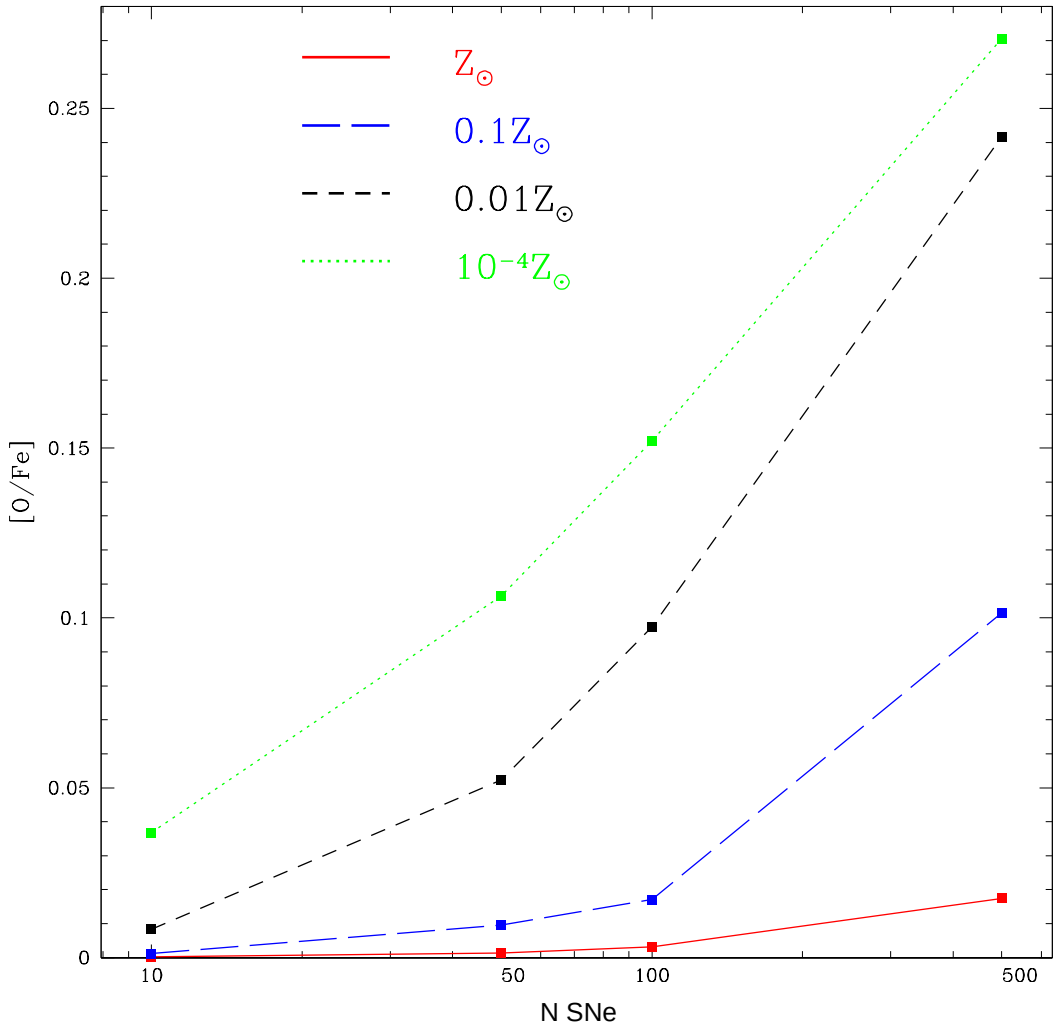

Figure 2.4: [O/Fe] ratios as functions of the number of SNe and of different disk gas metallicities in the case of R_0=8 kpc using stellar yields given by Woosley & Weaver (1995).

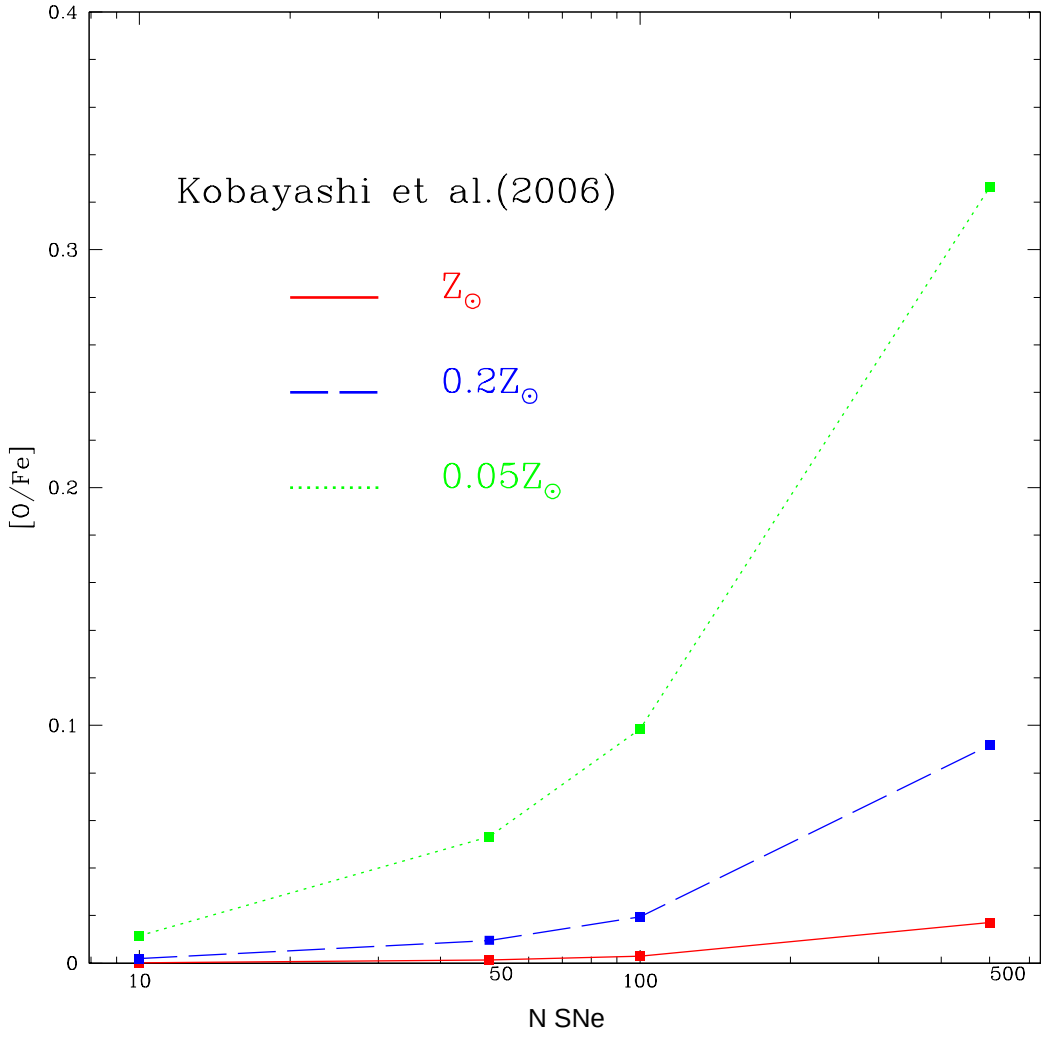

Figure 2.5: As in Fig.2.4 using stellar yields given by Kobayashi et al. (2006).

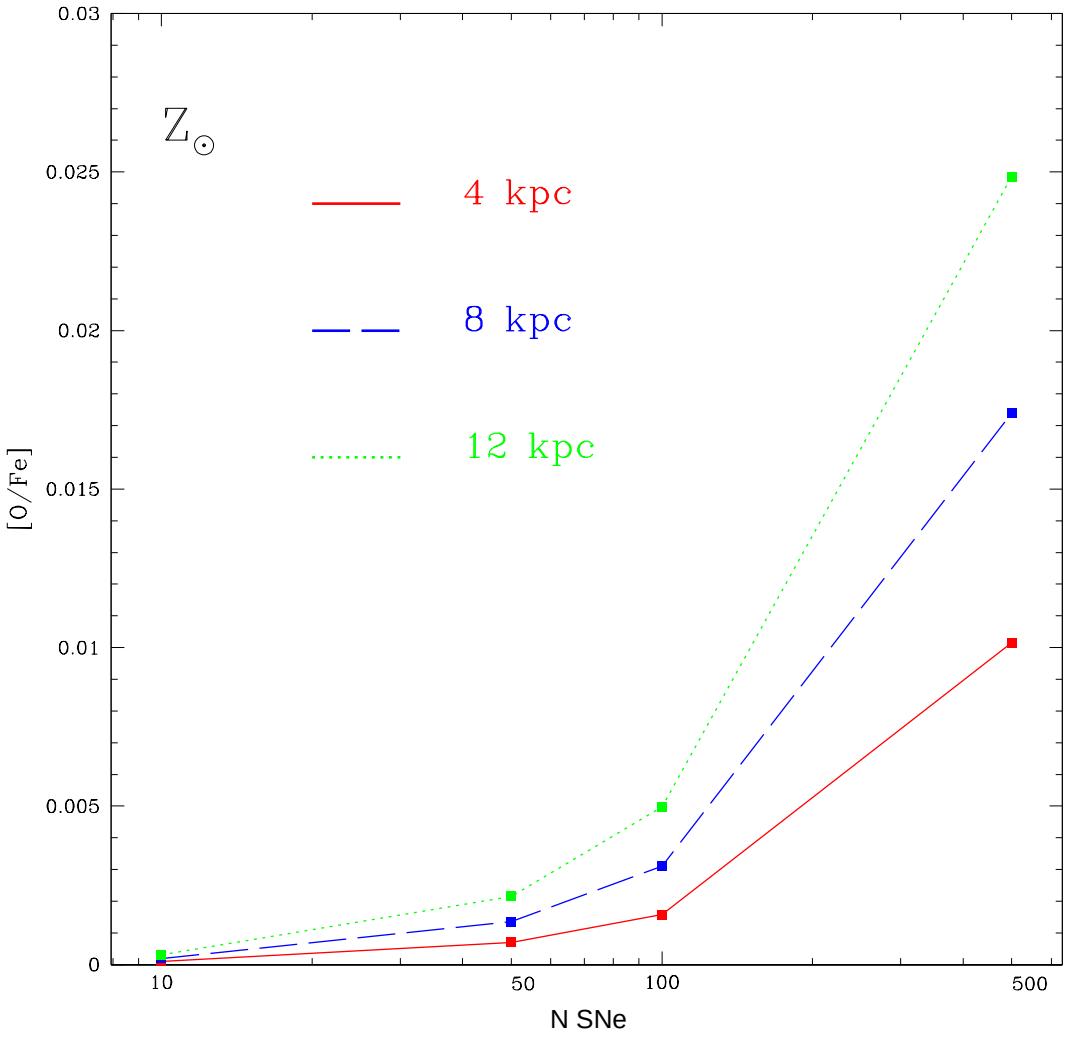

Figure 2.6: [O/Fe] ratios as functions of the number of SNe and the throwing radial coordinate in the case of solar metallicity using stellar yields given by Woosley & Weaver (1995).

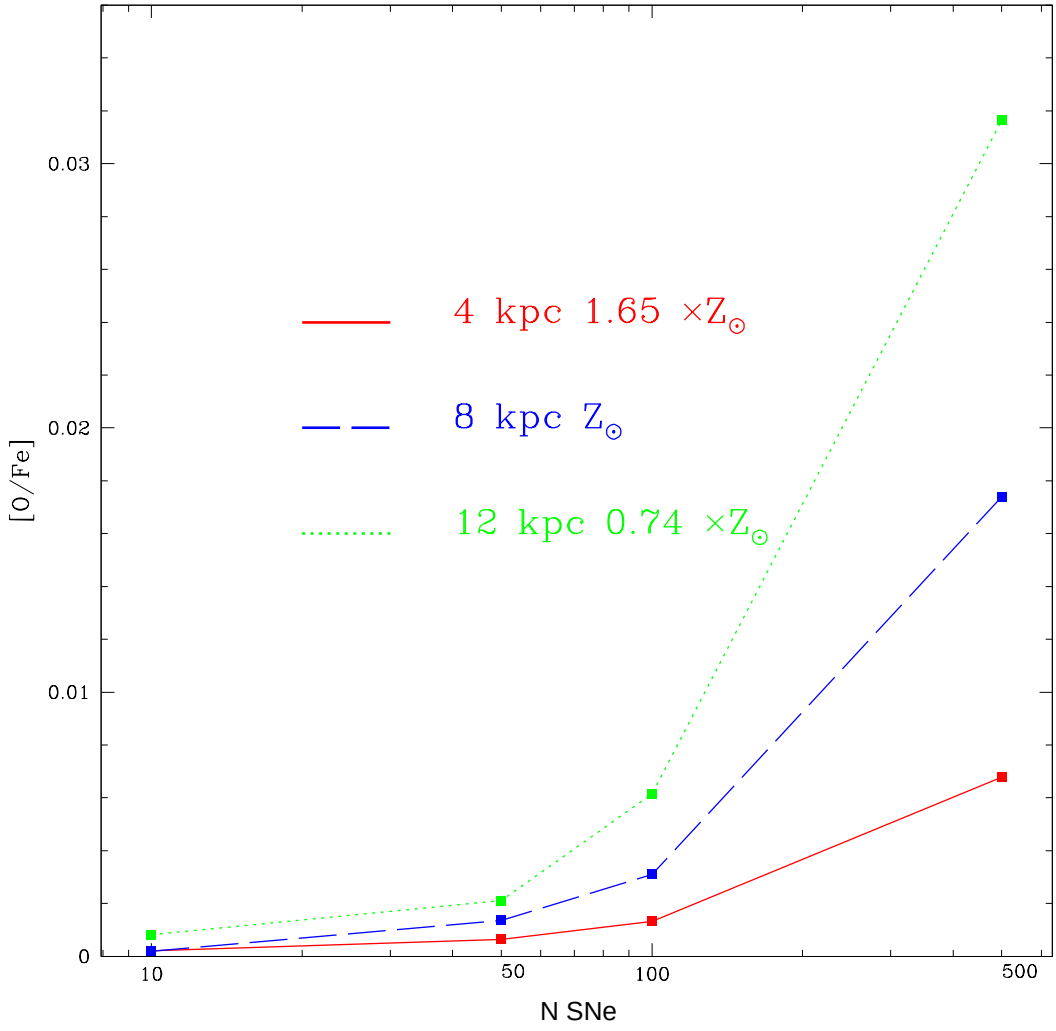

Figure 2.7: [O/Fe] ratios as functions of the number of SNe and the initial throwing radial coordinate, taking for the ISM metallicities the average observed values along the Galactic disk from Cepheids by Andrievsky et al. (2002a-c, 2004) and Luck et al. (2003) (see Cescutti et al. 2006).

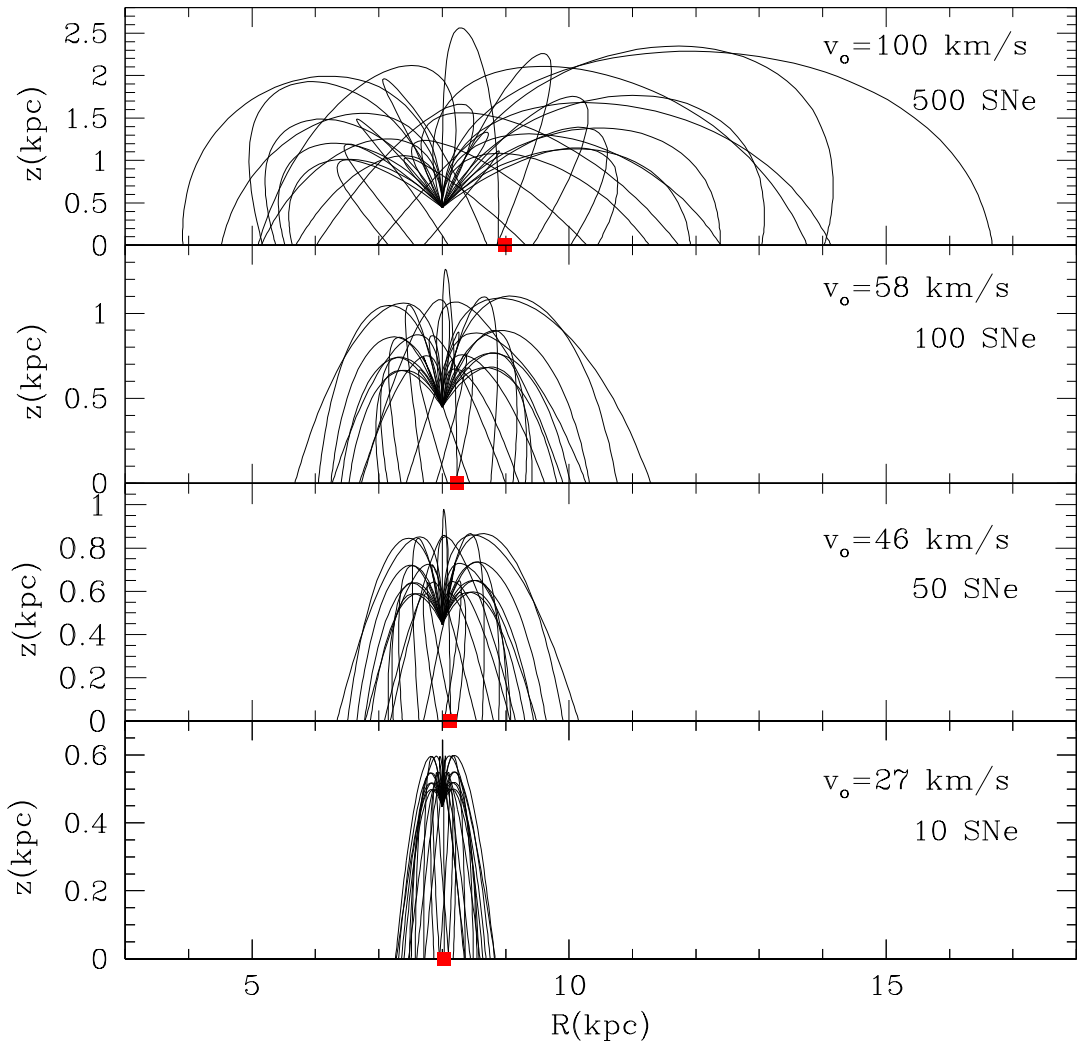

Figure 2.8: Galactic fountains in the meridional plane in the purely ballistic model with the same spatial initial conditions: (R, z)=(8 kpc, 448 pc). Red squares on the R axis are the average falling radial coordinate.

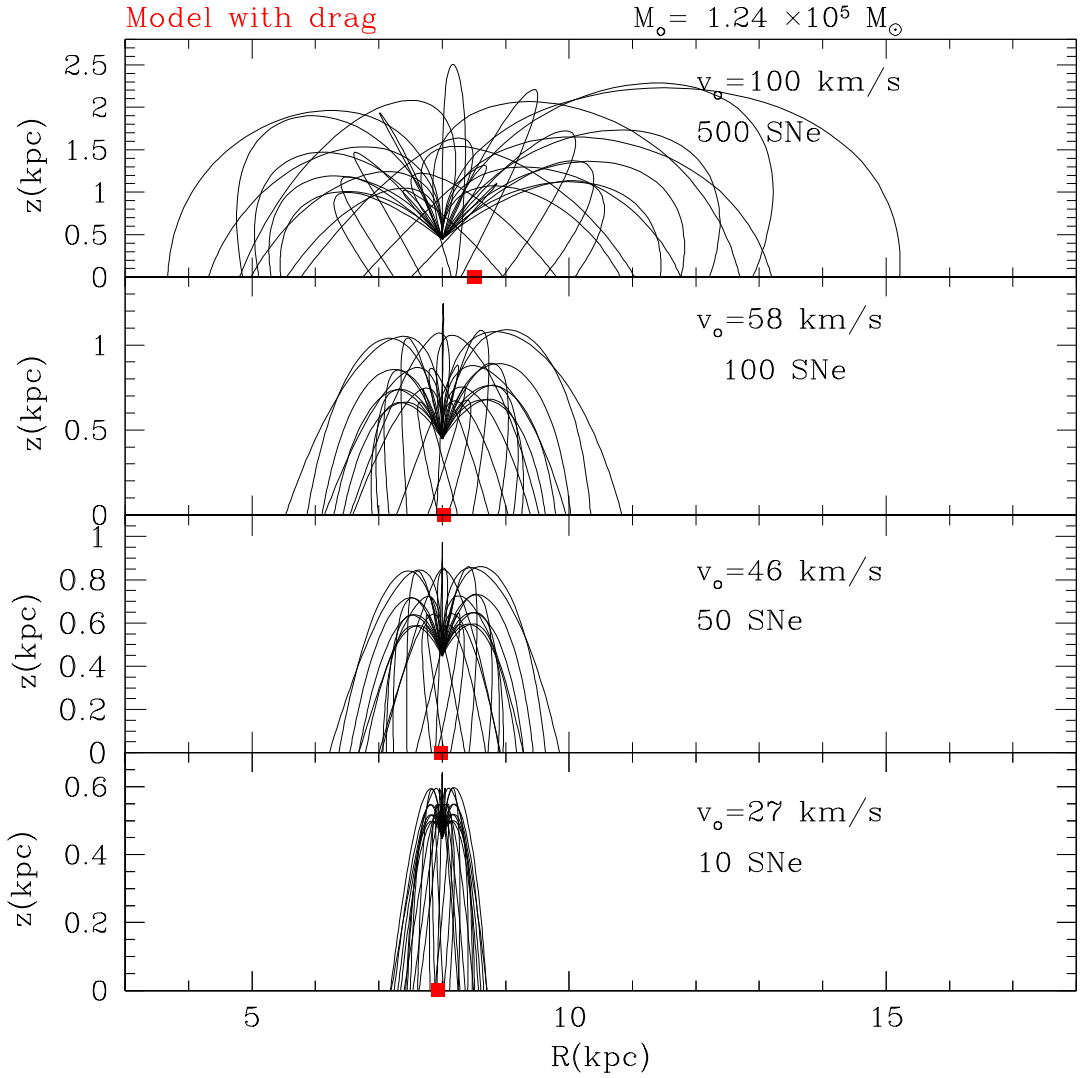

Figure 2.9: Galactic fountains in a model with drag with the initial radial coordinate R_0=8 kpc. In this case the orbits depend on the mass of the cloud ejected (indicated on the top of the panels). The natural effect of the viscous interaction is to decelerate the clouds. Red squares on the R axis are the average falling radial coordinate.

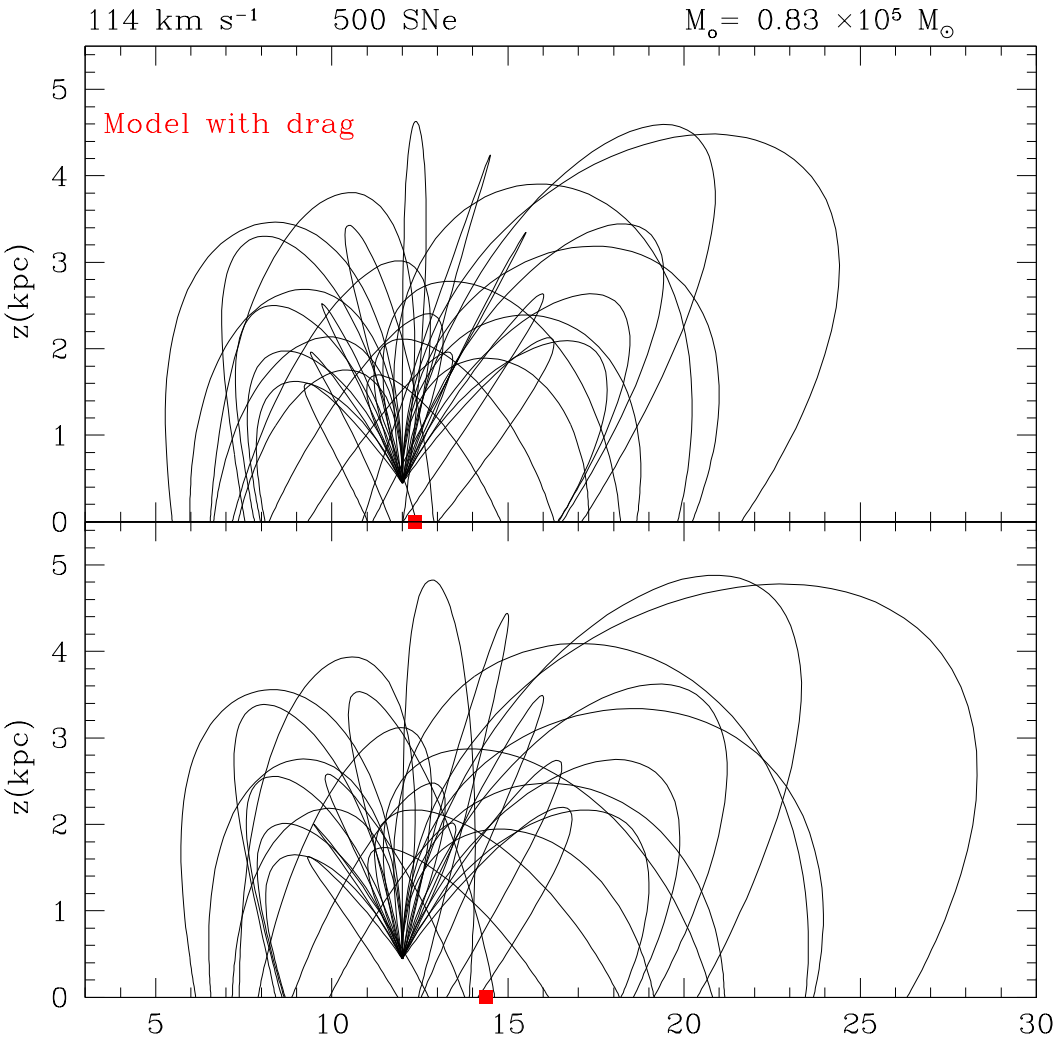

Figure 2.10: Fountains that reach the maximum height in our model.

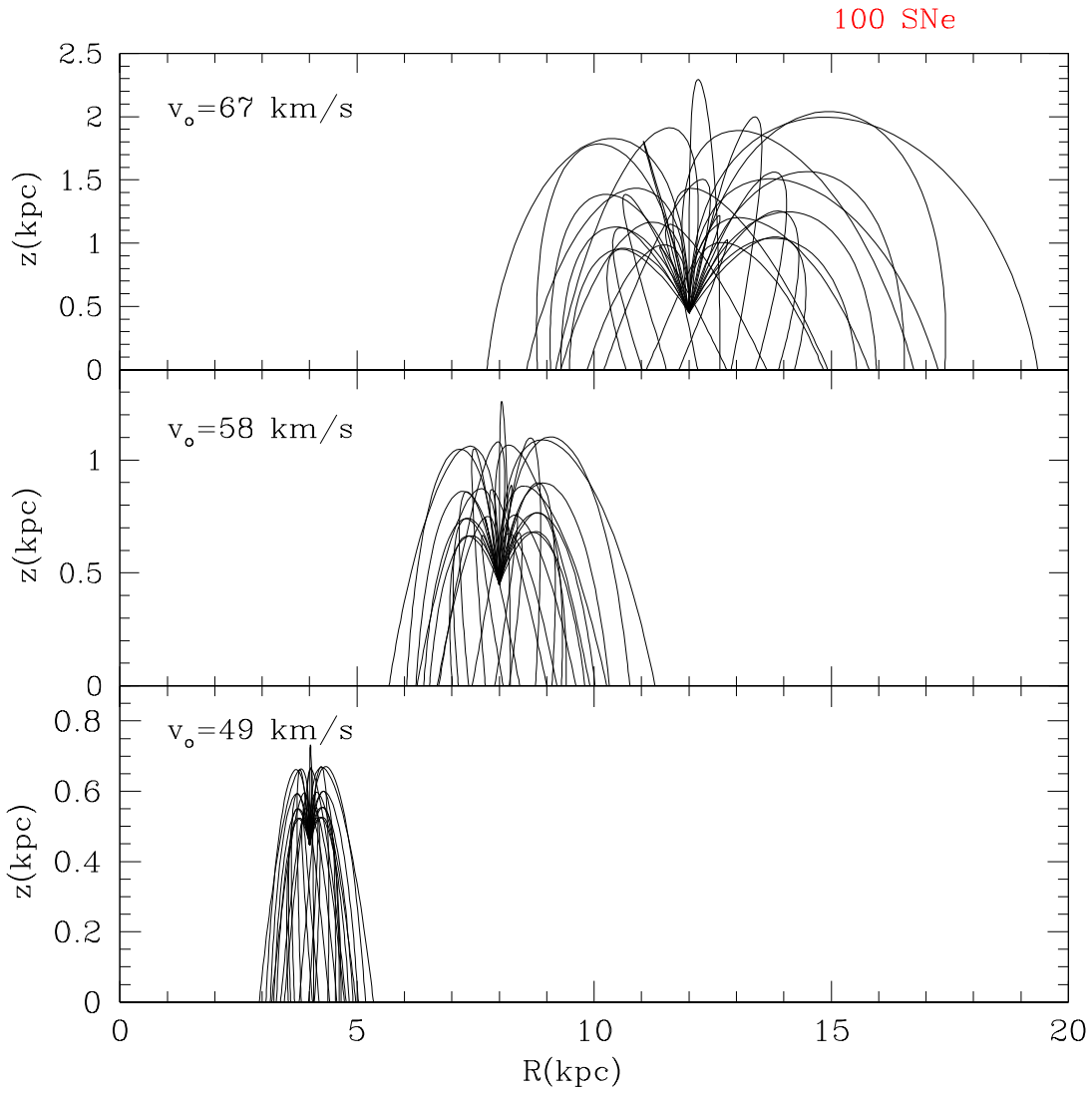

Figure 2.11: Fountains in the purely ballistic model driven by a sequential explosion of 100 SNe .Red squares on the R axis are the average falling radial coordinate.

Chapter 3

Chemical evolution models

Galactic chemical evolution is the study of the evolution in time and in space of the abundances of the chemical elements in the interstellar gas in galaxies. This process is influenced by many parameters such as the initial conditions, the star formation and evolution, the nucleosynthesis and possible gas flows.

3.1 Simple models

Although the simple models of galactic chemical evolution are not able to follow the evolution of single elements especially those produced on long timescales since they assume *instantaneous recycling approximation*, they can be useful to study some galactic properties for elements produced on short time-scales such as oxygen ($\sim$ total metallicity). We are showing here some analytical solution which are often used in the literature. We also present our new analytical solution for the galactic fountain in the simple model framework.

3.1.1 Closed model solutions

As it is well known, the so-called *Simple Model* of chemical evolution is based on the following assumptions:

1. the system is one-zone and closed, namely there are no inflows or outflows.

2. The initial gas is primordial (no metals).

3. The IMF is constant in time.

4. The gas is well mixed at any time (*instantaneous mixing*).

5. Stars more massive than 1 $M_{\odot}$ die instantaneously; stars smaller than 1 $M_{\odot}$ live forever (*instantaneous recycling approximation* or IRA).

These simplifying assumptions allow us to calculate analytically the chemical evolution of the galaxies. We define here the fundamental quantity R, the returned fraction,

$$R = \frac{\int_1^\infty (m - M_R)\phi(m)dm}{\int_0^\infty m\phi(m)dm}, \tag{3.1}$$

namely the total mass fraction of gas restored by a stellar generation; $\phi(m)$ is the IMF and M_R is the mass of the remnant. For the IMF we use the normalization as follow:

$$\int_0^\infty m\phi(m)dm = 1. \tag{3.2}$$

We also introduce the galactic yield y_z defined as:

$$y_Z = \frac{1}{1-R}\int_1^\infty m p_{Z,m}\phi(m)dm, \tag{3.3}$$

namely the ratio between the total mass of newly formed and ejected by all stars larger than 1 $M_\odot$ and the amount of mass locked up in low mass stars and remnants. $p_{Z,m}$ is the stellar yield by a star of mass m. The well known solution of the closed box model (Tinsley 1980) is:

$$Z = y_Z \ln(\mu^{-1}), \tag{3.4}$$

where μ is the gas fraction $M_g(t)/M_{tot}(t)$ and $Z = M_z/M_g$ is the total gas metallicity. This result is obtained by assuming that the galaxy initially contains only gas and has the remarkable property that it does not depend on the particular star formation history of the galaxy. To obtain eq. (3.4) one has to assume that y_Z does not depend on metallicity. Nucleosynthesis can indeed depend on metallicity, especially for secondary elements. In the general case in which $y_Z = f(Z)$ the evolution of the metallicity is governed by the following equation:

$$\int_0^Z \frac{dw}{f(w)} = \ln(\mu^{-1}). \tag{3.5}$$

3.1.2 Leaky box solutions

Relaxing the first of the assumptions of the simple model, we obtain models including gas flows, also known as *leaky box* models. Analytical solutions of simple models of chemical evolution including infall or outflow are known since at least 30 years (Pagel & Patchett 1975; Hartwick 1976; Twarog 1980; Edmunds 1990). Here, we follow the approach and the terminology of Tinsley (1980) and Matteucci (2001), namely we assume for simplicity *linear* flows (we assume gas flows proportional to the star formation rate (SFR)). Therefore, the outflow or wind rate $W(t)$ is given by:

$$W(t) = \lambda(1 - R)\psi(t), \tag{3.6}$$

where $\psi(t)$ is the SFR, and the infall rate $A(t)$ is given by:

$$A(t) = \Lambda(1 - R)\psi(t). \tag{3.7}$$

Here λ and Λ are two proportionality constants larger than zero. The first assumption is justified by the fact that, the larger the SFR is, the more intense are the energetic events associated with it (in particular SN explosions and stellar winds), therefore the larger is the chance of having a large-scale outflow (see e.g. Silk 2003). A proportionality between $A(t)$ and $\psi(t)$ instead does not have a clear physical justification. .

The system of equations we need to solve is therefore:

$$\begin{cases} \dfrac{dM_{tot}}{dt} = (\Lambda - \lambda)(1 - R)\psi(t), \\ \dfrac{dM_g}{dt} = (\Lambda - \lambda - 1)(1 - R)\psi(t), \\ \dfrac{dM_Z}{dt} = (1 - R)\psi(t)[\Lambda Z_A + y_Z - (\lambda + 1)Z]. \end{cases} \tag{3.8}$$

where M_Z is the mass of metals ($M_Z = Z \cdot M_g$) and Z_A is the metallicity of the infalling gas.

The general solution of this system in the presence of infall of gas with a general metallicity Z_A and outflow is:

$$Z = \frac{\Lambda Z_A + y_Z}{\Lambda}\left\{1 - \left[(\Lambda - \lambda) - (\Lambda - \lambda - 1)\mu^{-1}\right]^{\frac{\Lambda}{\Lambda - \lambda - 1}}\right\}. \tag{3.9}$$

To find this solution we have made use of the initial conditions $Z(0) = 0$, $M_g(0) = M_{tot}(0) = M_{g,0}$. It is worth pointing out that the explicit dependence of Z on time is hidden in the time dependence of μ.

We show in Fig. 3.1 the evolution of Z/y_Z versus μ in the case $Z_A = 0$ for different values of λ and Λ. It is worth reminding that $\mu = 1$ at the beginning of the evolution of the galaxy and its value decreases with time. Therefore, the time axis is inverted compared to the μ-axis in this figure and in similar ones. We can see that all the models with gas flows produce metallicities smaller than the ones predicted by the closed box model (solid line). This is in agreement with the first and the third of Edmund's theorems (Edmunds 1990), since we have assumed that the infalling gas is pristine ($Z_A = 0$). Fig. 3.2 shows the effective yields $y_{eff} = Z/\ln(\mu^{-1})$ (normalized to y_Z) of the same models presented in Fig 3.1. y_{eff} is often used in literature to interpret data and to analyze to what extent the chemical evolution of a galaxy deviates from the behavior predicted by the closed box model (Garnett 2002; Tremonti et al. 2004). We can notice from eq. (3.9) that the solution diverges for models in which $\lambda > \Lambda$ when μ approaches 0, therefore, we show Z/y_Z and y_{eff}/y_Z versus μ only until $\mu \sim 0.1$. Indeed, Prantzos & Aubert (1995) pointed out that IRA cannot be applied in situations in which low μ values are obtained, because

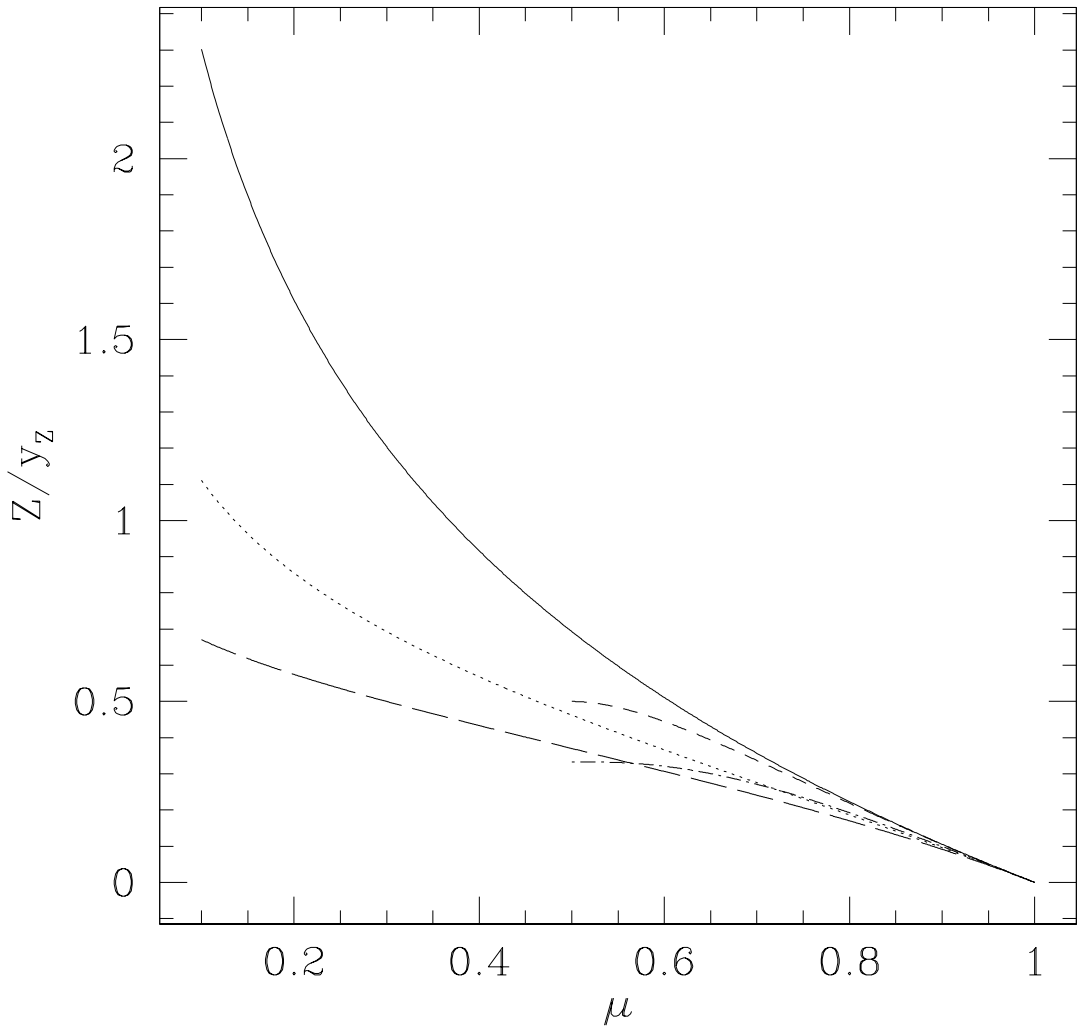

Figure 3.1: Evolution of the metallicity as a function of μ for the closed box model (solid line) and models with gas flows: $\lambda = 2$ and $\Lambda = 0$ (dotted line); $\lambda = 0$ and $\Lambda = 2$ (short-dashed line); $\lambda = 3$ and $\Lambda = 1$ (long-dashed line); $\lambda = 1$ and $\Lambda = 3$ (dot-dashed line). The metallicity of the infalling gas Z_A is assumed to be 0.

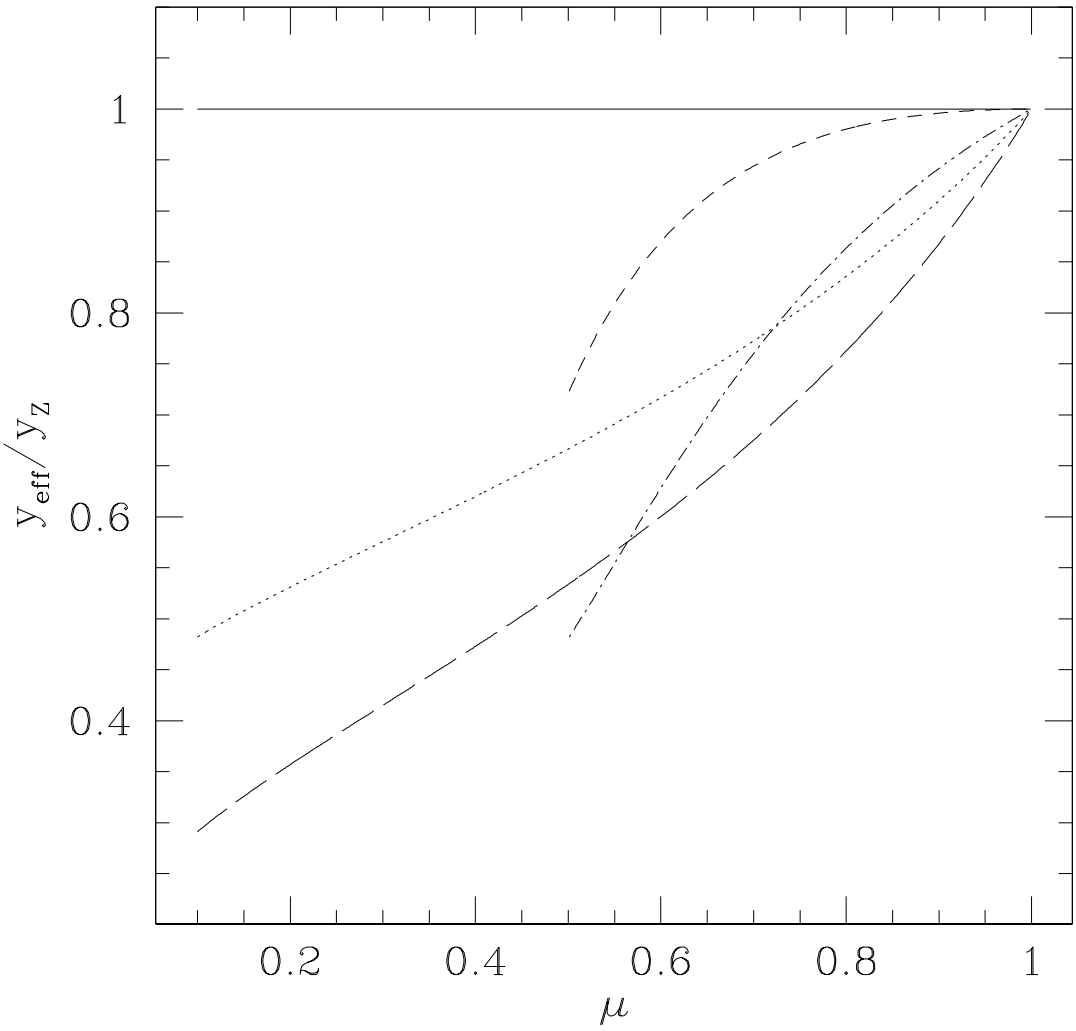

Figure 3.2: Normalized effective yield as a function of μ. Notation as in Fig. 3.1

the amount of gas ejected by low mass stars at late times can substantially modify the final abundances, also for elements produced on short timescales by massive stars. We notice here also that, in models in which the infall rate is larger than the outflow rate, not all the values of μ are possible. Solving the first two equations of the system (3.8), we get:

$$\mu = \frac{\Lambda - \lambda - 1}{\Lambda - \lambda} + \frac{1}{\Lambda - \lambda}\frac{M_{g,0}}{M_g}. \tag{3.10}$$

In the models in which $\Lambda > \lambda + 1$, M_g is always increasing (eq. 3.8), therefore μ ranges between 1 and a minimum value:

$$\mu_{\rm min} = \frac{\Lambda - \lambda - 1}{\Lambda - \lambda}. \tag{3.11}$$

For models in which $\lambda + 1 > \Lambda > \lambda$ there is no $\mu_{\rm min}$ but there is a upper limit reachable by the gas mass which is given by $M_{g,lim} = M_{g,0}/(\lambda + 1 - \Lambda)$. For this reason, we plotted in Figs. 3.1 and 3.2 the model with $\lambda = 0$ and $\Lambda = 2$ (short-dashed line) and the model with $\lambda = 1$ and $\Lambda = 3$ (dot-dashed line) only for $\mu \geq \mu_{\rm min} = 0.5$.

3.2 The galactic fountain in Simple models

3.2.1 The framework of the differential winds

We present in this section the chemical evolution of galaxies in which a differential wind is assumed, namely in which the metals are more easily channelled out of the parent galaxy than the pristine gas. The easiest way to consider a differential wind in the framework of simple models of chemical evolution is to assume that the metallicity of the gas carried out in the galactic wind is proportional to the metallicity of the ISM with a proportionality constant larger than one. If we define Z^o as the metallicity of the outflowing gas, this condition implies that $Z^o = \alpha Z$ with the ejection efficiency $\alpha > 1$. In the metallicity budget (third equation in (3.8)) we assume that the negative term due to the galactic wind is given by $W(t)Z^o = \alpha Z \lambda (1 - R)\psi(t)$. With our simple approach we are able to determine analytical expressions for the evolution of Z, which allow us to understand more clearly the effect of galactic winds on the chemical evolution of galaxies.

The set of the equations we have to solve in this case is very similar to (3.8), with the only difference given by the metallicity budget equation, which we modify as follows:

$$\frac{dM_Z}{dt} = (1 - R)\psi(t)[\Lambda Z_A + y_Z - (\lambda\alpha + 1)Z]. \tag{3.12}$$

The solution of this new set of equations is given by:

$$Z = \frac{\Lambda Z_A + y_Z}{\Lambda + (\alpha - 1)\lambda}\left\{1 - \left[(\Lambda - \lambda) - (\Lambda - \lambda - 1)\mu^{-1}\right]^{\frac{\Lambda + (\alpha-1)\lambda}{\Lambda - \lambda - 1}}\right\}. \tag{3.13}$$

It is straightforward to see that we can obtain eq. (3.9) in the case $\alpha = 1$ (i.e. in the case in which the galactic wind is not differential). We remind here that this solution is valid only for primary elements. The evolution of secondary elements (namely elements synthesized from the metals present in the stars at birth) in the framework of simple models with gas flows has been extensively studied by Köppen & Edmunds (1999) and we refer the reader to this paper to find out more about it.

Assuming again for simplicity an infall of pristine gas (i.e. $Z_A = 0$) we can see how the chemical evolution of the galaxy varies with the ejection efficiency α. In Figs. 3.3 and 3.4 we show Z/y_Z vs. μ for different values of α and gas flow parameters (λ, Λ) taken as (3, 1) and (1, 3), respectively. The first couple of values can be attributed to objects in which galactic winds have a prominent role. This is usually the case in dwarf galaxies, since the potential well of these objects is very shallow and large-scale outflows must be common (Dekel & Silk 1986). The second set of parameters ($\lambda = 1$, $\Lambda = 3$) can more properly refer to spiral galaxies, although large outflow episodes in massive spirals are not very likely. In general, the effect of differential winds can be more clearly distinguished in models in which the outflow is prominent compared to the infall.

As expected, the differential wind determines a significant reduction of the metallicity of the galaxy. It can be shown analytically that, for each value of $\alpha > 1$, eq. (3.13) produces metallicities systematically smaller that the ones obtained from eq. (3.9). Moreover, it is evident from these plots that the asymptotic trend of Z/y_Z as μ approaches 0 or μ_{min}. From eq. (3.13) it is easy to see that, in both cases, Z/y_Z asymptotically tends to the value $[(\alpha - 1)\lambda + \Lambda]^{-1}$ provided that $Z_A = 0$, therefore Z/y_Z decreases almost linearly with α when μ is small and $\alpha \gg 1$.

3.2.2 The analytical solution in the presence of galactic fountains

A special case of variable infall metallicity is represented by the situation in which $Z_A = Z^o = \alpha Z$, namely the metallicity of the infalling gas is set to be always proportional to the one of the ISM of the galaxy as for the wind. This condition implies therefore that the very same gas that has been driven out of the galaxy by energetic events can subsequently rain back to the galaxy, due to the pull of its gravitational potential. In order to solve the chemical evolution in this special case, we have necessarily to assume that $\lambda \geq \Lambda$ since the reservoir for the infall gas is given by the gas expelled out of the galaxy through galactic winds. The solution of the chemical evolution in the presence of galactic fountains is given by:

$$Z = \frac{y_Z}{(\lambda - \Lambda)(\alpha - 1)} \left\{ 1 - \left[(\Lambda - \lambda) - (\Lambda - \lambda - 1)\mu^{-1} \right]^{\frac{(\lambda-\Lambda)(\alpha-1)}{\Lambda-\lambda-1}} \right\}. \tag{3.14}$$

A comparison of this solution with the solution of eq. (3.13) with infall of pristine gas ($Z_A = 0$) is shown in Fig. 3.5. For both models plotted in this figure we have assumed $\lambda = 3$, $\Lambda = 1$ and $\alpha = 5$. As expected, the galactic fountain model predicts larger values for Z.

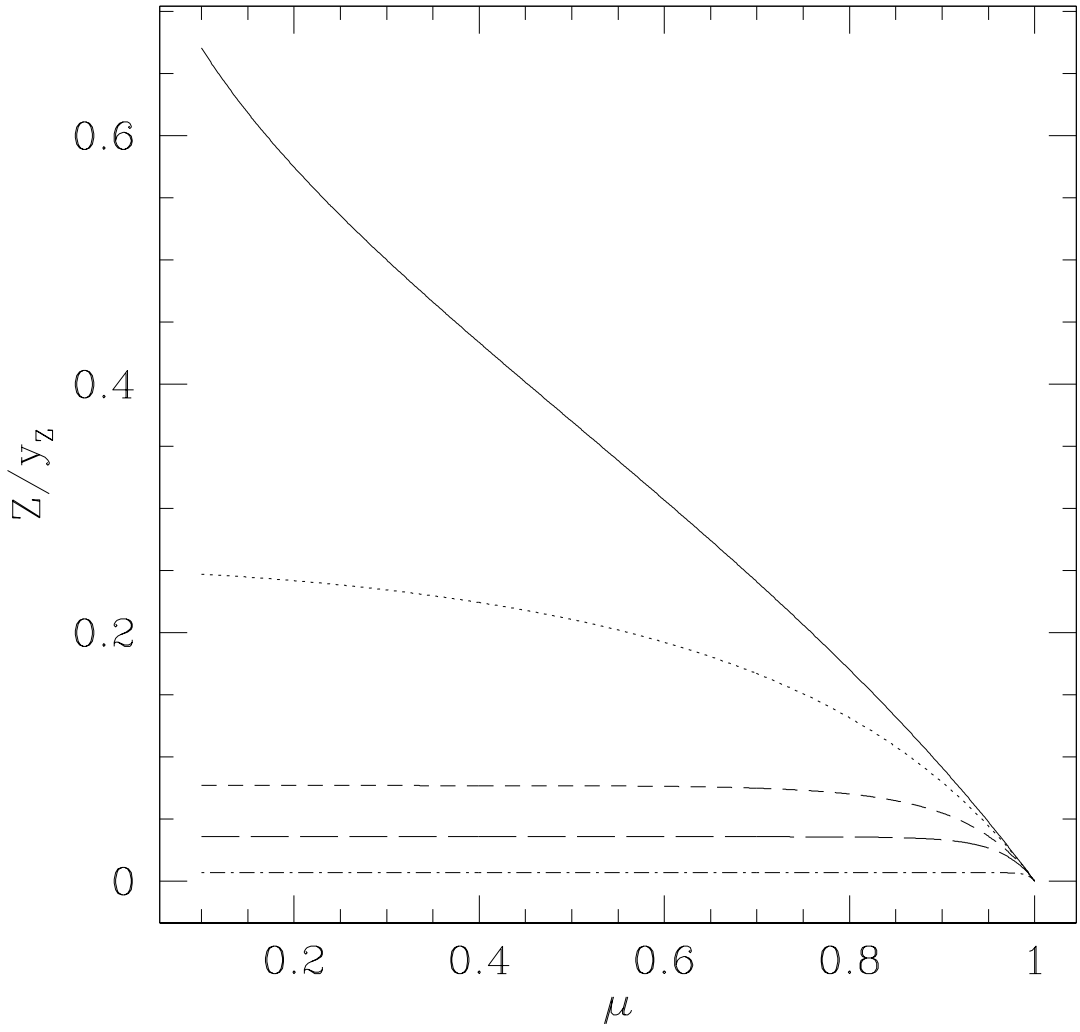

Figure 3.3: Evolution of the metallicity as a function of μ for simple models with differential winds, $\lambda = 3$, $\Lambda = 1$ and $Z_A = 0$. Plotted are models with the differential wind parameter $\alpha = 2$ (dotted line), 5 (short-dashed line), 10 (long-dashed line) and 50 (dot-dashed line). For reference, also the model with $\alpha = 1$ (normal wind) is plotted (solid line).

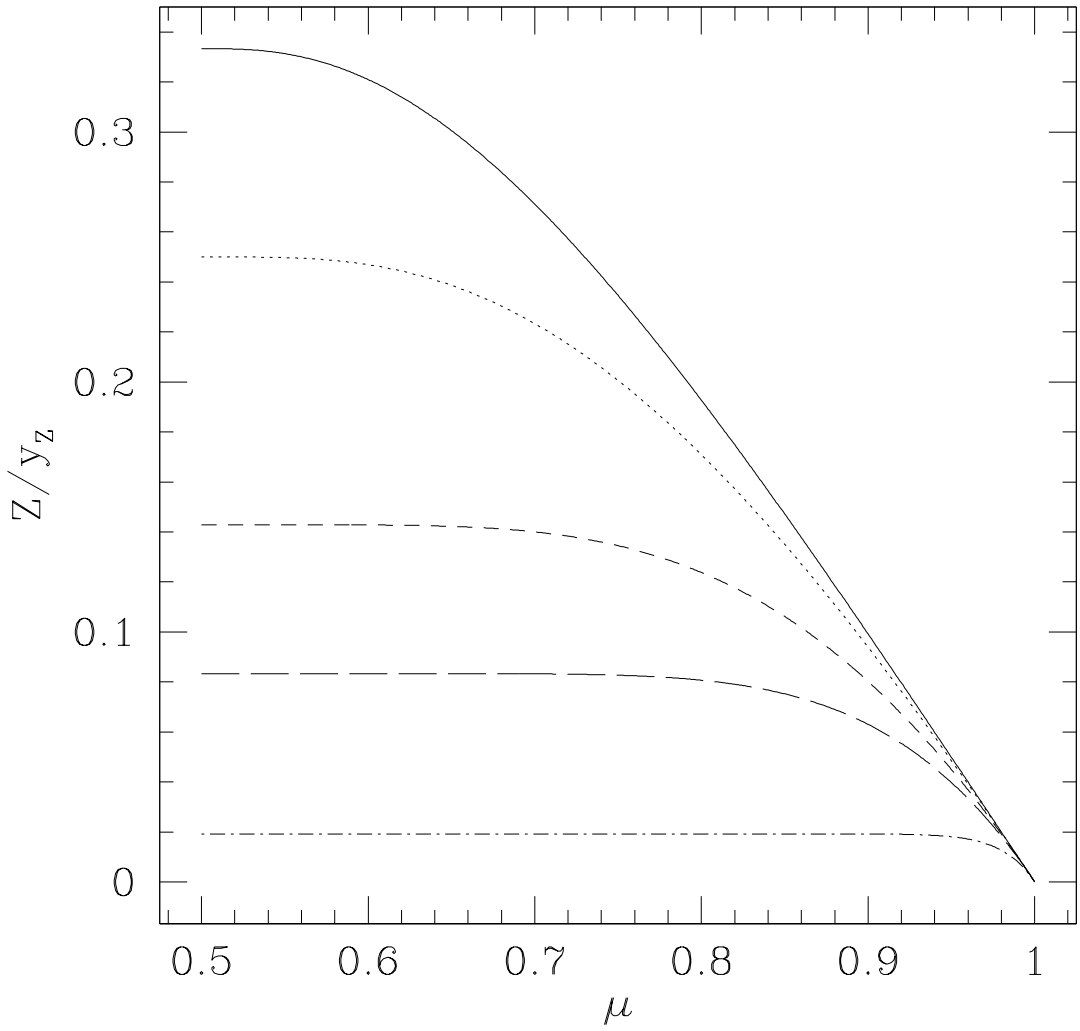

Figure 3.4: As in Fig. 3.3 but for $\lambda = 1$ and $\Lambda = 3$

.

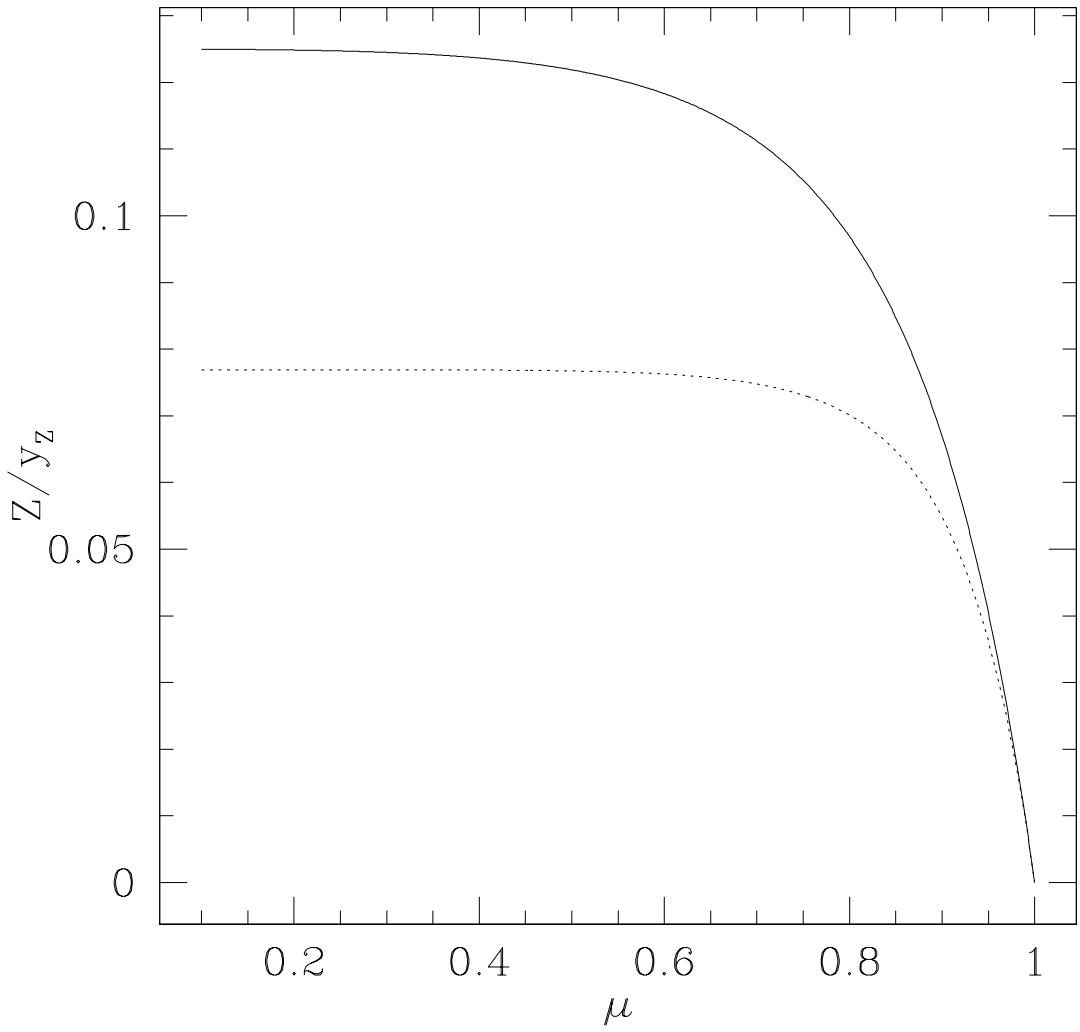

Figure 3.5: Comparison of the chemical evolution of a galactic fountain model (solid line) with a model with infall of pristine gas ($Z_A = 0$, dotted line). For both models, $\lambda = 3$, $\Lambda = 1$ and $\alpha = 5$.

From eqs. (3.13) and (3.14) we can also notice that the metallicity ratio tends asymptotically to the value $[(\alpha-1)\lambda+\Lambda]/[(\lambda-\Lambda)(\alpha-1)]$ which is always larger than one (for the special choice of parameters it is equal to 13/8) but it tends to 1 for $\alpha \gg 1$. In our example, only an infall of pre-enriched gas, whose metallicity is larger than 5/8 y_Z can therefore produce a metallicity in the galaxy larger than the one attained by the galactic fountain model. From eq. (3.14) we can also see that, in the special case in which $\lambda = \Lambda$, Z/y_Z tends to the solution of the closed box model (eq. 3.4). This is due to the fact that, in the framework of the simple models of chemical evolution, having outflow and infall with the same rate and metallicity or not having gas flows at all is formally the same. Indeed, as we have shown in Chapter 2 the fountains take a finite and non-negligible time to orbit around and fall back to the galaxy. This implies a delay in the mixing of metals in the ISM, which conflicts with the fourth assumption of the simple models of chemical evolution (Sect. 3.1.1), therefore only detailed numerical models can ascertain the effect of this delay on the chemical evolution of galaxies.

3.3 Numerical models of chemical evolution

In order to build a detailed chemical evolution model one needs to specify the initial conditions, namely whether the system is closed or open and whether the gas is primordial (no metals) or already chemically enriched. Then, it is necessary to define the stellar birthrate function, which is generally expressed as the product of two independent functions, the SFR and the IMF, namely:

$$B(m,t) = \psi(t)\varphi(m)\ dt\ dm \tag{3.15}$$

where $\varphi(t)$ is the SFR and $\psi(m)$ is the IMF. The SFR is assumed to be only a function of the time and the IMF only a function of the mass. This oversimplification is due to the absence of a clear knowledge of the star formation process.

Moreover, it is necessary to know the stellar lifetime and the nuclear burnings which take place in the stellar interiors during the stellar lifetime and produce new chemical elements, in particular metals. These metals, together with the pristine stellar material are restored into the ISM at the star death. This process clearly affects crucially the chemical evolution of the ISM. Finally, supplementary parameters as the infall of extragalactic gas, radial flows and galactic winds, are important ingredients in building galactic chemical evolution models.

The SFR is one of the most important drivers of galactic chemical evolution: it describes the rate at which the gas is turned into stars in galaxies. Since the physics of the star formation process is still not well known, several parameterizations are used to describe the SFR. A common aspect to the different formulations of the SFR is that they include a dependence upon the gas density. Here we recall the most commonly used parameterizations for the SFR adopted so far in the literature. An exponentially decreasing SFR provides an easy to handle formula:

$$\psi(t) = \nu e^{-t/\tau_\star} \tag{3.16}$$

with $\tau_\star$ = 5-15 Gyr in order to obtain a good fit to the properties of the solar neighborhood (Tosi, 1988) and ν= 1 - 2 Gyr^{-1}, being ν the efficiency of star formation which is expressed as the inverse of the timescale of star formation. However, the most famous formulation and most widely adopted for the SFR is the Schmidt (1959) law:

$$\psi(t) = \nu\sigma_{gas}^{k} \tag{3.17}$$

which assumes that the SFR is proportional to some power of the volume or surface gas density (σ_{gas}). The exponent suggested by Schmidt was k = 2 but Kennicutt (1998) suggested that the best fit to the observational data on spiral disks and starburst galaxies is obtained with an exponent k = 1.4± 0.15. A more complex formulation, including a dependence also on the total surface mass density (σ_{tot}), which is induced by the SN feedback, was suggested by the observations of Dopita & Ryder (1994) who proposed the following formulation:

$$\psi(t) = \nu\sigma_{tot}^{k1}\sigma_{gas}^{k2} \tag{3.18}$$

Kennicutt suggested also an alternative law to the Schmidt-like one discussed above:

$$\psi(t) = 0.017\Omega_{gas}\sigma_{gas} \tag{3.19}$$

being Ω_{gas} the angular rotation speed of the gas.

The most common parameterization for the IMF is that proposed by Salpeter (1955), which assumes a one-slope power law with x = 1.35, in particular:

$$\varphi(m) = Am^{-(1+x)} \tag{3.20}$$

$\varphi(m)$ is the number of stars with masses in the interval M, M+dM, and A is a normalization constant. More recently, multi-slope expressions of the IMF have been adopted since they better describe the luminosity function of the main sequence stars in the solar vicinity (Scalo 1986, 1998; Kroupa et al. 1993). Generally, the IMF is assumed to be constant in space and time, with some exceptions such as the one suggested by Larson (1998), which adopts a variable slope:

$$x = 1.35(1 + m/m_1)^{-1} \tag{3.21}$$

where m_1 is variable with time and associated to the Jeans mass, (the typical mass at which the internal pressure is no longer strong enough to prevent gravitational collapse). The effects of a variable IMF on the galactic disk properties have been studied by Chiappini et al. (2000), who concluded that only a very "ad hoc" variation of the IMF can reproduce the majority of observational constraints, thus favoring chemical evolution models with IMF constant in space and time.

The stellar yields are fundamental ingredients in galactic chemical evolution. In the past ten years a large number of calculations has become available for stars of all masses and metallicities. However, uncertainties in stellar yields are still present. This is due to uncertainties in the nuclear reaction rates, treatment of convection, mass cut, explosion energies, neutron fluxes and possible fall-back of matter onto

the proto-neutron star. Moreover, the ^{14}N nucleosynthesis and its primary and/or secondary nature are still under debate. Depending on the galactic system, the infall rate (IR) can be assumed to be constant in space and time, or more realistically the infall rate can be variable in space and time:

$$IR(r,t) = A(r)e^{-t/\tau(r)} \tag{3.22}$$

with $\tau(r)$ constant or varying along the disk. The parameter A(r) is derived by fitting the present time total surface mass density in the disk of the Galaxy, $\sigma_{tot}(t_{now})$. Otherwise, for the formation of the Galaxy one can assume two independent episodes of infall during which the halo and perhaps part of the thick-disk formed first and then the thin-disk, as in the two-infall model of Chiappini et al. (1997).

For the rate of gas outflow or galactic wind there are no specific prescriptions but generally one simply assumes that the wind rate (W) is proportional to the SFR (Hartwick 1976, Matteucci & Chiosi 1983):

$$W(t) \propto \lambda\psi(t) \tag{3.23}$$

with λ being a free parameter.

A good model of chemical evolution should be able to reproduce a minimum number of observational constraints and the number of independent observational constraints should be larger than the number of free parameters which are: τ, k_1, k_2, the $\varphi(m)$ slope(s) and the parameter describing the wind, λ if adopted.

The main observational constraints in the MW, in particular in the solar vicinity, that a good model should reproduce (see Chiappini et al. 2001) are:

- The present time surface gas density: Σ_{gas} = 13±3 $M_\odot pc^{-2}$
- The present time surface star density $\Sigma_\star$= 35±5 $M_\odot pc^{-2}$
- The present time total surface mass density: Σ_{tot} = 48±9 $M_\odot pc^{-2}$
- The present time SFR: ψ_0 = 2 - 5$M_\odot$ $pc^{-2}Gyr^{-1}$
- The present time infall rate: 0.3 - 1.5$M_\odot$ pc^{-2} Gyr^{-1}
- The present day mass function (PDMF).
- The solar abundances, namely the chemical abundances of the ISM at the time of birth of the solar system 4.5 Gyr ago.
- The age-metallicity relation, namely the relation between the ages of the stars and the metal abundances of their photospheres, assumed to be equivalent to the stellar [Fe/H][1].

[1]We adopt the usual spectroscopic notations that [A/B]= $log_{10}(N_A/N_B)_\star - log_{10}(N_A/N_B)_\odot$ and that $log\epsilon(A) = log_{10}(N_A/N_H) + 12.0$, for elements A and B

- The G-dwarf metallicity distribution, namely the number of stars with a lifetime equal or larger than the age of the Galaxy as a function of their metallicities.
- The distributions of gas and stars formation rate along the disk.
- The average SNII and Ia rates along the disk (SNII=1.2±0.8 cen^{-1} and SNIa=0.3±0.2 cen^{-1}).
- The observed abundances in the stars and the [A/Fe] vs. [Fe/H] relations.

The chemical compositions of stars of all Galactic generations contains very important information about the cumulative nucleosynthesis history of our Galaxy. The difference in the timescales for the occurrence of SNII and Ia produces a timedelay in the Fe production relative to the α-elements (Tinsley 1979; Greggio & Renzini 1983b; Matteucci 1986). In fact, in the single degenerate scenario for a SNIa, originally proposed by Whelan and Iben (1973), the SNIa explodes due to a C-deflagration in a C-O white dwarf (WD) reaching the Chandrasekhar mass limit, M_{Ch}= 1.44$M_{\odot}$, after accreting material from a red giant companion. The progenitors of C-O WDs lie in the range 0.8 - 8.0$M_{\odot}$, therefore, the most massive binary system of two C-O WDs is the 8$M_{\odot}$ + 8$M_{\odot}$ one. The clock of the system in this scenario is provided by the lifetime of the secondary star (i.e. the less massive one in the binary system). This implies that the minimum timescale for the appearence of the first type Ia SNe is the lifetime of the most massive secondary star. In this case the time is $t_{SNIamin}$=0.03 Gyr (Greggio & Renzini 1983a; Matteucci & Greggio, 1986; Matteucci & Recchi, 2001). On this basis we can interpret all the observed abundance ratios plotted as functions of metallicity. In particular, this interpretation is known as time-delay model and only a model including both contributions in the percentages of 30% (SNII) and 70% (SNIa) can reproduce the data.

3.4 The detailed chemical evolution model for the Milky Way of François et al. (2004).

We started from the model of François et al. (2004) (hereafter F04) which is an upgrade of the original model of Chiappini et al. (1997), where the Galaxy is assumed to have formed by means of two main infall episodes. The first formed the halo and the thick disk, the second the thin disk. The time-scale for the formation of the halo-thick disk is 0.8 Gyr and the entire formation period does not last more than 2 Gyr. The time-scale for the thin disk is much longer, 7 Gyr in the solar vicinity, implying that the infalling gas forming the thin disk comes mainly from the intergalactic medium and not only from the halo. Moreover, the formation timescale of the thin disk is assumed to be a function of the galactocentric distance, leading to an inside out scenario for the Galaxy disk build-up (Matteucci & François 1989). The galactic thin disk is approximated by several independent rings, 2 kpc wide, without exchange of matter between them.

The main characteristic of the two-infall model is an almost independent evolution between the halo and the thin disk (see also Pagel & Tautvaisienne 1995). A threshold gas density of $7 M_{\odot} pc^{-2}$ in the star formation process (Kennicutt 1989, 1998, Martin & Kennicutt 2001) is also adopted for the disk.

This model already reproduces an extended set of observational constraints. Some of the most important observational constraints are represented by the various relations between the abundances of metals (C,N,O,α-elements, iron peak elements) as functions of the [Fe/H] abundance (see Chiappini et al. 2003a, b and F04) and by the G-dwarf metallicity distribution. Although this model is probably not unique, in this respect it reproduces the majority of the observed features of the MW. Many of the assumptions of the model have been shared by other authors (e.g. Prantzos & Boissier 2000, Alibés et al. 2001, Chang et al. 1999).

The equation below describes the time evolution of G_i, namely the mass fraction of the element i in the gas:

$$\dot{G}_i(r,t) = -\psi(r,t) X_i(r,t)$$

$$+ \int_{M_L}^{M_{Bm}} \psi(r, t-\tau_m) Q_{mi}(t-\tau_m) \phi(m) dm$$

$$+A_{Ia} \int_{M_{Bm}}^{M_{BM}} \phi(M_B) \cdot \left[\int_{\mu_m}^{0.5} f(\mu) \psi(r, t-\tau_{m2}) Q_{mi}^{SNIa}(t-\tau_{m2}) d\mu \right] dM_B$$

$$+(1-A_{Ia}) \int_{M_{Bm}}^{M_{BM}} \psi(r, t-\tau_m) Q_{mi}(t-\tau_m) \phi(m) dm$$

$$+ \int_{M_{BM}}^{M_U} \psi(r, t-\tau_m) Q_{mi}(t-\tau_m) \phi(m) dm$$

$$+X_{A_i} A(r,t) \tag{3.24}$$

where $X_i(r,t)$ is the abundance by mass of the element i and Q_{mi} indicates the fraction of mass restored by a star of mass m in form of the element i, the so-called "production matrix" as originally defined by Talbot & Arnett (1973). We indicate with M_L the lightest mass which contributes to the chemical enrichment and it is set at $0.8 M_{\odot}$; the upper mass limit, M_U, is set at $100 M_{\odot}$.

The SFR $\psi(r,t)$ is defined as:

$$\psi(r,t) = \nu \left(\frac{\Sigma(r,t)}{\Sigma(r_{\odot},t)} \right)^{2(k-1)} \left(\frac{\Sigma(r,t_{Gal})}{\Sigma(r,t)} \right)^{k-1} G_{gas}^{k}(r,t), \tag{3.25}$$

where ν is the efficiency of the star formation process and is set to be 2 Gyr^{-1} for the Galactic halo and 1 Gyr^{-1} for the disk. $\Sigma(r,t)$ is the total surface mass density, $\Sigma(r_\odot,t)$ the total surface mass density at the solar position, $G_{gas}(r,t)$ the surface density normalized to the present time total surface mass density in the disk $\Sigma_D(r,t_{Gal})$, where $t_{Gal}=14$ Gyr is the age assumed for the MW and $r_\odot=8$ kpc is the solar galactocentric distance (Reid 1993). The gas surface exponent, k, is set equal to 1.5. With these values of the parameters, the observational constraints, in particular in the solar vicinity, are well fitted. Below a critical threshold of the gas surface density ($7M_\odot pc^{-2}$), we assume no star formation. This naturally produces a hiatus in the SFR between the halo-thick disk and the thin disk phases.

The Scalo (1986) IMF, constant in time and space is adopted. τ_m is the evolutionary lifetime of stars as a function of their mass m (Maeder & Maynet 1989).

The Type Ia SN rate has been computed by assuming as progenitor model for Type Ia SNe the single degenerate model (see also Chapter 5). We followed Greggio & Renzini (1983a) and Matteucci & Greggio (1986) formulation which is expressed as:

$$R_{SNeIa}=A_{Ia}\int_{M_{Bm}}^{M_{BM}}\phi(M_B)\left[\int_{\mu_m}^{0.5}f(\mu)\psi(t-\tau_{M_2})d\mu\right]dM_B \tag{3.26}$$

where M_2 is the mass of the secondary, M_B is the total mass of the binary system, $\mu=M_2/M_B$, $\mu_m=max\left[M_2(t)/M_B,(M_B-0.5M_{BM})/M_B\right]$, $M_{Bm}=3M_\odot$, $M_{BM}=16M_\odot$. The IMF is represented by $\phi(M_B)$ and refers to the total mass of the binary system for the computation of the Type Ia SN rate, $f(\mu)$ is the distribution function for the mass fraction of the secondary:

$$f(\mu)=2^{1+\gamma}(1+\gamma)\mu^\gamma \tag{3.27}$$

with $\gamma=2$; A_{Ia} is the fraction of systems in the appropriate mass range, which can give rise to Type Ia SN events. This quantity is fixed to 0.05 by reproducing the observed Type Ia SN rate at the present time (Mannucci et al. 2005). Note that in the case of the Type Ia SNe the"production matrix" is indicated with Q_{mi}^{SNIa} because of its different nucleosynthesis contribution (for details see Matteucci & Greggio 1986 and Matteucci 2001).

The term $A(r,t)$ represents the accretion term and is defined as:

$$A(r,t)=a(r)e^{-t/\tau_H(r)}+b(r)e^{-(t-t_{max})/\tau_D(r)}. \tag{3.28}$$

X_{A_i} are the abundances in the infalling material, which is assumed to be primordial, while $t_{max}=1$ Gyr is the time for the maximum infall on the thin disk, $\tau_H=0.8$ Gyr is the time scale for the formation of the halo thick-disk and $\tau_D(r)$ is the timescale for the formation of the thin disk and is a function of the galactocentric distance (inside-out formation, Matteucci and François, 1989; Chiappini et al. 2001).

In particular, it is assumed that:

$$\tau_D=1.033r(\mathrm{kpc})-1.267\ \mathrm{Gyr}. \tag{3.29}$$

Finally, the coefficients $a(r)$ and $b(r)$ are obtained by imposing a fit to the observed current total surface mass density in the thin disk as a function of galactocentric distance given by:

$$\sigma(r) = \sigma_D e^{-r/r_D}, \tag{3.30}$$

where σ_D=531 $M_\odot$ pc^{-2} is the central total surface mass density and $r_D = 3.5$ kpc is the scale length assumed for the disk of the Galaxy.

3.4.1 Nucleosynthesis prescriptions

For the nucleosynthesis prescriptions of the Fe and the other elements (namely O, S, Si, Ca, Mg, Sc, Ti, V, Cr, Zn, Cu, Ni, Co and Mn), we adopted those suggested in F04. They compared theoretical predictions for the [el/Fe] vs. [Fe/H] trends in the solar neighborhood for the above mentioned elements and they selected the best sets of yields required to best fit the data. In particular, for the yields of SNe II they found that the Woosley & Weaver (1995) (hereafter WW95) ones provide the best fit to the data. No modifications are required for the yields of Ca, Fe, Zn and Ni as computed for solar chemical composition. For oxygen, the best results are given by the WW95 yields computed as functions of the metallicity. For the other elements, variations in the predicted yields are required to best fit the data (see F04 for details).

In particular, the Mg yields require some adjustments since Mg yields from massive stars are generally too low and predict a too low Mg solar abundance. However, this fact does not affect the [Mg/Fe] vs. [Fe/H] diagram if the predicted ratios are normalized to the predicted solar abundances. What matters in these diagrams are the proportions of a given element produced in different mass ranges: Mg is mainly produced in massive stars and therefore, irrespective of the predicted Mg abundance, one always obtains an overabundance of Mg relative to Fe in metal poor stars followed by a decrease of the Mg/Fe ratio at the onset of Type Ia SNe which produce the bulk of Fe. F04 artificially increased the yields of Mg from WW95 to obtain also a good solar Mg abundance and to give an indication to nucleosynthesis modelers about what might be necessary to fit the absolute Mg abundance. For the Fe-peak elements, the situation is more complex and still very uncertain and we do not show results for these elements in this work. Concerning O, the best agreement with the [O/Fe] vs. [Fe/H] and the solar O abundance, as measured by Asplund et al. (2005), is obtained by adopting the original WW95 yields from massive stars as functions of metallicity. The same is not true for Fe: it was already known from the paper of Timmes & al. (1995) that the Fe yields as functions of metallicity overestimate the solar Fe and many people use those yields divided by a factor of 2. Alternatively, one can use the yields for solar chemical composition for the whole galactic lifetime and the result is the same. This is due to the still existing uncertainties in the Fe yields.

Concerning the yields from Type SNeIa, revisions in the theoretical yields by Iwamoto et al.(1999) are required for Mg, Ti, Sc, K, Co, Ni and Zn to best fit the data. The prescription for single low-intermediate mass stars is by van den Hoek

& Groenewegen (1997), for the case of the mass loss parameter, which varies with metallicity (see Chiappini et al. 2003a, model5).

3.5 Inserting Galactic Fountains in a detailed chemical evolution model

As we have shown in Chapter 2 the range of the cloud orbits originated from the break out of a supershell is quite small. The clouds are generally directed outwards but the average landing coordinates differ from the throwing coordinates by at most $\sim$ 1 kpc. Therefore, it is unlikely that galactic fountains can affect abundance gradients on large scales. However the fountains take a finite and non-negligible time to orbit around and fall back into the Galaxy. This implies a delay in the mixing of metals in the ISM, which conflicts with the IMA assumption.

In this thesis we also test the effect on the chemical evolution of different values of the delay generated by sequential SN explosions at different galactocentric distances.

3.5.1 The relaxation of the IMA

While the IRA has been relaxed in most of the recent chemical evolution models, there have been only a few attempts to relax the IMA mainly because of difficulties in estimating the dispersal and mixing time of the chemical elements (Roy & Kunth 1995) and because models which retain the IMA provide nevertheless an excellent fit to the data in the MW (e.g. Chiappini et al. 1997). Although there is no doubt that IMA is not realistic (Schmidt 1963; Tinsley 1975), the validity of this assumption depends on the time-scale of the mixing processes. Malinie et al.(1993) claimed that due to chemical inhomogeneities in the disk, mixing and star formation could be delayed by 10^{8-9} yr.

One of the very few studies in which IMA has been relaxed is the one of Thomas et al. (1998). They proposed a model in which relaxing IMA was included by splitting the gas components into two different phases: the inactive and active gas phases. The first one consists of a hot and not homogeneously distributed component; stars cannot form out of this phase. The active phase is instead assumed to be cool and well mixed. They discussed various time-scales for the mixing of the stellar ejecta, and they found that a delay of the order of 10^8 years leads to a better fit of the observational data in the [Mg/Fe]-[Fe/H] diagram than in the IMA hypothesis.

We test the relaxation of the IMA in the detailed chemical evolution model of F04, considering two physically motivated time delays: i) the "galactic fountain time delay" effect and ii) the delay produced by the cooling of the metals ("metal cooling delay model").

The second delay is due to the fact that stars form only in cold gas and that hot gas takes a finite time to cool. However, there is still some debate in the literature on the cooling time-scale. Recchi et al. (2001) studied the effect of a single, instantaneous starburst on the dynamical and chemical evolution of a gas-rich dwarf

galaxy. They found that most of the metals already reside in the cold gas phase after a few tens of Myr. This result is mainly due to the assumed low SNII heating efficiency, and justifies the generally adopted homogeneous and instantaneous mixing of gas in chemical evolution models. On the other hand, Rieschick & Hensler (2000) presented a chemodynamical model for the evolution of a dwarf galaxy in which most of the metals undergo a cycle lasting almost 1 Gyr before being incorporated into the ISM. A similar result has been obtained by Tenorio-Tagle (1996). More recently, in the work of Harfst et al. (2006), a multi-phase description of the ISM was implemented: the ISM was treated as two dynamically independent gas phases: a cloudy and a diffuse one. The two gas phases are linked by the processes of condensation/evaporation and a drag force. In this model, it is assumed that stars form in clouds and that clouds are destroyed by stellar feedback, thereby self-regulating the star formation. Each cloud is assumed to form stars only *after a time of inactivity*, because not all the gas in clouds is dense or unstable enough for immediate star formation. In this work the time of inactivity considered is a few hundred Myr.

Here, we simply implement our "metal cooling delay model" in the detailed chemical evolution model of F04 by means of a delay in the chemical enrichment.

The galactic fountain delay model

We implemented this delay in the chemical evolution model of F04 only during the thin disk phase. In fact, the dynamical effect of a galactic fountain requires the presence of a stratified ISM, which arises only after the end of the halo phase. In the past, several authors (i.e. MM89 and Tenorio-Tagle 1996) studied the supershell evolution produced by a sequential explosion of Type II SNe. They emphasized that a break-out event, necessary for a galactic fountain, requires that the OB associations must sit on a *plane stratified disk* where the density decreases along the z direction. In the work of MM89 a scale height of 100 pc for the ISM was considered. This is the reason why OB associations existed at early times during the formation of the halo but did not produce galactic fountains. Galactic fountains could have formed perhaps during the thick disk phase. However, by computing a fountain with a scale height of 1 kpc (typical of the thick disk), the fountains start at $\simeq 3$ kpc, i.e. well within the halo. At this height, the stratification is much weaker and the ISM temperature is high, therefore the sound speed is high and the shock can be easily dissipated through sound waves. Moreover the thick disk phase lasts for a very short time (see Fig. 4.1). We can then conclude that (hypothetical) thick disk fountains would have a negligible impact on the chemical evolution of the Galaxy.

Therefore, we consider the galactic fountain delay only for ejecta from massive stars (with mass $> 8\ M_{\odot}$) born after the halo-thick disk transition.

The metal cooling delay model

Roy & Kunth (1995) studied the dispersal and mixing of oxygen in the ISM of gas-rich galaxies. Due to a variety of hydrodynamical processes operating at

scales ranging from 1 pc to greater than 10 kpc in the ISM, there are difficulties in estimating the dispersal and mixing timescale: (*i*) on large galactic scales ($1 \geq l \geq 10$ kpc), turbulent diffusion of interstellar clouds in the shear flow of galactic differential rotation is able to remove azimuthal O/H fluctuations in less than 10^9 yrs; (*ii*) at the intermediate scale ($100 \geq l \geq 1000$ pc), cloud collisions and expanding supershells driven by evolving associations of massive stars, differential rotation and triggered star formation will redistribute and mix gas efficiently in about 10^8 yrs; (*iii*) at small scales ($1 \geq l \geq 100$ pc), turbulent diffusion may be the dominant mechanism in cold clouds, while Rayleigh-Taylor and Kelvin-Helmhotz instabilities quickly develop in regions of gas ionized by massive stars, leading to full mixing in $\leq 2 \times 10^6$ yrs. Malinie et al. (1993) claimed that due to chemical inhomogeneities observed for example in the age-metallicity relation in the solar neighborhood, remixing and star formation may be delayed by 10^{8-9} yr.

Following the work of Thomas et al. (1998), we relaxed the IMA in the chemical evolution model by splitting the gas component into two different phases (cold and warm). The gas in the interstellar medium is heated by SN events and the stars cannot form in this "warm gas phase"; only after the gas cools can stars form and then pollute the ISM. We implemented the two gas phases simply by means of a delay in the chemical enrichment. In this case: i) all stellar masses (both Type II and Type Ia SNe) and ii) both halo and disk stars, are affected by this delay.

The implementation of a delay in the chemical evolution model

We treated the time delay in the mixing by simply considering a time delay in the stars deaths due to galactic fountains (Δt_1) and gas cooling (Δt_2). In particular in eq. (3.24)

Concerning the galactic fountain delay model, in eq. (3.24) in all quantitities related to Type II SNe we replace $(t - \tau_m)$ (in the SFR, ψ and in the fraction of mass restored by a star of mass m, Q_{mi}) with $(t - \tau_m - \Delta t_1)$. Since the galactic fountain delay affect only Type II SNe, all the quantities appearing in the second integral remain as function of $(t - \tau_{m2})$.

For the gas cooling model all stellar masses (both Type II and Type Ia SNe) are affected by this delay and we replace in all quantities $(t - \tau_m)$ with $(t - \tau_m - \Delta t_2)$ and $(t - \tau_{m2})$ with $(t - \tau_{m2} - \Delta t_2)$.

In our model the SFR history is not modified, we have simply delayed the pollution of the ISM by died stars.

We want to stress out that for the model with the galactic fountain delay we expect an halt in the pollution of the α-elements, at the time t_0 of the death of the first type II SNe affected by the galactic fountains the Fe from Type Ia SNe continues to be produced. Then in the classical plot of chemical evolution model $[\alpha/Fe]$ vs $[Fe/H]$ we forecast a drop in the $[\alpha/Fe]$ quantity in the interval $[t_0, t_0 + \Delta t_1]$.

3.6 Considering different Type Ia SN Progenitors in the chemical evolution model

The Type Ia SN rate, which depends on the SN Ia progenitor model and the star formation history, is a fundamental ingredient in models of galactic chemical evolution. The progenitor model can be described simply by a delay time distribution (DTD) function, which is the distribution of the explosion times. In the pioneering work of Greggio & Renzini (1983a, hereafter GR83) there was, for the first time, an expression for the Type Ia SN rate in the scenario of the single degenerate model. The DTD of this model arises from the scenario described in the introduction and predicts the explosion times of binary systems with the appropriate characteristics. An alternative model for progenitors of Type Ia SNe was proposed by Iben & Tutukov (1984) considering the double white progenitor model.

Tornambé & Matteucci (1986) formulated a Type Ia SN rate in this scenario and applied it to galactic chemical evolution models. In the following, Matteucci & Greggio (1986) tested the GR83 rate by means of a detailed chemical evolution model of the MW and interpreted the [α/Fe] ratios versus [Fe/H] as due to the delay in the Fe production from Type Ia SNe, thus confirming previous suggestions (Tinsley, 1979; Greggio & Renzini 1983b). In the chemical evolution model of F04 described above it was considered this implementation for the type Ia SN rate (see eq. 3.26).
In recent years other authors (Dahlen et al. 2004; Strolger et al. 2004; Mannucci et al. 2005, 2006; Scannapieco & Bildsten, 2005; Sullivan et al. 2006; Aubourg et al. 2008; Pritchet et al. 2008; Totani et al. 2008) have proposed Type Ia SN rates based on DTDs derived empirically. One example is the rate of Mannucci et al. (2005;2006): they suggested that two populations of progenitors of Type Ia SNe are needed to explain the dependence of the rates on the colors of the parent galaxy. The presence of Type Ia SNe in old, red, quiescent galaxies is an indication that part of these SNe originate from old stellar populations. On the contrary, the increase of the rate in blue galaxies (by a factor of 30 going from (B-K) $\sim$2 to (B-K) $\sim$ 4.5) shows that part of the SN Ia progenitors is related to young stars and closely follows the evolution of the SFR. Mannucci et al.(2006, hereafter MVP06), on the basis of the previously described relation between the Type Ia SN rate and the color of the parent galaxies, their radio power as measured by Della Valle et al. (2005), and cosmic age, concluded that there are two populations of progenitors of Type Ia SNe. They have suggested (but see Greggio et al. 2008) that the current observations can be accounted for only if about half of the SNe Ia (*prompt SNe Ia*) explode within 10^8 years after the formation of their progenitors, while the rest explode during a wide period of time extending up to 10 Gyrs (*tardy SNe Ia*). Matteucci et al. (2006) applied this formulation of the Type Ia SN rate to chemical evolution models of galaxies of different morphological type. They concluded that a fraction of 50% of prompt Type Ia SNe worsens the agreement with abundance data, especially in the MW, and suggested that prompt Type Ia SNe should indeed exist but their fraction should not be larger than 30%. They also found a possible scenario for SN

Ia progenitors in the MVP06 framework: a possible justification for this strongly bimodal DTD can be found in the framework of the single degenerate model for the progenitors of Type Ia SNe. In fact, such a DTD can be found if one assumes that the function describing the distribution of mass ratios inside the binary systems, is a multi-slope function. In particular, this choice means that in the range 5-8 $M_{\odot}$ are preferred the systems where $M_1 \sim M_2$, whereas for lower mass progenitors are favored systems where $M_1 >> M_2$. Another suggestion came from Dahlen et al. (2004) and Strolger et al.(2004, 2005), on the basis of the observational cosmic Type Ia SN rate. They suggested a DTD with no prompt Type Ia SNe with a maximum occurring at 3-4Gyr. More recently, a direct determination of the DTD function has been reported by Totani et al. (2008), on the basis of the faint variable objects detected in Subaru/XMM-Newton Deep Survey (SXDS). They concluded that the DTD function is inversely proportional to the delay time, i.e. the DTD can be well described by a featureless power law (DTD $\propto t^{-n}$, with $n \sim 1$). A similar suggestion came from Pritchet et al. (2008), who suggested a DTD $\propto t^{-0.5\pm0.2}$.

The maximum at which the Type Ia SN rate occurs is a very important parameter which affects the shape of the [α/Fe] relation in galaxies. This timescale depends on the fraction of prompt/tardy Type Ia SNe and on the specific history of star formation in galaxies, as shown by Matteucci & Recchi (2001), being shorter than in the solar neighbourhood for ellipticals and longer for irregular systems.

In this work, for the first time we show the effects of adopting different DTDs in a model for the chemical evolution of the MW: in particular, we will focus on three relevant observational costraints: i) the [O/Fe] vs.[Fe/H] relation in the solar vicinity for which many accurate data are now available, ii) the Type Ia SN rate at the present time and iii) the G-dwarf metallicity distribution. To do that we we adopt five different DTDs, two of which are empirically derived (see Chapter 5).

Chapter 4

Effects of Galactic Fountains and delayed mixing in the chemical evolution of the Milky Way

In this Chapter we show our results concerning the relaxation of the IMA in the detailed chemical evolution model described before by means the i) the galactic fountain delay effect and ii) the metal cooling delay effect, presented in the previous Chapter.

4.1 The time delay originated by a galactic fountain

In Chapter 2 we used the Kompaneets (1960) approximation for the evolution of the superbubble driven by sequential supernova explosions. We assumed that supershells are fragmented by Rayleigh-Taylor instabilities, and considered each fragment as a cloud with an initial velocity given by the supershell velocity at the moment of fragmentation. Then, we followed the orbit of the clouds either ballistically (the cloud is subject only to the gravitational potential of the Galaxy) or taking into account viscous interaction between the extra-planar halo gas and the cloud.

In Tables 2.3-2.5 the results are summarized for fragmentation times (t_{final}) and the velocities (v_n) of the supershells in the direction perpendicular to the galactic plane at those times for initial throwing coordinates fixed at 4 kpc, 8 kpc and 12 kpc. In Table 4.1 we report the average time $< t_{total} >$ necessary to create a cloud from a supershell plus the time necessary for the cloud to fall back onto the Galactic disk:

$$< t_{total} >= t_{final} + < t_{orbit} >, \tag{4.1}$$

where $< t_{orbit} >$ is the average time required for a cloud to return to the galactic disk once it leaves the supershell. These average values are calculated in the case of OB associations with 10, 50, 100, 500 SNe at 3 galactocentric distances: 4 kpc, 8

kpc, 12 kpc. In Table 4.2 we show the maximum delay time t_{total} , at a fixed initial galactocentric distance of ejection.

As explained in Chapter 3, we consider the galactic fountain delay only for ejecta from massive stars (with mass $> 8\ M_{\odot}$) born after the halo-thick disk transition. In Fig. 4.1 we show the predicted SFR expressed in $M_{\odot}$ pc^{-2} Gyr^{-1} as a function of the galactic time (Gyr) predicted by our chemical evolution model. We note that the SFR is the same for all galactocentric distances during the halo phase. The effect of the two infall model in presence of the threshold in the star formation is clearly shown: the star formation halts during the halo-thin disk transition and the duration of the gap varies as a function of galactocentric distance. At the solar neighborhood the gap is $\simeq 0.3$ Gyr. This gap seems to be observed in the abundance ratio distribution as shown in Gratton et al. (2000) and Fuhrmann (1999). In Table 4.3 we report the times at different galactocentric distances at which the SFR in the thin disk begins (t_{SFR}). At late times the substantially effect of the threshold is to produce a oscillating SFR on very short timescales resulting in practice in a constant SFR. Ejecta of intermediate-mass stars and Type Ia SNe (which are most probably not clumped in OB associations) are not subject to the galactic fountain delay.

Table 4.1: The average time $< t_{total} >$ [Myr].

	4 kpc	8 kpc	12 kpc
10 SNe	43	53	75
50 SNe	36	54	87
100 SNe	36	57	96
500 SNe	38	75	133

Table 4.2: The maximum t_{total} as a function of the galactocentric distance.

	4 kpc	8 kpc	12 kpc
Maximum delay	48 Myr	114 Myr	245 Myr

As shown in Table 4.2, a single superbubble can produce a delay in the mixing up to $\sim$ 250 Myr, but the average values are smaller, spanning the range between 40 - 140 Myr (Table 4.1). In the simulation, we considered different values up to 1 Gyr. It is possible that the MW formed super-star clusters during more intense phases of star formation, as observed in M82 (Melo et al. 2005). A delay of 1 Gyr can then be obtained if the number of massive stars in a cluster is $\sim 10^4$, which is consistent with the mass of the largest super-star clusters observed in M82. We considered this long delay as an extreme case.

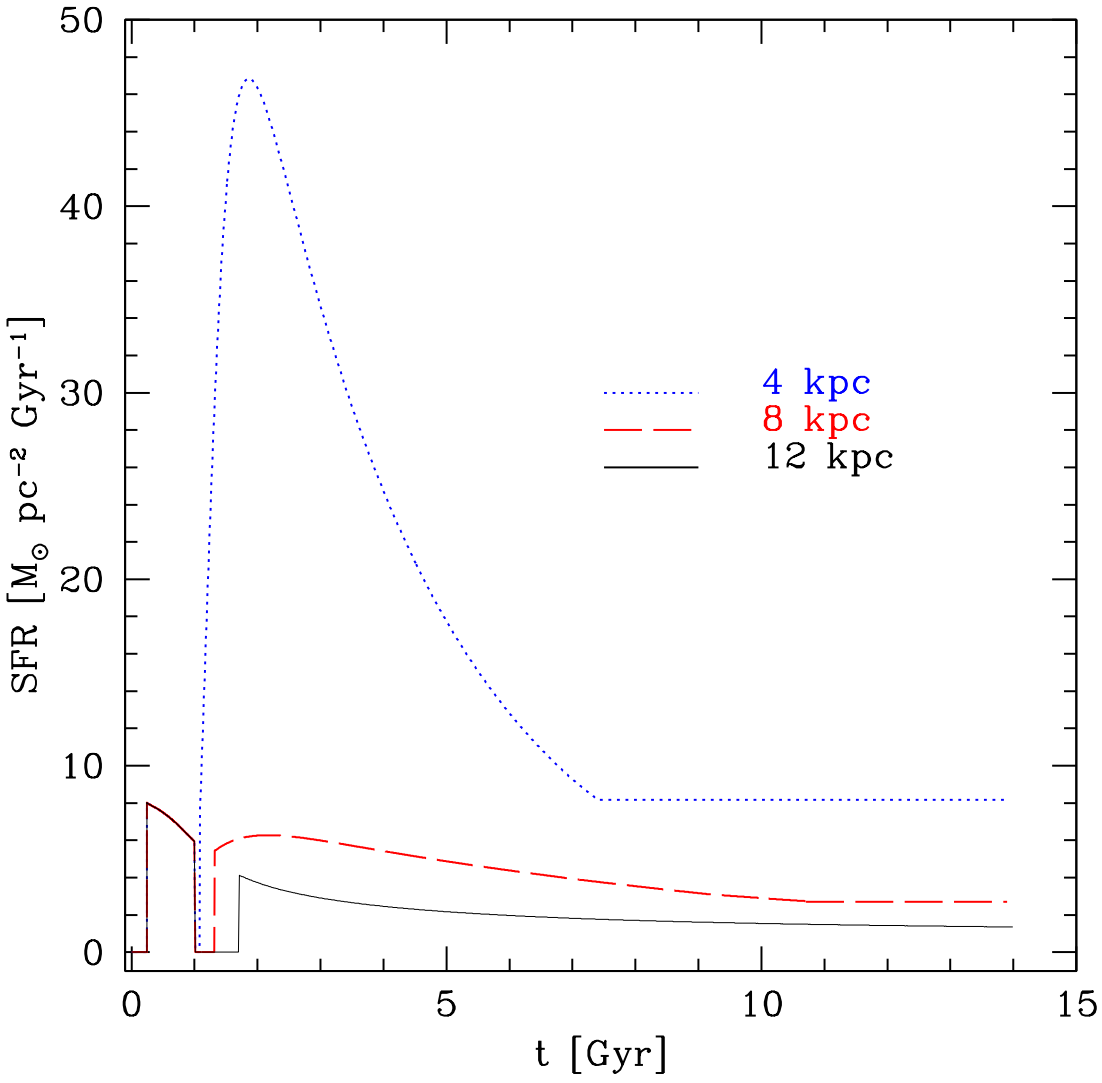

Figure 4.1: The SFR expressed in $M_{\odot}$ pc^{-2} Gyr^{-1} as a function of the galactic time (in Gyr), as predicted by the standard two infall model at 4 (dotted line), 8 (dashed line) and 12 kpc (solid line).

Table 4.3: Beginning of the star formation in the disk after the halo-thick disk transition (t_{SFR}).

	4 kpc	8 kpc	12 kpc
Beginning of SF in the disk	1.1 Gyr	1.3 Gyr	1.7 Gyr

4.2 Observational data

We used the collection of data elaborated in the work of F04, who adopted a data sample for stars in the solar neighborhood spanning a metallicity range from -4 dex to solar. In particular, for the very metal poor stars ([Fe/H] between -4 and -3 dex), the results from the UVES Large Program " First Stars" (Cayrel et al. 2003) were adopted.

For the abundances in the remaining range of [Fe/H], they adopted already published data in the literature from various sources: for all the elements studied here (O, Mg, Si), F04 used the data of Carney et al. (1997), Nissen & Schuster (1997), Ryan et al. (1991), Edvardsson et al. (1993), Matteucci et al. (1993 and references therein). Moreover, concerning the Mg and Si, but not O, the collection of F04 includes the data of Stephens (1999), Carretta et al. (2002), McWilliam et al. (1995), Fulbright (2000), Gratton & Sneden (1988). For the O, F04 also used the data of Nissen et al. (2002). Here, for O, we also took into account the data of Bensby et al. (2004).

All of these data are normalized to the solar abundances of Grevesse & Sauval (1998) with the exception of oxygen for which we adopted the value of Asplund et al. (2005).

For the galactic abundance gradient for the oxygen, we used the set of data given by Andrievsky et al. (2002a,b) and Luck et al. (2003) (see also Cescutti at al. 2007).

4.3 Results

In this section we discuss our results. First we show how a galactic fountain delay can affect the chemical evolution model, then we present the results for the metal cooling delay model.

We show the model predictions for O, Mg, Si and Fe obtained in particular for the relations [el/Fe] versus [Fe/H] compared with the observational data and try to put constraints on the maximum acceptable delay.

4.3.1 Results for the galactic fountain delay model

We have taken into account different values for the delay generated by galactic fountain events from sequential SN explosions: 0.1 Gyr, 0.2 Gyr, 0.5 Gyr, 1 Gyr.

We tested the delay effect at different galactocentric distances: 4, 8, 12 kpc.

Concerning the solar neighborhood, in Table 4.4 we report the solar abundances by mass as predicted by the chemical model with IMA and the delay models compared to the solar values. In Fig. 4.2 we show the results for [O/Fe] versus [Fe/H] in the solar neighborhood compared to the observational data described in Sect 4.2. Our results are normalized to the "best model" of F04 values at 9.5 Gyr (the age of the formation of the solar system). As we can see from this figure and from Table 4.4, the solar abundances predicted by our models are substantially in agreement with the obtained abundances. The standard model with no delay shows a discontinuity at ~ -0.8 dex, and this is due to the gap in the SFR discussed before. In fact, during the gap, O stops being produced whereas Fe keeps being produced by Type Ia SNe. The effect of the delay due to the fountains is therefore to increase this effect by increasing the duration of the gap.

Table 4.4: Mass fractions of several elements aspected by the standard chemical evolution model with IMA and by the delay model at the galactic age of 9.5 Gyr compared to the solar values of Asplund et al. (2005).

	$X_{\odot oss}$	$X_{\odot th}$				
	Asplund et al. (2005)	François et al. (2004)	0.1 Gyr	0.2 Gyr	0.5 Gyr	1 Gyr
He	2.55×10^{-1}	2.52×10^{-1}	2.52×10^{-1}	2.52×10^{-1}	2.52×10^{-1}	2.52×10^{-1}
C	2.21×10^{-3}	2.03×10^{-3}	2.05×10^{-3}	2.06×10^{-3}	2.11×10^{-3}	2.17×10^{-3}
N	6.32×10^{-4}	9.73×10^{-4}	9.75×10^{-4}	9.77×10^{-4}	9.81×10^{-4}	9.85×10^{-4}
O	5.48×10^{-3}	5.27×10^{-3}	5.31×10^{-3}	5.35×10^{-3}	5.46×10^{-3}	5.62×10^{-3}
Mg	6.17×10^{-4}	6.66×10^{-4}	6.70×10^{-4}	6.74×10^{-4}	6.86×10^{-4}	7.03×10^{-4}
Si	6.80×10^{-4}	8.14×10^{-4}	8.17×10^{-4}	8.20×10^{-4}	8.30×10^{-4}	8.43×10^{-4}
S	3.31×10^{-4}	3.95×10^{-4}	3.97×10^{-4}	3.98×10^{-4}	4.03×10^{-4}	4.09×10^{-4}
Ca	6.13×10^{-5}	5.40×10^{-5}	5.42×10^{-5}	5.44×10^{-5}	5.50×10^{-5}	5.58×10^{-5}
Fe	1.18×10^{-3}	1.14×10^{-3}	1.15×10^{-3}	1.15×10^{-3}	1.15×10^{-3}	1.16×10^{-3}

In the description of the delay model, we emphasized that galactic fountains can be seen only in disk stars. The typical delay, due to the fact that massive stars are clumped in OB associations, is 0.1 Gyr. Referring to Fig. 4.2 we present a first strong result: *a delay of 0.1 Gyr produces a negligible effect on the chemical evolution of the Galaxy in the solar neighborhood.* We note that the data show a spread in the halo-thick disk transition phase ([Fe/H]$\simeq$-0.77). This spread can be explained in terms of a combination of: i) a threshold in the star formation, ii) a delay in the chemical enrichment from the massive stars as due a to galactic fountain effect. Moreover, we note that the maximum possible delay, in order not to break the agreement with data, must be lower than 1 Gyr.

The same effect is shown in Fig. 4.3 and in Fig. 4.4 where we analyzed the behavior of such a delay in a chemical evolution model for other two α elements: Mg and Si.

It is also interesting to test the fountain delay at different galactocentric distances. In Figs. 4.5, 4.6 and 4.7 we report our results for O, Mg and Si, respectively. In each figure we plot the [el/Fe] vs. [Fe/H] at 4 and 12 kpc galactocentric distances. We note that the results are strongly dependent on the galactocentric distance. In fact, as explained before, the drop of the [el/Fe] ratio in the [el/Fe] vs. [Fe/H] plot

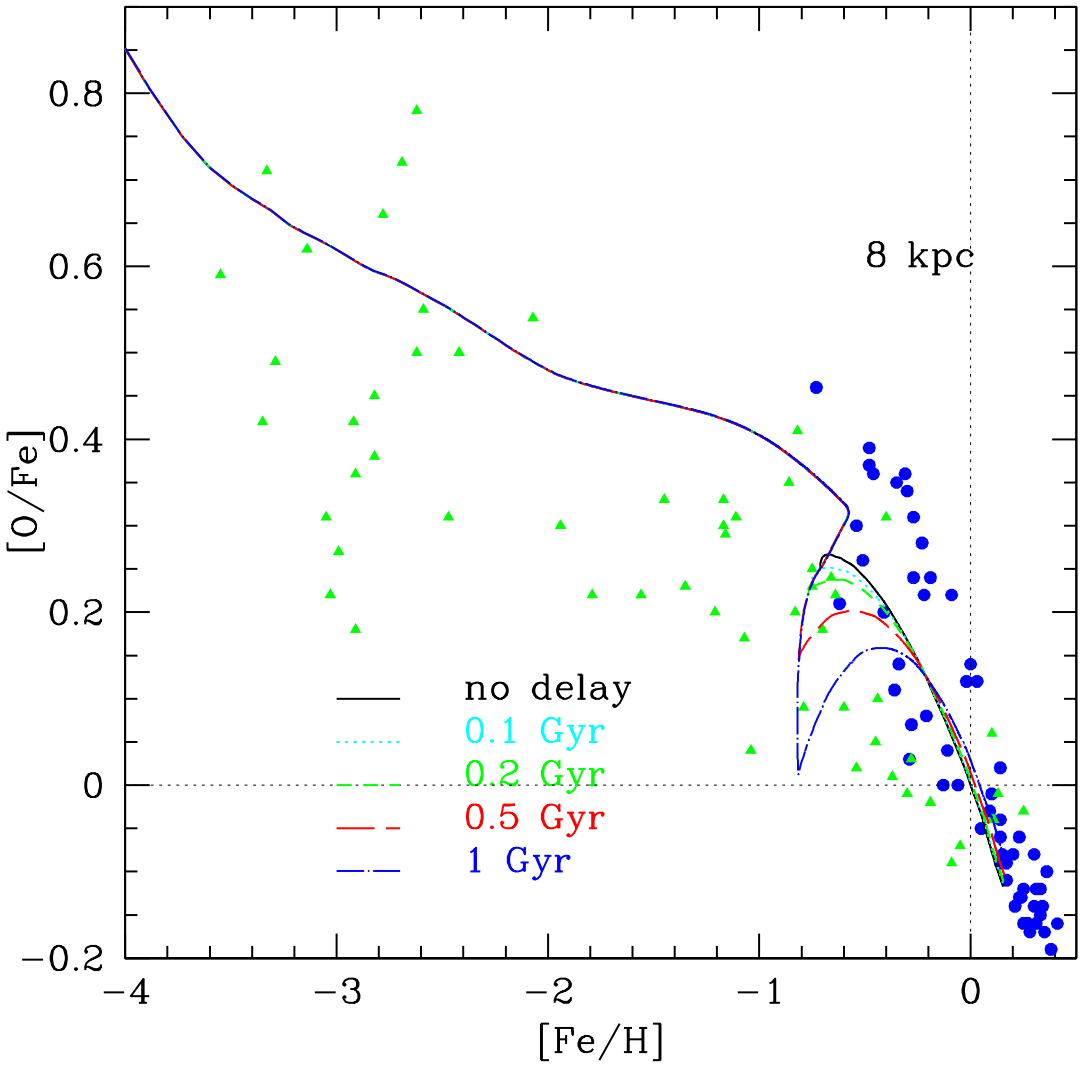

Figure 4.2: The abundance ratio [O/Fe] as a function of [Fe/H] in the solar neighborhood. We compared the François et al. (2004) model (solid line) with our galactic fountain delay models: dotted line (0.1 Gyr), short dashed line (0.2 Gyr), long dashed line (0.5 Gyr), dashed dotted line (1 Gyr). The data are taken from the collection used in François et al. (2004) (filled green triangles) and from Bensby et al. (2005) (filled blue circles).

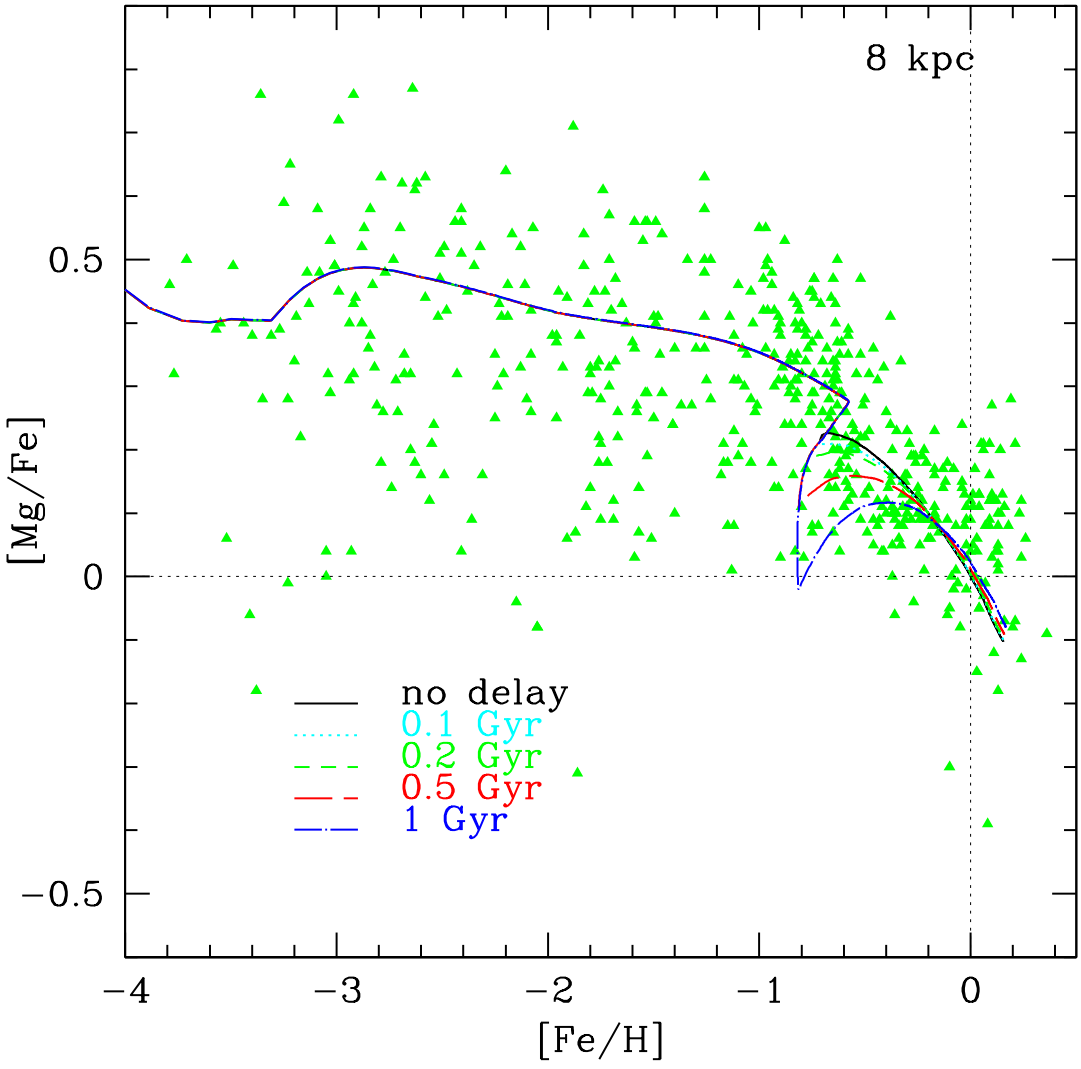

Figure 4.3: The abundance ratio [Mg/Fe] as a function of [Fe/H] in the solar neighborhood. Notation as in Fig. 4.2.

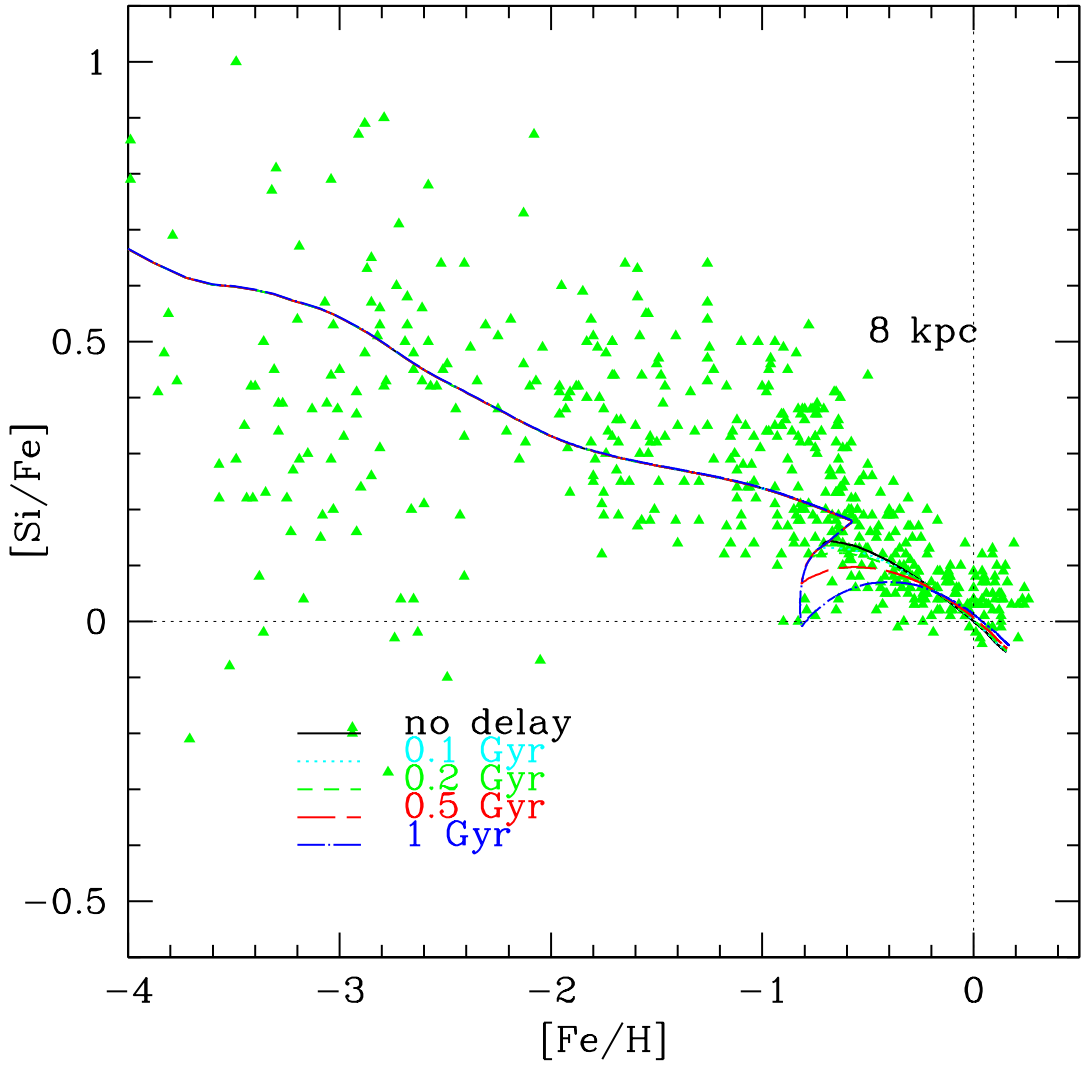

Figure 4.4: The abundance ratio [Si/Fe] as a function of [Fe/H] in the solar neighborhood. Notation as in Fig. 4.2.

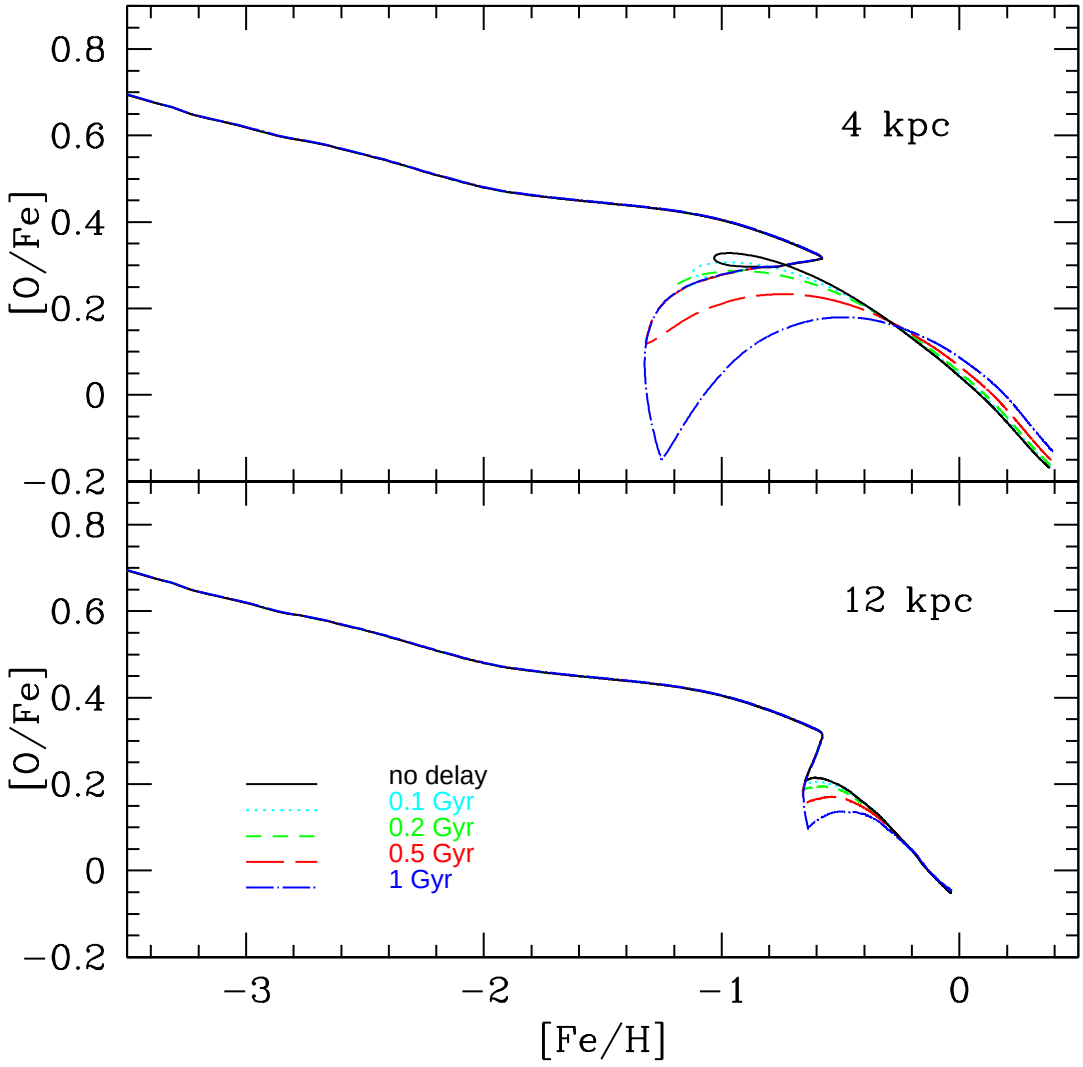

Figure 4.5: The abundance ratio [O/Fe] as a function of [Fe/H] at 4 and 12 kpc. Notation as in Fig. 4.2.

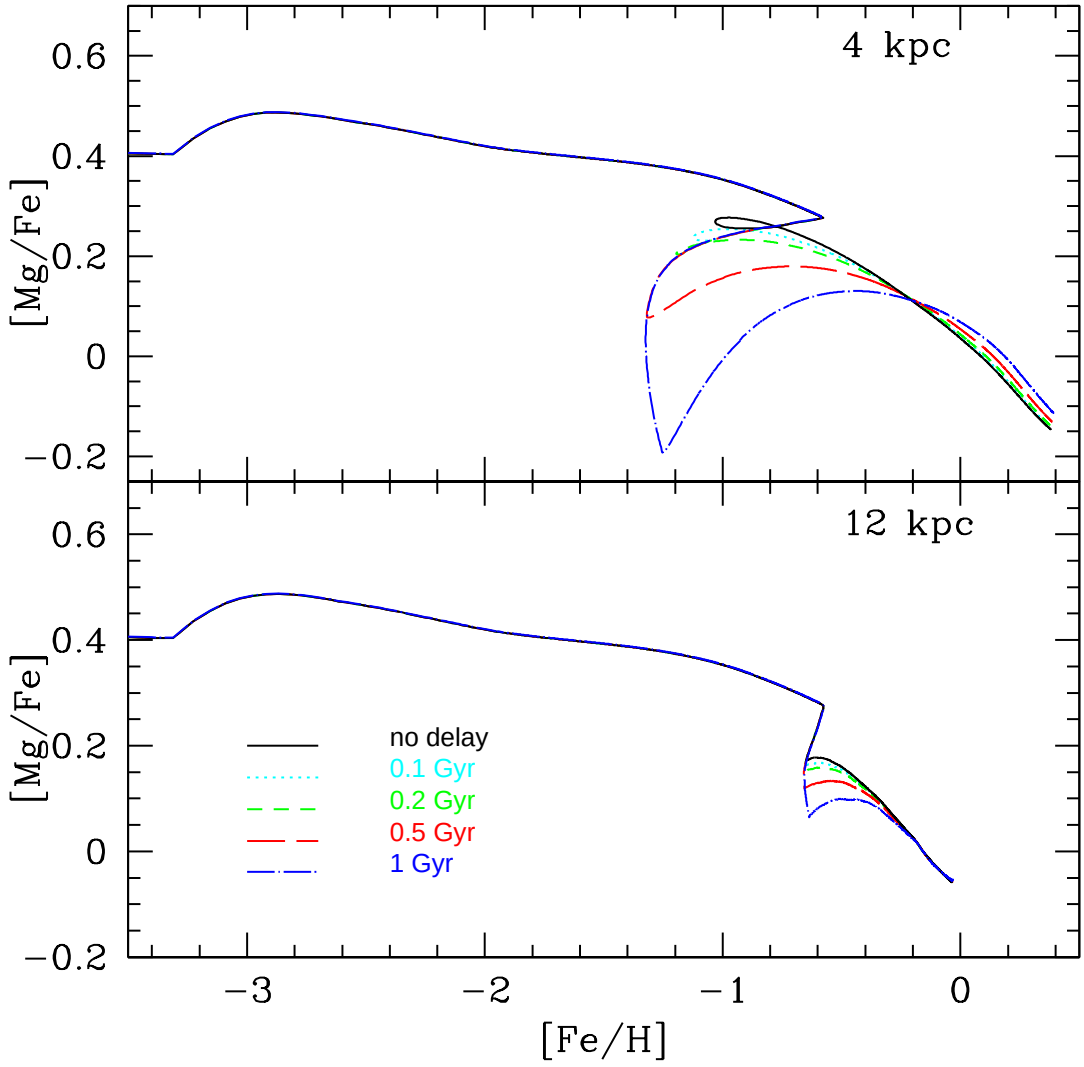

Figure 4.6: The abundance ratio [Mg/Fe] as a function of [Fe/H] at 4 and 12 kpc. Notation as in Fig. 4.2.

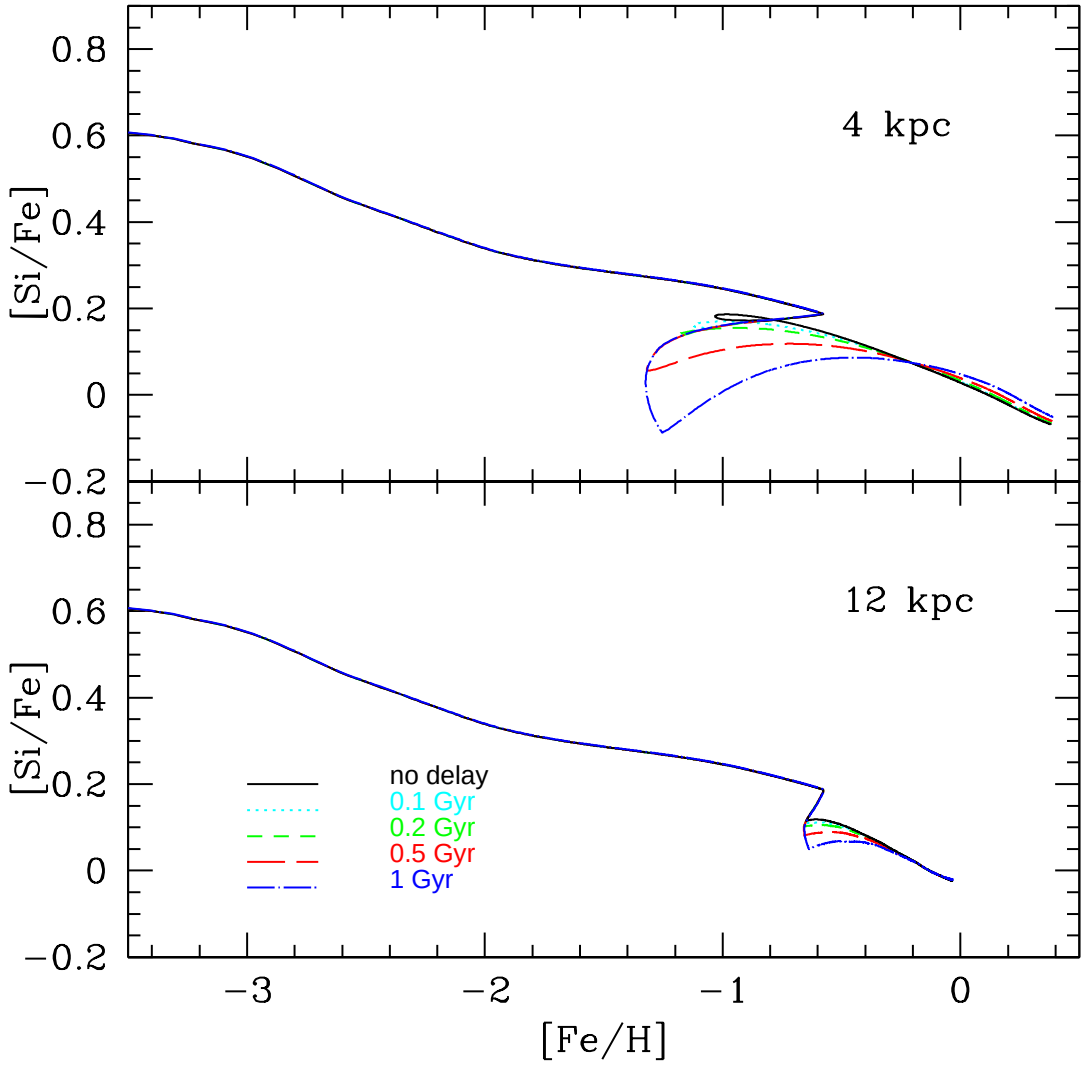

Figure 4.7: The abundance ratio [Si/Fe] as a function of [Fe/H] at 4 and 12 kpc Notation as in Fig. 4.2.

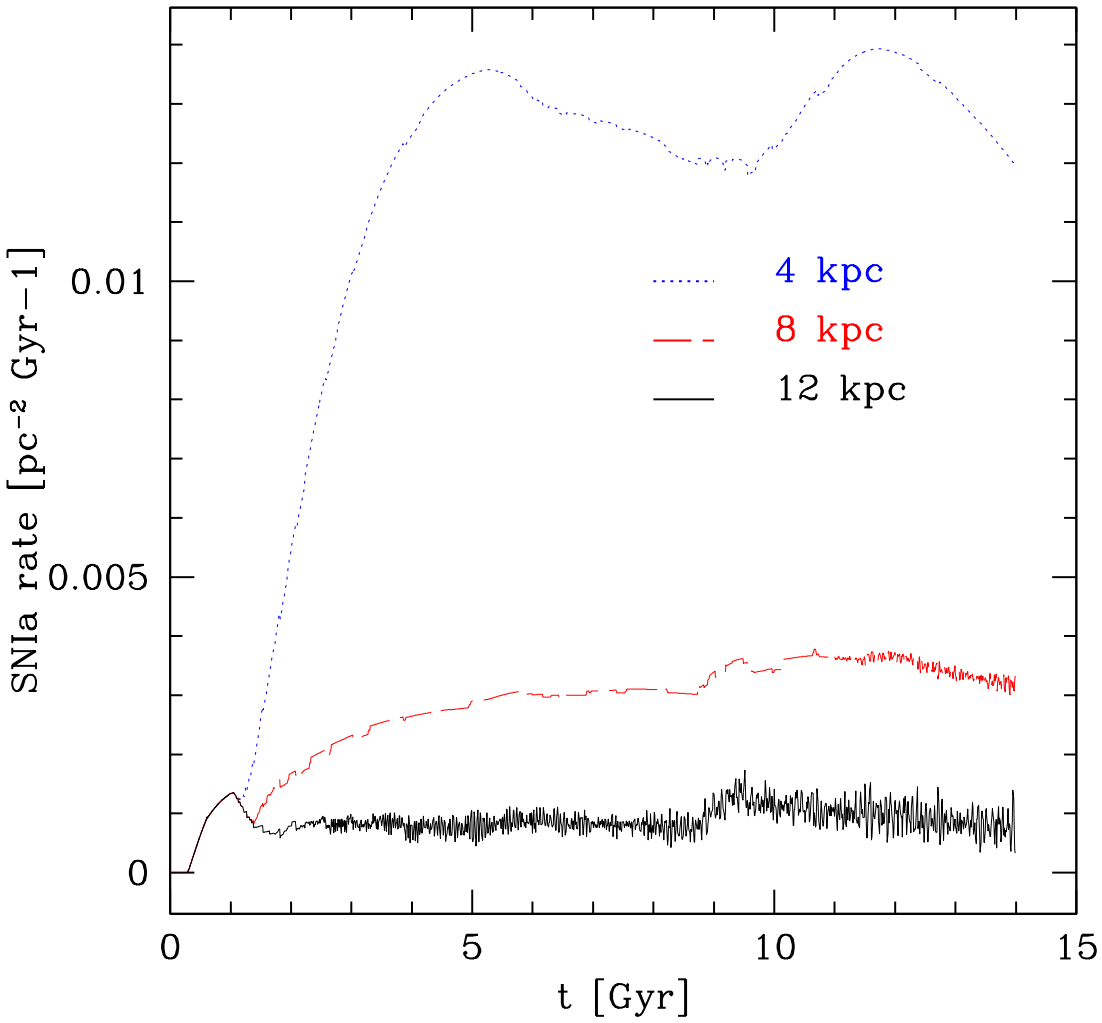

Figure 4.8: The Type Ia SN rate expressed in pc^{-2} Gyr^{-1} as a function of the galactic time (Gyr), as predicted by the standard two infall model at 4, 8 and 12 kpc.

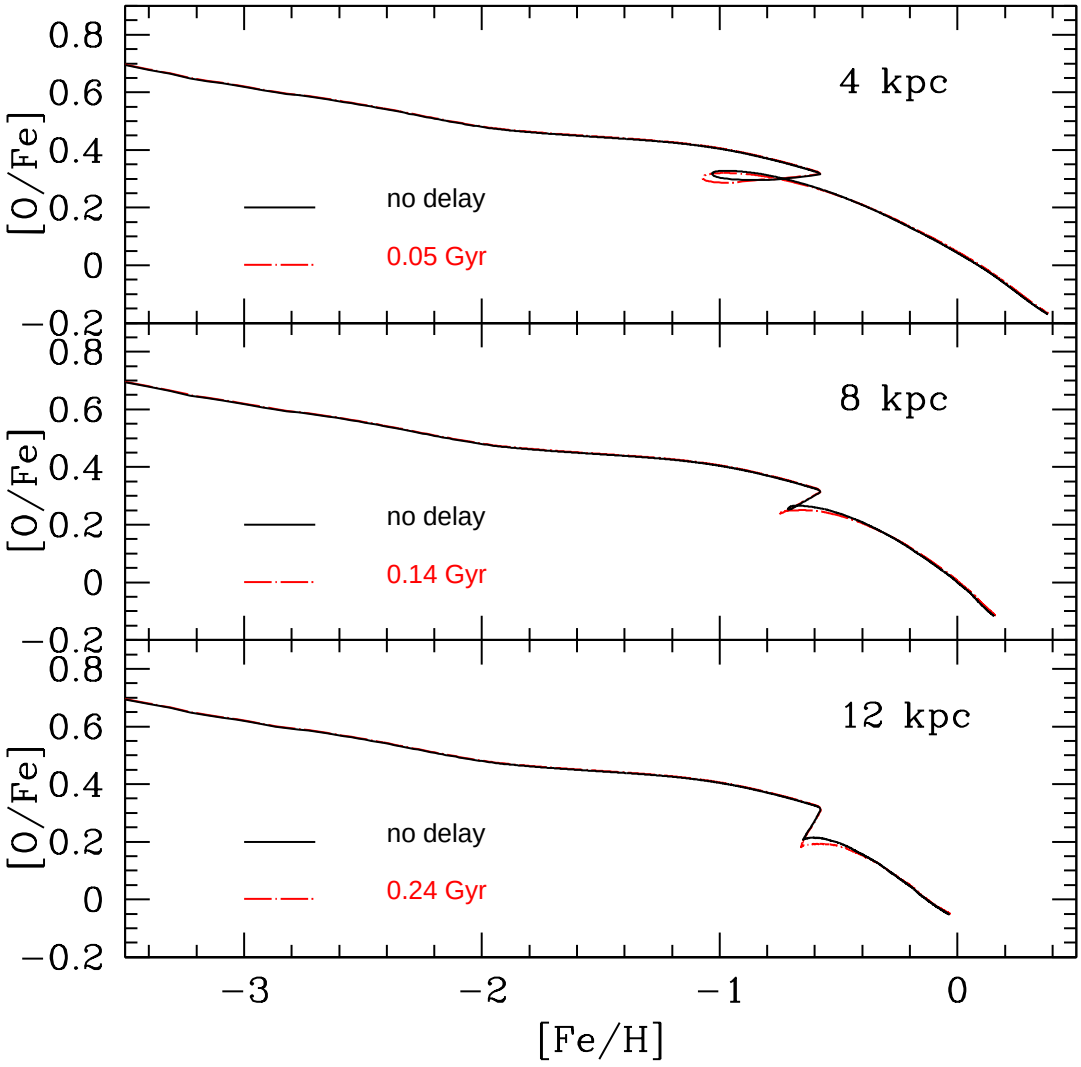

Figure 4.9: The abundance ratio [O/Fe] as a function of [Fe/H] at 4, 8 and 12 kpc for relative maximum delays as reported in Table 4.2.

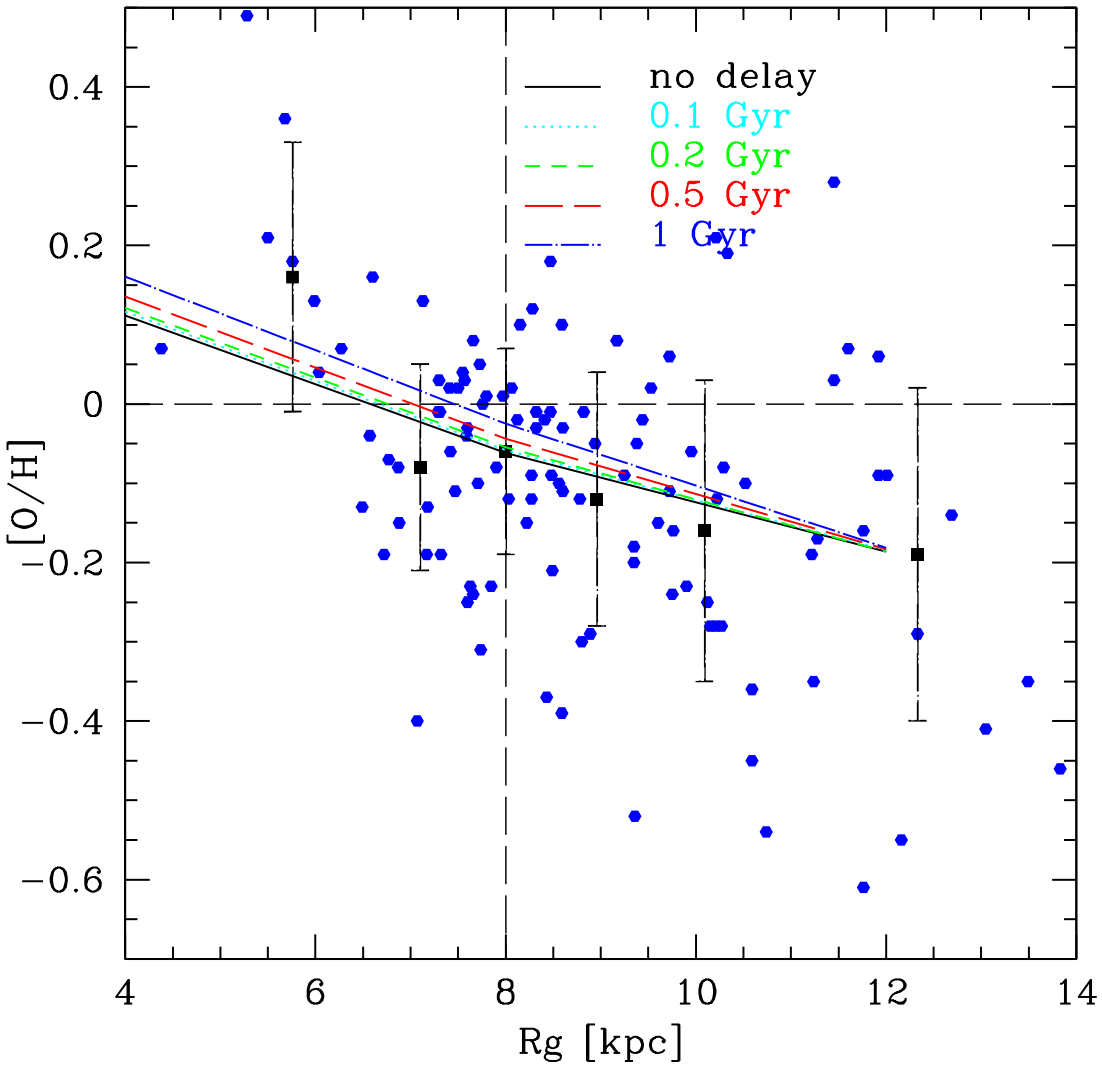

Figure 4.10: Predicted and observed O abundance gradients in the galactocentric distance range 4-14 kpc. The data points are from Cepheids. The large squares with error bars represent average of the points with their errors. The black solid line is the François et al. (2004) model normalized to the mean value of the bin centered at 8 kpc (see Cescutti et al. 2007).

is due to the iron ejected by the Type Ia SNe. The discontinuity predicted at 4 kpc is larger than that predicted at larger galactocentric distances. This effect is due to the higher specific Type Ia SN rate at 4 kpc than at larger distances. The specific Type Ia SN rate is the SNIa rate per unit mass of gas and it increases toward the Galactic center, the reason being that while the Type Ia SN rate is a factor of 8 higher than that in the solar vicinity, because of the higher SFR, the mass of gas is higher by only a factor of 2 relative to the solar region. Therefore, the effect of the pollution by Type Ia SNe during the gap is enhanced.

Again in Figs. 4.5, 4.6 and 4.7 we note that, at a fixed galactocentric distance, the effect of the galactic fountain delay depends also on the considered element: the Si which is also produced by Type Ia SNe in a non negligible amount shows a smaller drop of the [Si/Fe] quantity compared to O and Mg.

Even if the galactic fountain effect in the [el/Fe] values is larger at 4 kpc because of the higher rate of Type Ia SNe, the delays expected at 4 kpc are smaller with respect to the outward galactocentric distances (as shown in Tables 4.1 and 4.2), as a consequence of the higher gravitational pull. In Fig. 4.9 we show the [O/Fe] vs [Fe/H] at 4, 8 and 12 kpc considering the maximum delays in each radius. In the case of a delay produced by a single OB association, the effect of galactic fountains is negligible.

Finally, we explored the effects of galactic fountains on the abundance gradient for oxygen. In Fig. 4.10 we plot the [O/H] as a function of the galactocentric distance. We note that the average delay due to galactic fountains is longer than 0.1 Gyr only for an OB association composed of 500 SNe at 12 kpc (Table 4.1); this event is very unlikely, thus the delay of 0.1 Gyr can be considered as an average upper limit for a delay produced by a single OB association at a galactocentric distance in the range 4-12 kpc. Referring to Fig.4.10 we can conclude that the time delay produced by a Galactic fountain generated by an OB association has a negligible effect on the abundance gradient in the Galaxy disk.

4.3.2 Results for the metal cooling delay model

In this section we present the results for the metal cooling delay model. Referring to Malinie et al. (1993), we considered mixing delays of 0.5 Gyr and 1 Gyr. In Figs. 4.11, 4.12 and 4.13 we show the effect of the metal cooling predicted by our model using the [el/Fe] vs. [Fe/H] plots. Thomas et al. (1998) already discussed the effect of a two- phase gas model relative to Mg. Referring to Fig. 4.12 we obtain a similar result, but the effect of our delay in the mixing is smaller. For the Si we have a similar behavior as can be seen in the Fig. 4.13. The differences between ours and Thomas et al.'s results are probably due to the different adopted yields for massive stars and IMF. In fact, Thomas et al. adopted Thielemann et al. (1996) yields and the Salpeter (1955) IMF.

A different result is obtained for the [O/Fe] vs [Fe/H] reported in Fig. 4.11. In this case, we find that the delay in the mixing leads to large differences in terms of chemical evolution models. We see that in the halo-thick disk phase, the predicted [O/Fe] values are much smaller than for the model with the IMA. The reason for this resides in the fact that in the model of F04 (our standard model), the yields used for O are the WW95 metallicity-dependent ones and in this case the delay induces a situation where the yields for Z=0, lower than those computed for the other metallicities, act for a longer time, thus producing the large depression in the [O/Fe] ratio. To demonstrate that this result is only due to the choice of nucleosynthetic yields, we plot in Fig. 4.14 the metal cooling delay model results using, for the oxygen, the yields at solar metallicity given by WW95. As we can see from this

figure, in this case the models with delay do not differ considerably from the standard model and the oxygen behaves similarly to the other α-elements. In Fig. 4.15 we report the [el/Fe] vs. [Fe/H] relations for the Mg and Si using for these two elements the metallicity dependent yields of WW95. As expected, the [el/Fe] ratios show a large depression in the halo-thick disk phase as in Fig. 4.11 due to the choice of metallicity-dependent yields. Therefore, we can conclude that the metallicity-dependent yields of WW95 are not compatible with a delayed enrichment of the halo.

Finally, in Figs. 4.16 and 4.17 we report age-metallicity relations in the solar neighborhood for [Fe/H] and [Mg/H] respectively, predicted by our metal cooling delay model using the stellar yields adopted in F04. Concerning the evolution of the [Fe/H], we compare our results with the observational data of Ramirez et al. (2007). As one can see, the effects of the delays are more visible in the age-metallicity relations than in the abundance ratios versus [Fe/H], and the reason is that in the abundance ratios these differences are partly erased. We conclude that all delays considered are compatible with the observations due to the very large data spread for the age metallicity relation, but we remind that the age-metallicity relation is not a good constraint for chemical models.

4.4 Summary

We studied the relaxation of IMA in chemical evolution models by means of the effects of a delay in the chemical enrichment produced by galactic fountain events and by means of a delay in the mixing due to chemical inhomogeneities in the disk (our metal cooling delay model).

Our main conclusions can be summarized as follows:

- In the solar neighborhood, we showed that the average delay produced by the galactic fountains has a negligible effect on the chemical evolution for all the α elements, we studied.

- In the [el/Fe] versus [Fe/H] relations, the main feature of the galactic fountain is an enhancement of the drop in the [el/Fe] ratios occurring because of the two infall scenario. In fact, the drop in the standard model of F04 is due to the halt of the SFR which produces a halt in the production of the α-elements whereas the Fe from Type Ia SNe continues to be produced. The galactic fountain delay has the effect of increasing the period during which there is no pollution from Type II SNe.

- Results produced by the model with a galactic fountain delay of 1 Gyr are not compatible with observational data. On the other hand, any delay < 1 Gyr could be acceptable, given the observed spread in the data.

- The time delay produced by a Galactic fountain generated by an OB association has a negligible effect on the abundance gradients in the Galaxy disk.

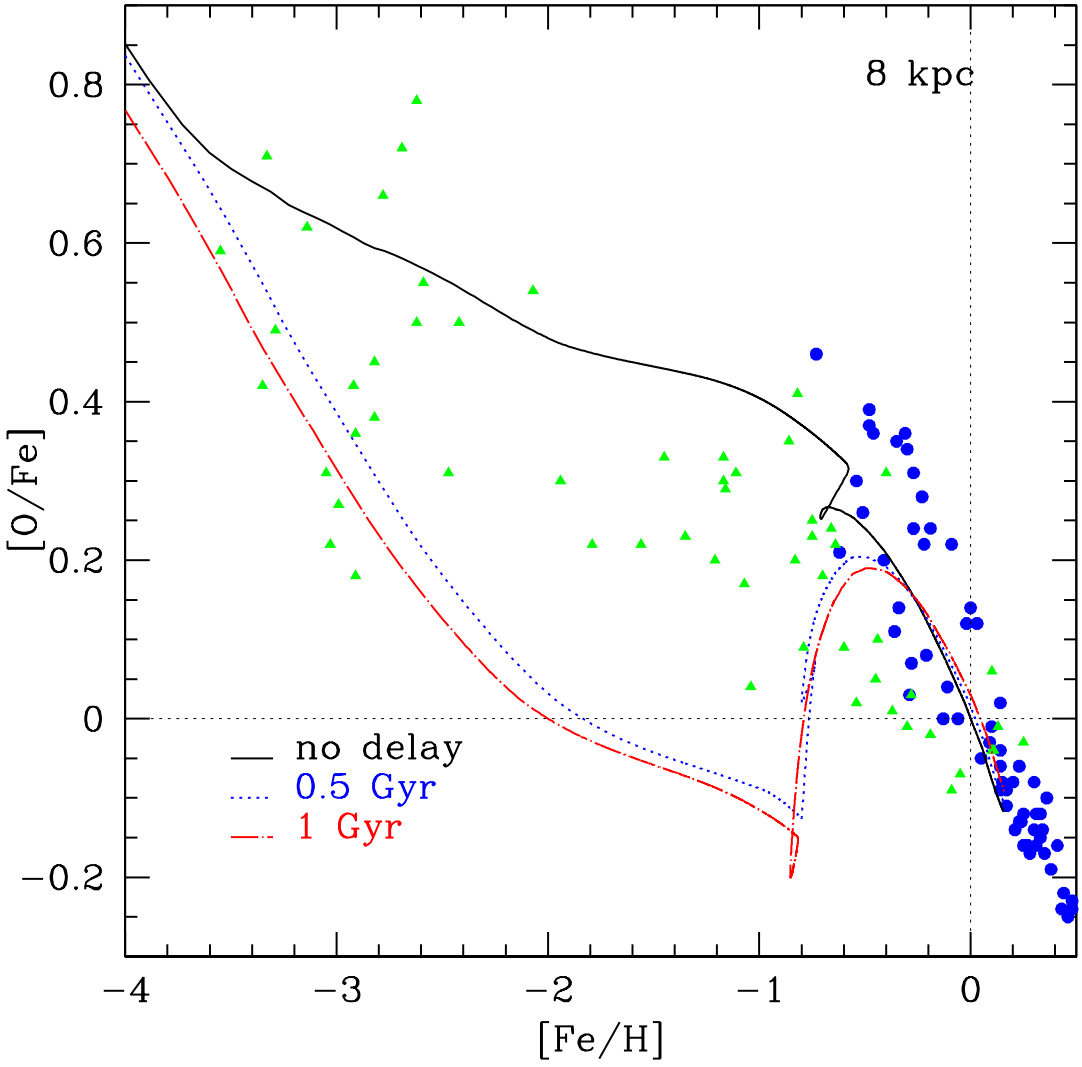

Figure 4.11: The abundance ratio [O/Fe] as a function of [Fe/H] in the solar neighborhood predicted by our metal cooling delay model. For the O we considered the metallicity dependent yields of WW95. Solid line: model without delay; dotted line and dashed dotted line: 0.5 and 1 Gyr delays, respectively. Symbols as in Fig. 4.2.

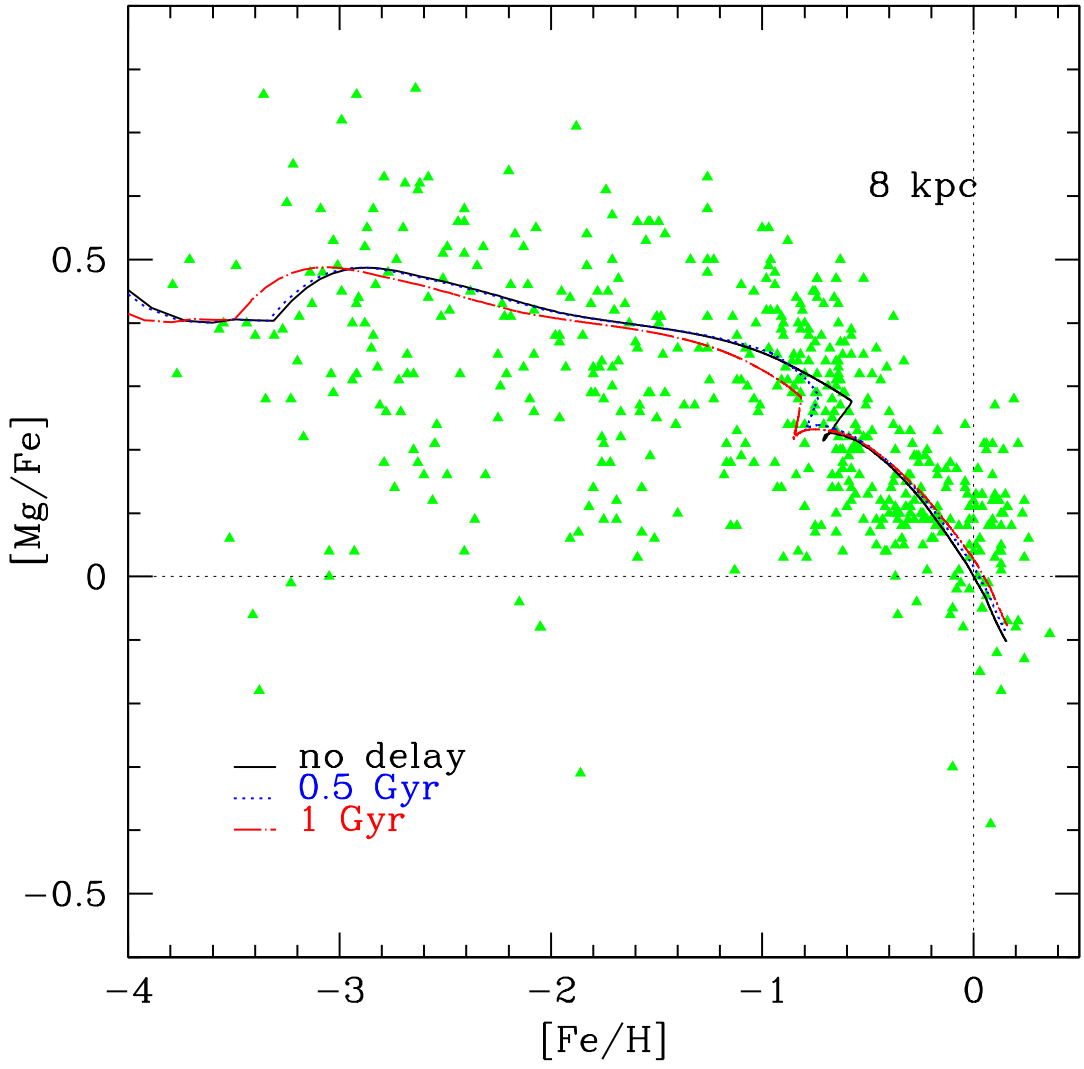

Figure 4.12: The abundance ratio [Mg/Fe] as a function of [Fe/H] in the solar neighborhood predicted by our metal cooling delay model. Notation as in Fig. 4.11.

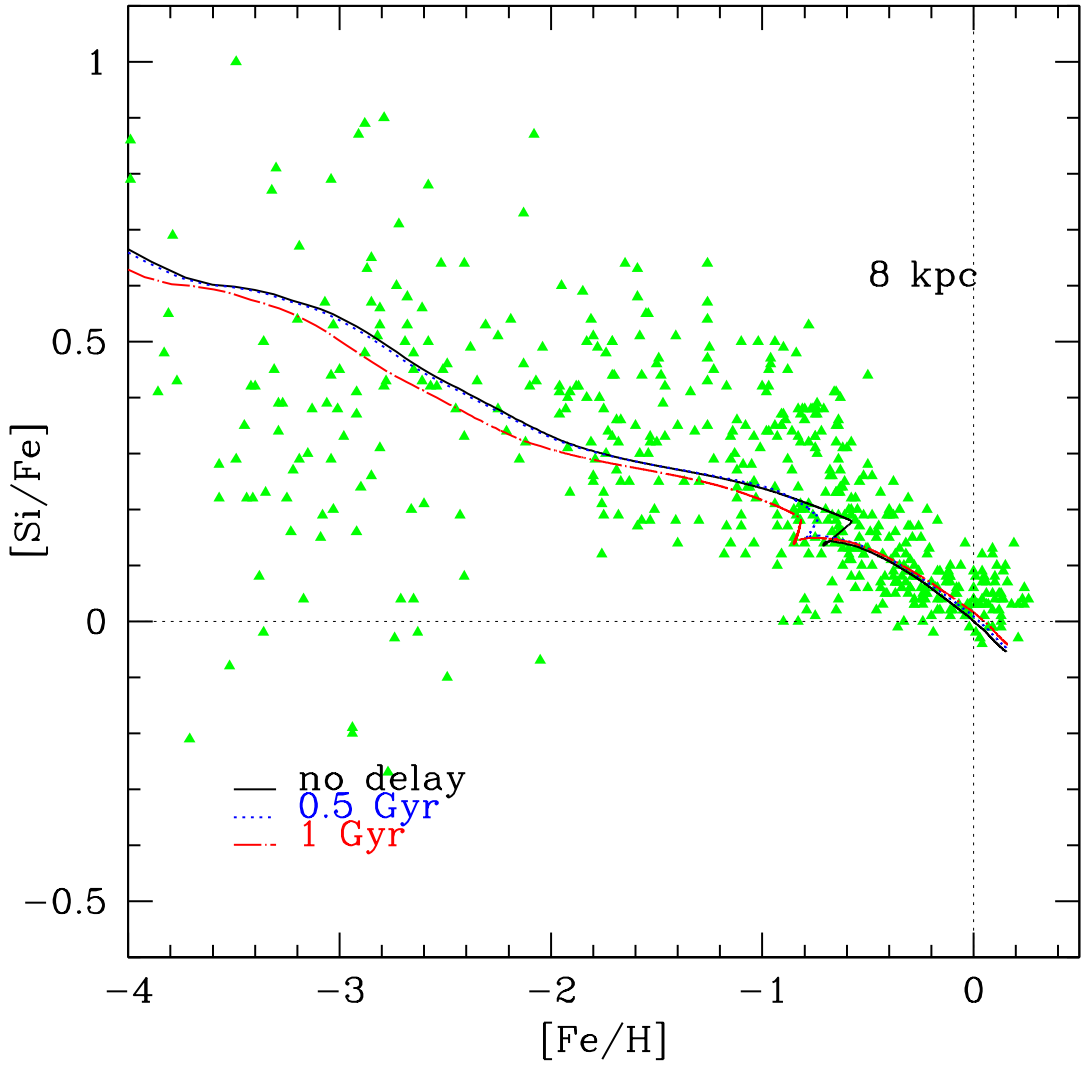

Figure 4.13: The abundance ratio [Si/Fe] as a function of [Fe/H] in the solar neighborhood predicted by our the metal cooling delay model. Notation as in Fig. 4.11.

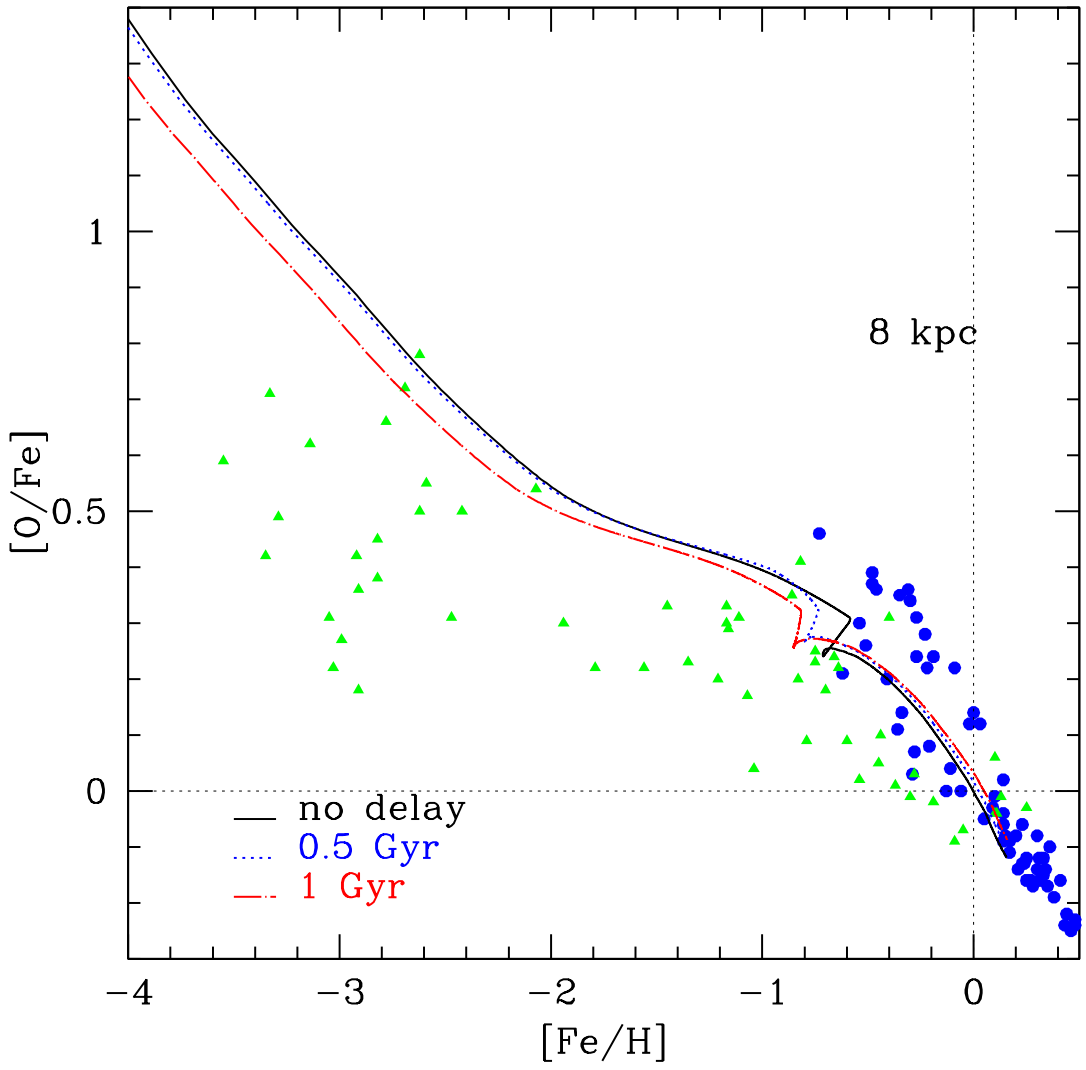

Figure 4.14: The abundance ratio [O/Fe] as a function of [Fe/H] in the solar neighborhood predicted by our metal cooling delay model. For the O we considered the solar yields of WW95. Notation as in Fig.4.11.

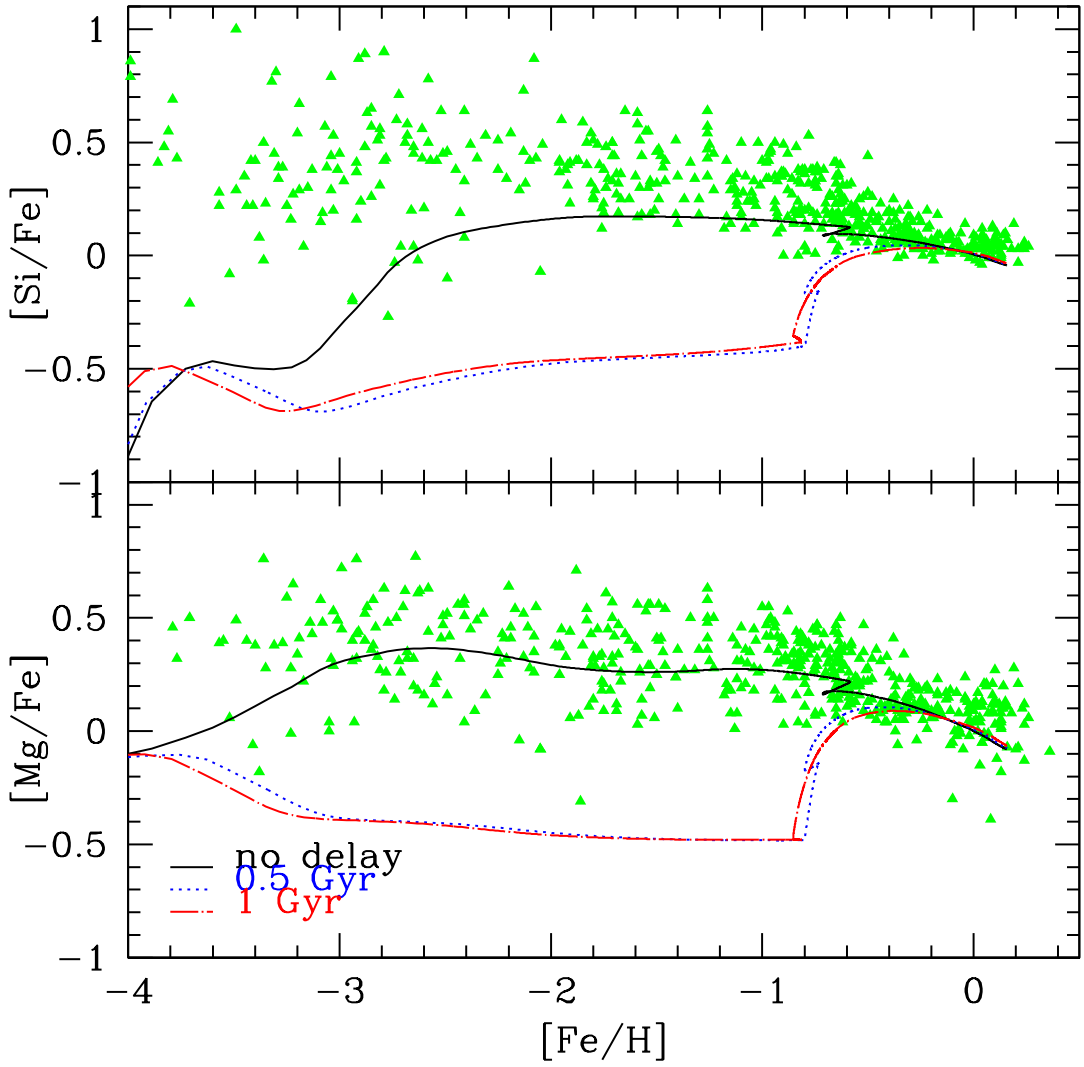

Figure 4.15: The abundance ratio [el/Fe] as a function of [Fe/H] for the Si and Mg in the solar neighborhood predicted by our metal cooling delay model. For the Si and Mg we considered the metal dependent yields of WW95. Notation as in Fig. 4.11.

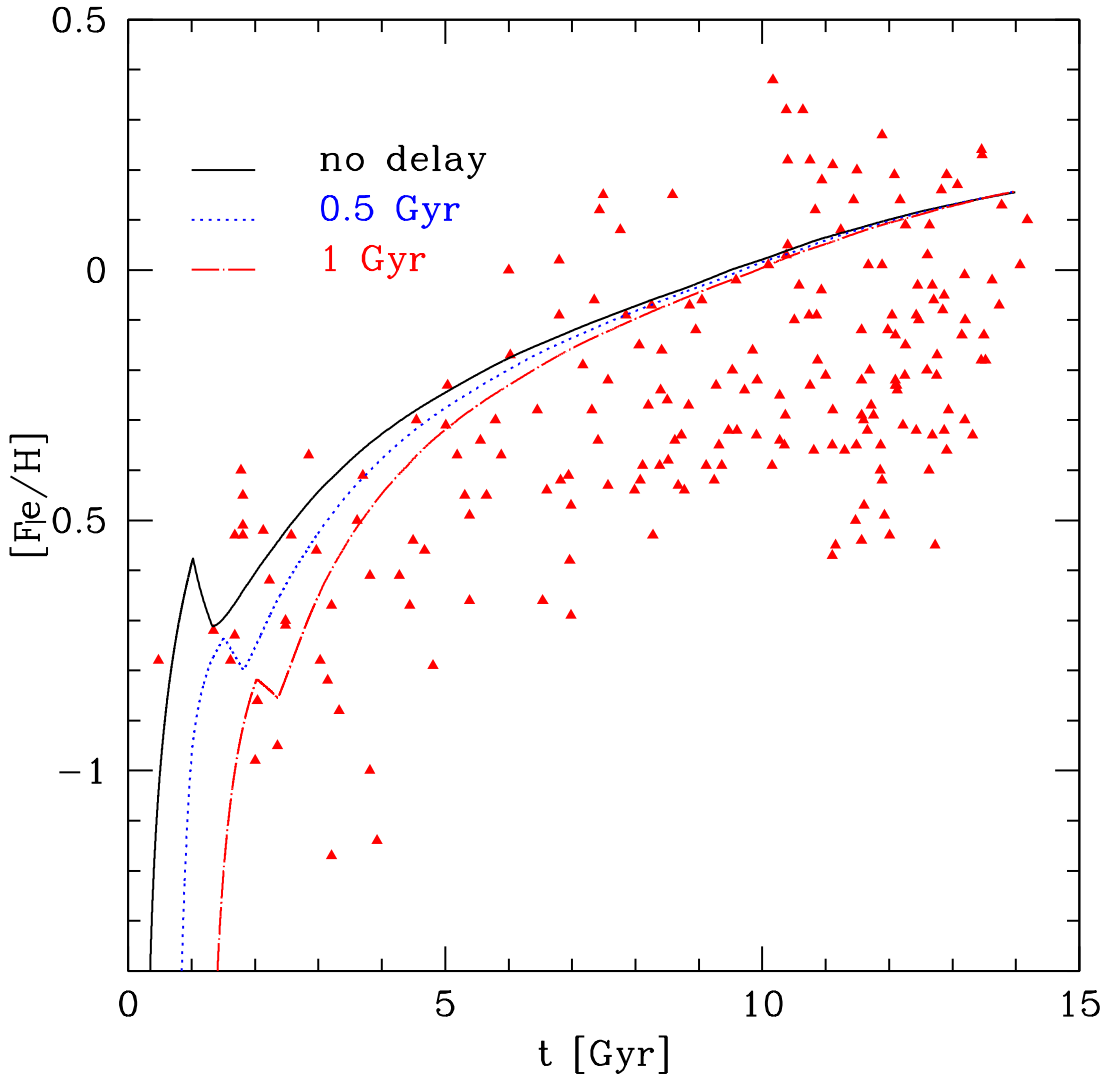

Figure 4.16: The abundance ratio [Fe/H] as a function of the galactic time [Gyr] in the solar neighborhood predicted by our metal cooling delay model. The data are taken from Ramirez et al. (2007) (filled red triangles). Notation as in Fig. 4.11.

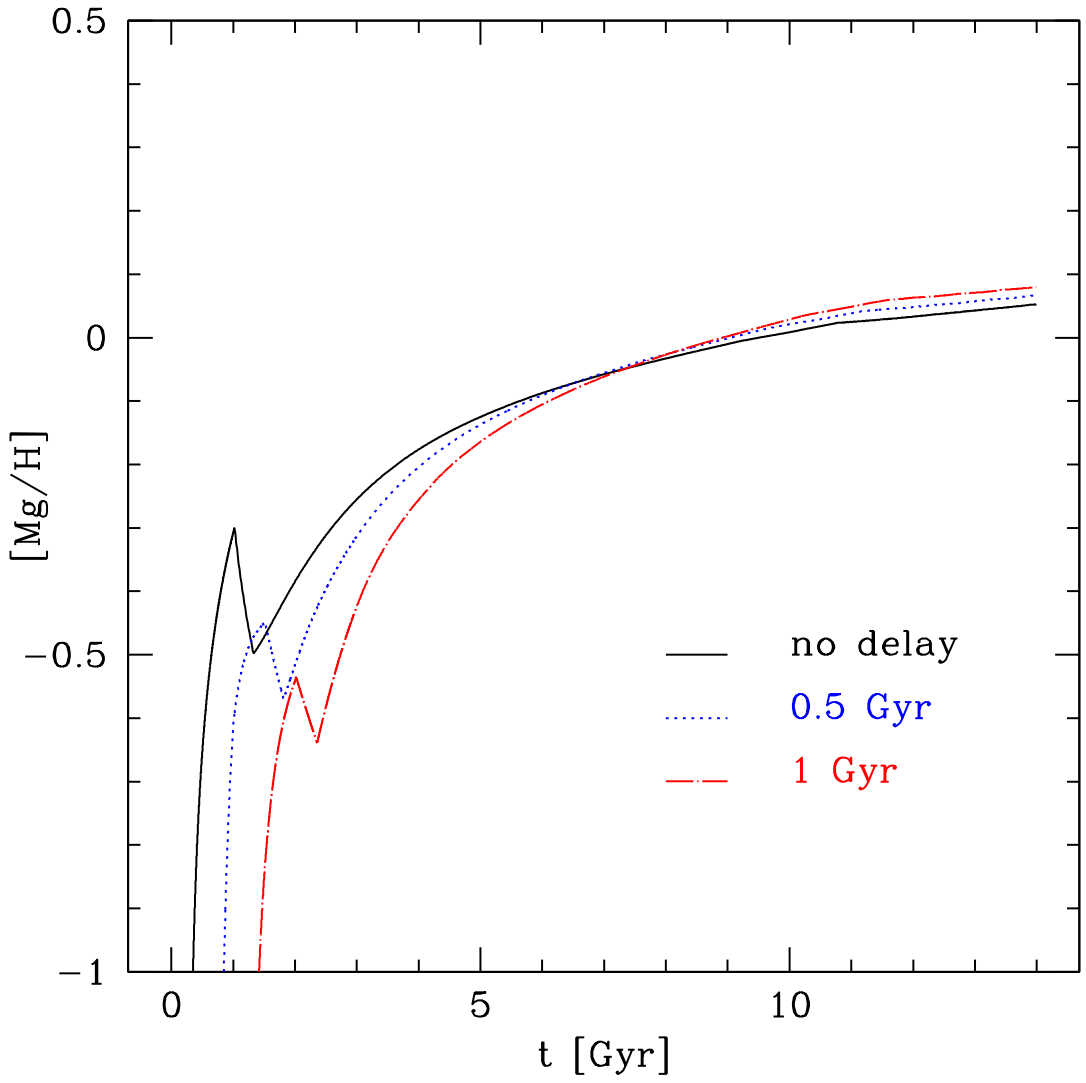

Figure 4.17: The abundance ratio [Mg/H] as a function of the galactic time [Gyr] in the solar neighborhood predicted by our metal cooling delay model. Notation as in Fig. 4.11.

- The metal cooling delay model with the assumed delays (which are those suggested in the literature) has a very small effect on the chemical evolution in the solar neighborhood if yields not depending on metallicity are used.
- On the other hand, in the case of the metal dependent yields of WW95, the results differ substantially from the reference model of F04 and do not fit the observations.

Chapter 5

The Effect of Different Type Ia Supernova Progenitors on Galactic Chemical Evolution

In this Chapter we show some results relative to the choice of the progenitors of Type Ia SNe. To do that we assumed the formulation described in Matteucci et al. (2006) of the delay time distribution (DTD) of the Type Ia SNe explosions, following Greggio (2005). The DTD describes the explosion times of Type Ia SNe and if convolved with the SFR if gives Type Ia SNe rate.

5.0.1 The assumed DTDs

As mentioned already in the Introduction there are several progenitor models proposed for Type Ia SNe. In particular:

- The merging of two C-O WDs, due to gravitational wave radiation, which reach the Chandrasekhar mass and explode by C-deflagration (Iben & Tutukov 1984). This is known as double-degenerate (DD) scenario. In the original paper of Iben & Tutukov the progenitor masses are in the range 5-9$M_{\odot}$ to ensure two WDs of at least $\sim 0.7M_{\odot}$ in order to reach the Chandrasekhar mass. In Greggio (2005) the range of progenitors is 2.0-8.0$M_{\odot}$, so that different combinations of WD masses are allowed, although always leading to exceed the Chandrasekhar mass. The clock for the explosion in this scenario is given by the lifetime of the secondary plus the gravitational time delay.

- The C-deflagration of a Chandrasekhar mass C-O WD after accretion from a non-degenerate companion (Whelan & Iben 1973; Munari & Renzini 1992; Kenyon et al. 1993). This model is known as the single-degenerate (SD) one. The main problem with this scenario is the narrow range of permitted values of the mass accretion rate in order to obtain a stable accretion, instead of an unstable accretion with a consequent nova explosion and mass loss. In this case, in fact, the WD never achieves the Chandrasekhar mass. In particular,

Nomoto et al. (1984) found that a central carbon-deflagration of a WD results for a high accretion rate ($\dot{M} > 4 \cdot 10^{-8}\, M_{\odot}\, \mathrm{yr}^{-1}$) from the secondary to the primary star (the WD). They found that $\sim (0.6 - 0.7)\ M_{\odot}$ of Fe plus traces of elements from C to Si are produced in the deflagration, well reproducing the observed spectra. The clock for the explosion here is given by the lifetime of the secondary star.

- A sub-Chandrasekhar C-O WD exploding by He-detonation induced by accretion of He-rich material from a He star companion (Tornambé & Matteucci 1987; Limongi & Tornambé 1991).

We test the effects of five DTDs on the detailed chemical evolution of F04:

- The Matteucci & Recchi (2001, hereafter MR01) one, which is practically the same as Greggio & Renzini (1983) (this model was included in the F04), and is based on the single degenerate model for Type I SN progenitors (see Matteucci et al. 2006 for details). In this DTD the fraction of prompt Type Ia SNe (Type Ia exploding inside the first 100 Myr since the beginning of star formation) is 13%.This formulation has proven one of the best to describe the chemical evolution of most galaxies. The very first SNe Ia to explode in this scenario are systems made of an 8+8 $M_{\odot}$ which take $\sim 30 - 35$ Myr.

- The DTD suggested by Greggio (2005) for the DD scenario: in particular, the DTD characterized by the exponent of the distribution function of the final separations, $\beta_a = -0.9$, by the exponent of the gravitational delay time distribution $\beta_g = -0.75$ and by a maximum nuclear delay time (lifetime of the secondary star) $\tau_{n,x} = 0.4$ Gyr. The reason for choosing these parameters resides in the fact that they ensure a not too flat distribution of separations, which seems to be required to reproduce the specific Type Ia SN rate in galaxies as a function of colors (see Greggio & Cappellaro 2009). In this DTD the fraction of prompt Type Ia SNe is 10%. The very first SNe Ia to explode in this scenario are systems made of an 8+8 $M_{\odot}$ which takes $\sim 30 - 35$ Myr plus the minimum gravitational time delay (1 Myr, Greggio 2005).

- The DTD of Mannucci et al (2006) (hereafter MVP06). Here the fraction of prompt Type Ia SNe is 50%. The very first systems explode also after 30-35 Myr. This DTD is practically bimodal with a fraction of also ~ 50 % of tardy Type Ia SNe (e.g. exploding after 100 Myr).

- The DTD proposed by Strolger et al. (2004), hereafter S04 with a maximum at 3-4 Gyr. Here the very first systems explode after $2.5 \cdot 10^8$ years. Therefore, there are no prompt Type Ia SNe.

- The DTD proposed by Pritchet et al. (2008, PHS08), with DTD $\propto t^{-0.5}$, where the fraction of prompt Type Ia SNe is $\sim 4\%$. The one proposed by Totani et al. (2008) goes like t^{-1} and we did not test it since these authors have already shown that it is very similar to the DTD of Greggio (2005) for the DD scenario.

In Fig. 5.1 we show the different DTDs including those mentioned above. As one can see, while the DTDs of the SD and DD scenarios are similar, those of MVP06 and S04 and PHS08 are quite different. We did not take into account the Hachisu et al. (1996; 1999) model since its effects have been already discussed in Kobayashi et al. (1998) and MR01.

5.0.2 The calculation of the Type Ia SN rate

Once a DTD has been assumed, the Type Ia SN rate is computed according to Greggio (2005):

$$R_{Ia}(t) = k_\alpha \int_{\tau_i}^{min(t,\tau_x)} A(t-\tau)\psi(t-\tau)DTD(\tau)d\tau \tag{5.1}$$

where $\psi(t)$ is the SFR and $A(t-\tau)$ is the fraction of binary systems which give rise to Type Ia SNe and in principle it can vary in time. Here we will assume A to be a constant. It is worth noting that the fraction A represents the fraction of binary systems with those particular characteristics to give rise to Type Ia SNe relative to the whole range of star masses (0.1-100$M_\odot$). We want to underline that the formulation used in eq. (3.26) for computing the Type Ia SN rate is equivalent to eq .(5.1) although A is defined as a fraction of binary systems rise to Type Ia SNe in the range 3 - 16 $M_\odot$. The time τ is the delay time defined in the range (τ_i, τ_x) so that:

$$\int_{\tau_i}^{\tau_x} DTD(\tau)d\tau = 1 \tag{5.2}$$

where τ_i is the minimum delay time for the occurrence of Type Ia SNe, in other words is the time at which the first SNe Ia start occurring, and τ_x is the maximum delay time. Clearly these delay times vary according to the assumed progenitor scenario: in particular, in the SD scenario τ_x is just the maximum nuclear delay time, namely the lifetime of the smallest secondary star, whereas in the DD model is the sum of the maximum nuclear delay time and the maximum gravitational delay time.

Finally, k_α is the number of stars per unit mass in a stellar generation and contains the IMF.

In particular:

$$k_\alpha = \int_{m_L}^{m_U} \phi(m)dm \tag{5.3}$$

with the normalization condition for the IMF being:

$$\int_{m_L}^{m_U} m\phi(m)dm = 1 \tag{5.4}$$

where $m_L = 0.1M_\odot$ and $m_U = 100M_\odot$ and define the whole range of existence of the stars.

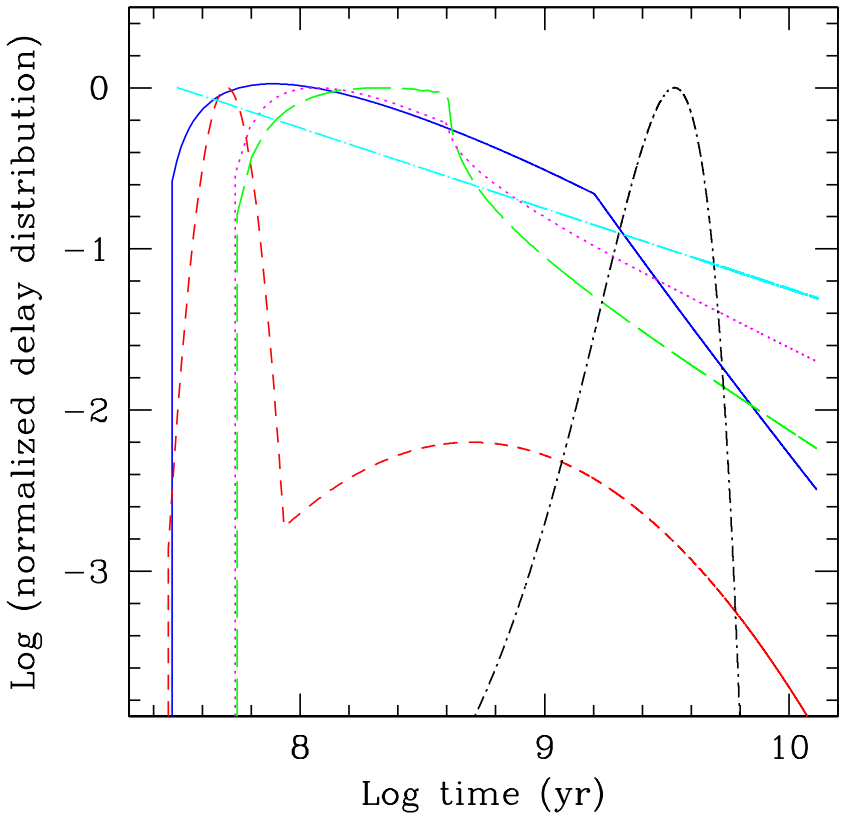

Figure 5.1: Various DTD functions normalized to their own maximum value: the continuous blue line is the DTD of MR01; the long dashed green line is the DTD of Greggio (2005) for the DD wide channel; the dotted magenta line is the DTD for the DD close channel of Greggio (2005); the dashed red line is the DTD of MVP06; the short dashed-dotted black line is the DTD of S04, the cyan long dashed-dotted line is the DTD of PHS08.

5.1 Predicted [O/Fe] vs. [Fe/H] with different DTDs

In Fig. 5.2 we show the predicted Type Ia SN rates for the solar vicinity in the framework of the two-infall model previously described and for the considered DTDs. We have chosen the parameter A in eq.(5.1) in order to reproduce the present time Type Ia SN rate in the Galaxy ($\sim 0.3\, SNe\, century^{-1}$, Cappellaro et al. 1999). It is worth noting that a value of A$\sim$ 0.0025 for all the DTDs was chosen, in agreement with Matteucci et al. (2006), with the exception of the PHS08 DTD for which the parameter A=0.0002. The PHS08 DTD is, in fact, predicting the largest fraction of SNe Ia exploding with large delays (see Fig. 5.1). That means that a larger fraction of long-living progenitors (born several Gyr ago, when the SFR was much higher, relative to the other models, is exploding at the present time. Therefore, a smaller value of A is required to reproduce the present-time SN Ia rate in the Galaxy. The oscillating behavior shown by some Type Ia SN rates in the last couple of Gyr is clearly related to the oscillations in the star formation rate, due to the assumed threshold in the gas density. In particular, models with a larger percentage of prompt Type Ia SNe show the oscillations at late times (SD model and MVP06 model), whereas the models of S04, Greggio (2005) and PHS08, having null, 10% and 4% fractions of prompt Type Ia SNe, respectively, show negligible oscillations.

As one can see, it is evident the effect of the gap in the star formation rate, as predicted by the two-infall model, for the DTDs of MVP06, SD, DD and PHS08 models. For the DTD of S04, there is no gap since the minimum delay in the occurrence of Type Ia SNe is much longer than for the other DTDs. There are no prompt Type Ia SNe and most of the SNe Ia start occurring only after the gap in the star formation.

In Fig. 5.3 we show the effect of the different DTDs on the [O/Fe] vs. [Fe/H] diagram. For [Fe/H]$>$ -1.0, the [O/Fe] ratio starts declining as a consequence of the increase of the Fe production from Type Ia SNe. Clearly, the DTD is fundamental in determining the moment, and therefore the [Fe/H] value, at which this process becomes important. We remind that this effect does not depend on details of the star formation history but mainly on the time delay between the chemical enrichment from SNe II and SNe Ia. On the basis of what just said, it is therefore important to see which DTD best fits the abundance data.

For the DTD suggested by S04 where the delay in the appearance of the first Type Ia SNe is much longer than in the other cases, the [O/Fe] ratio shows a longer plateau than in the other models, and the knee in the [O/Fe] ratio occurs at [Fe/H]$\sim$ -0.6 dex. The PHS08 DTD produces results not very different from the SD model but it predicts a too low solar Fe abundance ($[Fe/H]_{\odot}$=-0.16dex) and a too high solar $[O/Fe]_{\odot}$=0.22dex, as opposed to all the other models where the solar $[Fe/H]_{\odot}$ and $[O/Fe]_{\odot}$ are very close to zero (see Table 5.1 where we show the predicted solar ratios). Note that the model results are always normalized to their own predicted solar values.

A larger number of prompt Type Ia SNe clearly produces lower [O/Fe] ratios

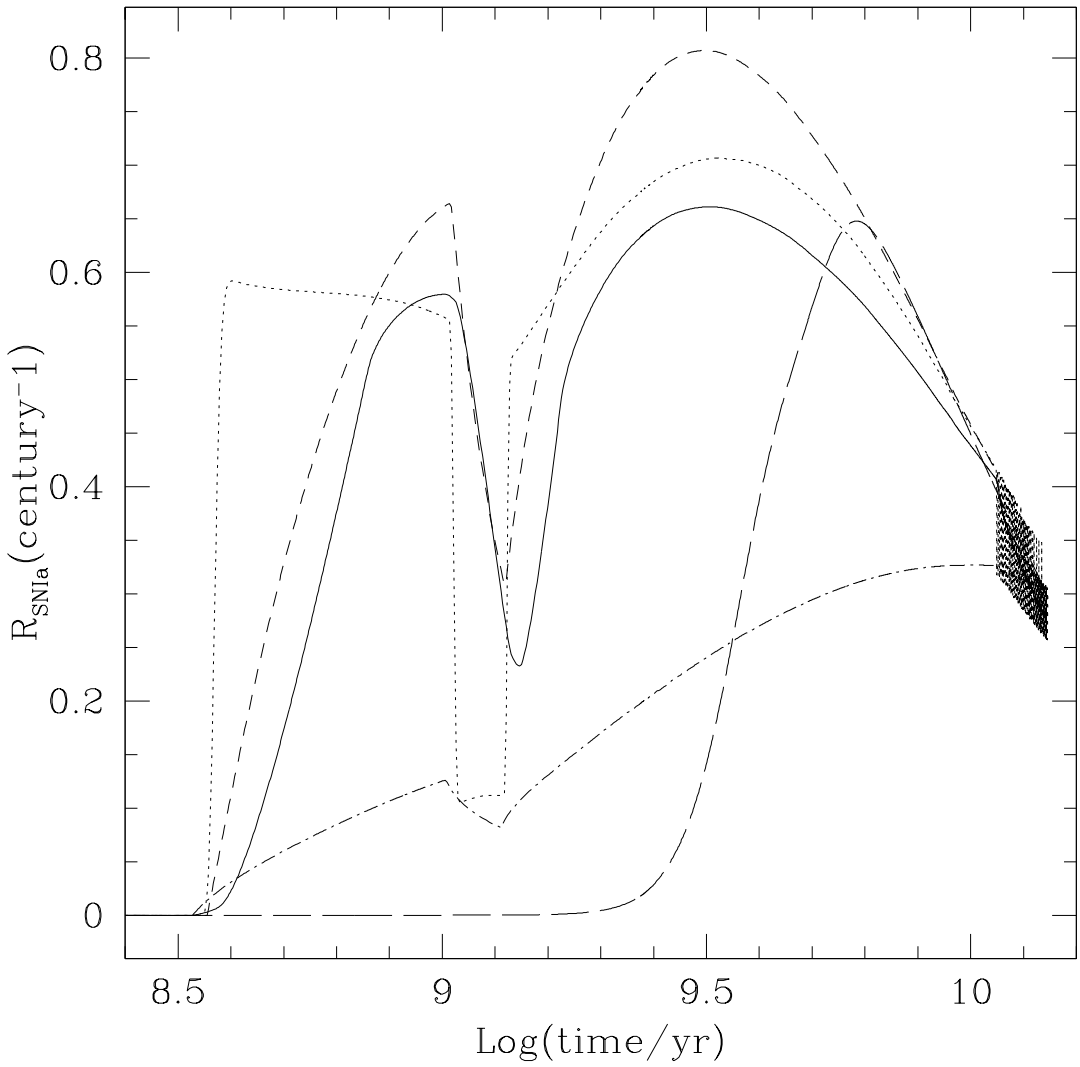

Figure 5.2: The predicted Type Ia SN rates in the solar vicinity in the framework of the two-infall model. The five curves refer to different DTDs. In particular, the dotted line represents the DTD of MVP06; the continuous line represents the SD model with the DTD from MR01 and the short dashed line the DD model with the DTD of Greggio (2005) for the DD wide channel. Finally, the long dashed line represents the DTD suggested by S04 and the dashed-dotted line the DTD of PHS08. The rates are expressed in SN per century, and are all normalized to reproduce the present time Type Ia SN rate in the MW.

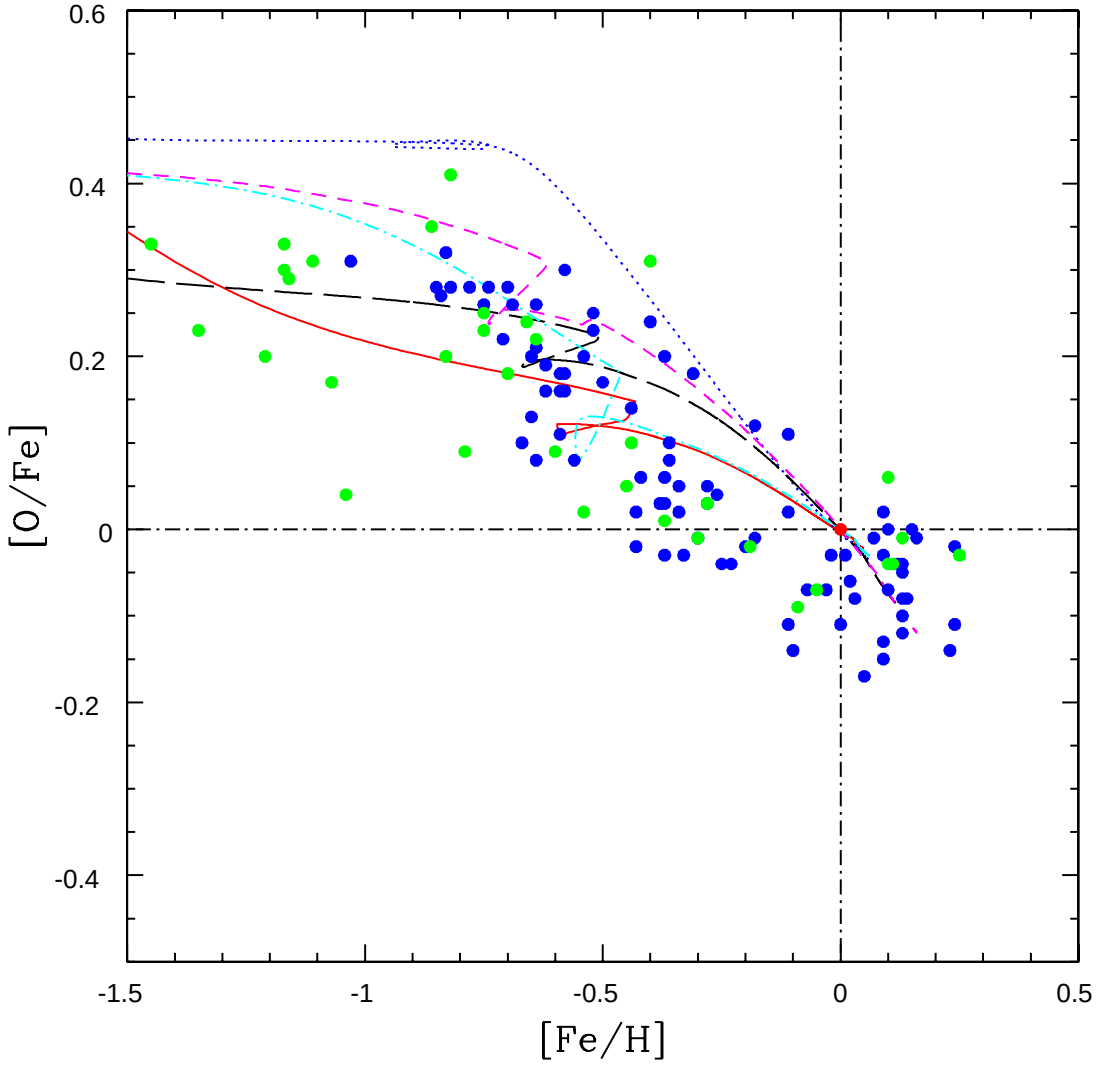

Figure 5.3: Comparison of all the models with all the studied DTDs: the short dashed curve refers to the DTD of MR01; the continuous curve refers tothe DTD of MVP06; the dotted line represents S04 DTD; the long dashed curve refers to the DTD of PHS08; the dashed-dotted curve refers to the DTD of the DD scenario (wide channel) of Greggio (2005). The model results are normalized to their own predicted solar values. The data are taken from the compilation of F04. The solar position is marked by a red dot.

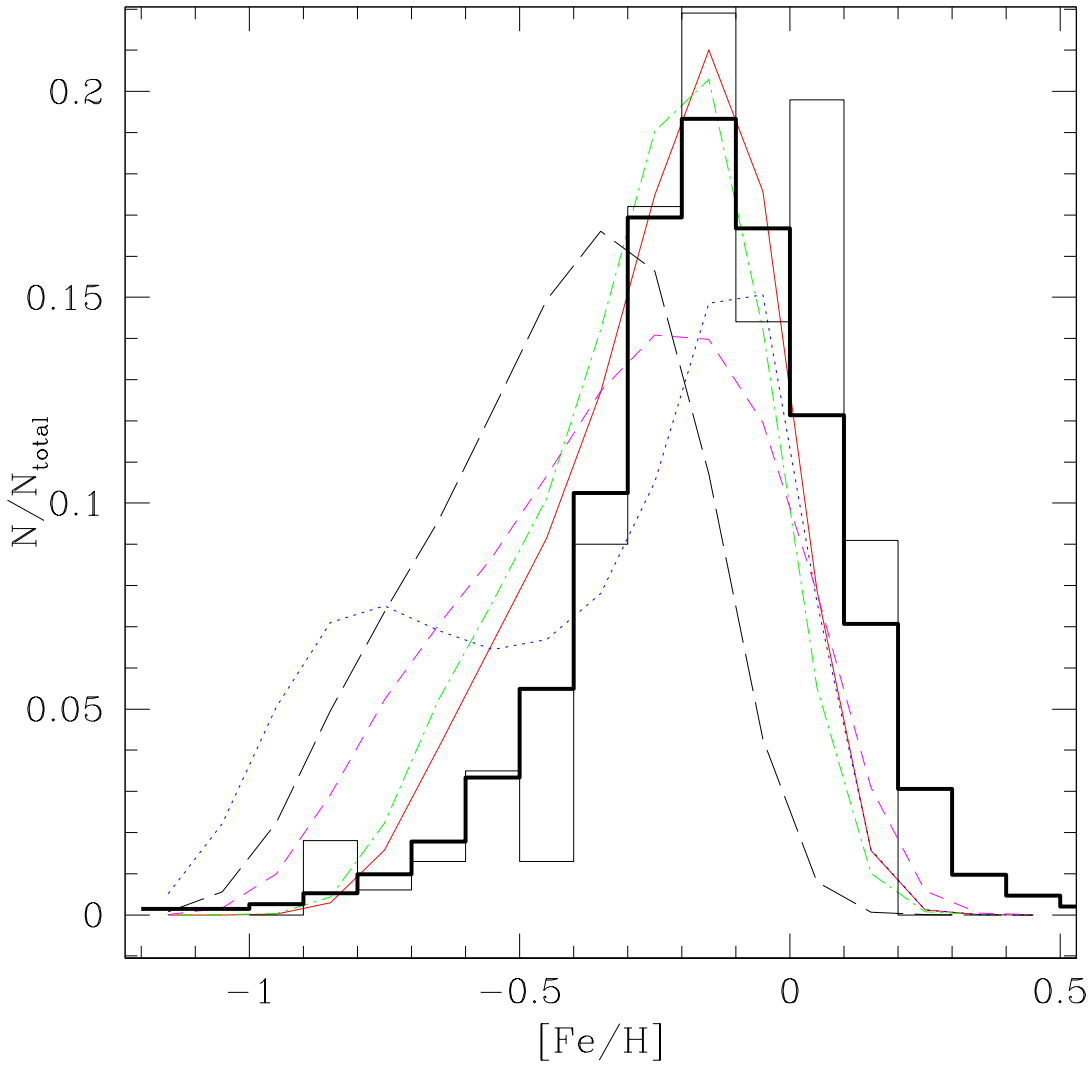

Figure 5.4: The G-dwarf metallicity distribution in the solar vicinity. The data are from the Geneva-Copenhagen Survey of the Solar Neighborhood, Nordström et al. (2004) (thick line histogram) and the data by Jørgensen (2000) (thin-line histogram). The models refer to: S04 DTD (dotted line), PSH08 DTD (long dashed line), DD model (dashed-dotted line), MVP DTD (continuous line) and SD model (short dashed line).

Table 5.1: Predicted $[O/Fe]_{\odot}$ and $[Fe/H]_{\odot}$ values at the time of formation of the solar system. Normalization to the solar values of Asplund et al. (2005). The solar values in these units are identically zero.

Model	$[O/Fe]_{\odot}$	$[Fe/H]_{\odot}$
SD	0.095	-0.013
DD	0.095	-0.038
MVP06	0.07	-0.003
S04	0.06	0.01
PHS08	0.22	-0.16

in this [Fe/H] range with respect to models depressing the number of prompt SNe in favor of tardy ones. Although the spread existing in the data prevents us from drawing firm conclusions, from this comparison it turns out that the S04 model tends to predict too high values of [O/Fe] in the range -1.5 $\leq$ [Fe/H]$\leq$ -0.2. On other hand, MVP06 DTD predicts too low [O/Fe] in the same range. From numerical experiments, we can say that the MVP06 DTD with $\sim$ 30% of prompt SNe would fit better the data, and it would be still compatible with the findings of MVP06. It is also interesting to note that the DTDs influence the [Fe/H] at which the gap in the star formation between the halo-thick disk and the thin disk phases is visible. This gap produces a loop in the [O/Fe] behaviour and is naturally produced by assuming a threshold gas density in the star formation. Observationally, a gap in the abundance ratios has been claimed by Fuhrmann (1998) and Gratton et al. (2000). In particular, the gap was observed at a [Fe/H] between -1.0 and -0.5 dex, corresponding to the transition phase between the thick and the thin disk. If confirmed, this gap can impose constraints on the history of star formation. In our plots the gap occurs at larger [Fe/H] values going from the SD to PHS08, DD and MVP06 DTD . For the S04 DTD, the gap is not visible and the reason is that Type Ia SNe start exploding in a non negligible number only after the gap. Therefore, the effect of the halt of oxygen production, while the Fe is still produced by the Type Ia SNe exploding during the gap, is lost. This effect produces in the other models the loop in the [O/Fe] ratio. If the gap really exists this would further strengthen the conclusion that prompt Type Ia SNe should exist and be a non negligible fraction of all SNe Ia.

In summary, the SD and DD models together with the bimodal distribution of MVP06 all produce acceptable results, although a 50% of prompt Type Ia SNe appears too large. The DTD from PHS08 and S04 are probably less likely although the spread in the data prevents us from drawing firm conclusions.

Therefore, we checked our results on a very important observational constraint: the G-dwarf metallicity distribution. In Fig. 5.4 we show the predictions for the G-dwarf metallicity distribution of all our models compared with observational data. This Figure shows that two models can be definitely ruled out: the PHS08 and the S04. Both of these models contain empirically derived DTDs. They predict too

many metal poor stars below [Fe/H]< -1.0 dex (the so-called G-dwarf problem), and this is due to the fact that in both cases the Fe abundance increases more slowly that in the other three models (SD, DD, MVP06) thus producing too many metal poor stars.The reason for that resides in the small number of prompt Type Ia SNe in the PHS08 and S04 models. In particular, the S04 model shows two distinct peaks in the G-dwarf metallicity distribution and this is due to the fact that at the beginning of the thin disk formation only SNeII enrich the gas in Fe and the bulk of Fe comes with a large delay, thus creating the second peak. On the other hand, the other models all produce acceptable results, with the DD and MVP06 models being the best. Note that all the models predict less metal rich stars than observed by Norström et al. (2004) which is the largest and more accurate survey of G and F dwarfs. This is a problem for pure models of chemical evolution which do not take into account the possibility of stellar migration. In fact, because of interaction between stars and transient spiral density waves (Roskar et al. 2008), stars born in the inner part of the disk can be scattered at larger galactocentric distances and this could be the explanation for the existence of metal rich stars in the solar vicinity.
In conclusion, the adoption of the DTD of MR01 which we have adopted throughout all this thesis is justified by the fact that is among the best ones to reproduce the main features of the MW.

Chapter 6

Conclusions

The main goal of this thesis work was the study the effects of galactic fountains on the chemical evolution of the Milky Way.

We first focused on the study of the chemical evolution of the superbubbles formed by multiple SN explosions and how they get polluted from the metals produced by SNe. We have studied the evolution of a supershell powered by the energetic feedback of a typical Galactic OB association at various Galactocentric radii. Based on the Kompaneets (1960) approximation, we have found analytical solutions for the temporal evolution of the supershell and we have established criteria for its fragmentation. From this fragmentation clouds are created and thrown out of the disk.

Given the self-similar behavior of the Kompaneets solution, the clouds are formed at the same scale height ($\sim$ 450 pc), irrespective of the number of SNe in the OB association or of the Galactocentric radius at which the OB association lies. Assuming that the ejecta of the dying stars of the OB association instantaneously mix with the supershell, we have been able to calculate the chemical composition of the clouds and in particular their $[O/Fe]$.

We have considered four different types of OB associations (containing 10, 50, 100 and 500 SNe, respectively) and three different initial throwing coordinates (4, 8 and 12 Kpc, respectively). Once the clouds are formed and can leave the disk, producing so called *galactic fountains*, we follow their orbits either assuming a purely ballistic model, or introducing a viscous force acting between the cloud and the surrounding hot halo gas. Our main conclusions can be summarized as follows:

- If the initial metallicity of the OB association is solar, the pollution from the dying stars has a negligible effect on the chemical composition of the clouds. In particular, the $[O/Fe]$ abundance ratio reaches at most ~ 0.025 dex in a model in which the throwing coordinate is $R_0 = 12$ kpc. Only starting from very low metallicities (less than $1/100\ Z_\odot$) it is possible to produce a significant enrichment of α-elements relative to Fe.

- Both in the ballistic and in the viscous interaction models the maximum height reached by the clouds is not very large. Only for OB associations composed

of 500 SNe it is possible to eject clouds up to heights larger than 2 kpc above the plane of the Galaxy.

- The range of the cloud orbits is also quite small. The clouds are generally directed outwards but the average landing coordinates differ from the throwing coordinates by $\sim$ 1 kpc at most. Only for a throwing coordinate of 12 kpc and an OB association made of 500 SNe does the ballistic model predict a landing coordinate $\sim$ 2 kpc larger than the throwing one.

- Models including a viscous interaction between clouds and the extra-planar gas predict smaller ranges of the cloud orbits. Indeed, the drag experienced by the cloud brakes it and therefore it shortens its journey above the Galactic plane.

- The high velocity cloud Complex C has a mass, velocity and inferred height above the plane inconsistent with the results of our models. Its oxygen over-abundance ($[O/Fe]$=0.12 dex) can be reproduced only if we assume a large OB association with metallicity 0.1 $Z_{\odot}$ or smaller, therefore its Galactic origin cannot be completely ruled out on the basis of its chemical composition alone, but the kinematical data suggest a different formation mechanism. The intermediate velocity cloud Arch IV instead has velocities and heights above the plane that are easily reproduced by our models, but its $[O/Fe]$ =0.25 dex is much larger than the one of Complex C, and it can be explained only by assuming initial metallicities smaller than 1/100 $Z_{\odot}$, which are unlikely at the present time for the Galactic disk. Therefore, it is unlikely that the two studied clouds originated in a Galactic fountain motion.

With this work for the first time we included in a detailed chemical evolution model for the Milky Way the effects of galactic fountains. As we have concluded that the range of the cloud orbits originated from the break out of a supershell is quite small, it is unlikely that galactic fountains can affect abundance gradients on large scales. However the fountains take a finite and non-negligible time to orbit around and fall back into the Galaxy. This implies a delay in the mixing of metals in the interstellar medium, which conflicts with the instantaneous mixing assumption.

We studied the relaxation of instantaneous mixing approximation in chemical evolution models by means of the effects of a delay in the chemical enrichment produced by galactic fountain events. We also studied the case of a delay in mixing due to the cooling timescale of the gas freshly produced by dying stars.

Our main conclusions can be summarized as follows:

- In the solar neighborhood, we showed that the average delay produced by the galactic fountains generated by typical OB associations has a negligible effect on the chemical evolution for all the α elements.

- In the $[\alpha/Fe]$ versus $[Fe/H]$ relations, the main feature of the galactic fountain is an enhancement of the drop in the $[\alpha/Fe]$ ratios occurring at $[Fe/H] \sim -1.0$

dex in all models and due to the two-infall episodes forming the Milky Way. In fact, the two infall model plus a gas threshold for star formation produce a gap in the SFR between halo-thick disk and thin disk formation. This drop of $[\alpha/Fe]$ is therefore due to the fact that α elements are not produced during the gap whereas Fe is continuously produced by Type Ia SNe. The galactic fountain delay has the effect of increasing the period during which there is no pollution from Type II SNe.

- Results produced by the model with a galactic fountain delay of 1 Gyr are not compatible with observational data. On the other hand, any delay < 1 Gyr could be acceptable, given the observed spread in the data. However, a delay of 1 Gyr can be produced only by super star clusters like the ones observed in M81 and not by the OB associations observed in the disk of the Galaxy.

- The time delay produced by a Galactic fountain generated by a typical OB association has also a negligible effect on the abundance gradients in the Galaxy disk.

- The metal cooling delay model with the assumed delays (which are those suggested in the literature) has a very small effect on the chemical evolution in the solar neighborhood if yields not depending on metallicity are used.

- On the other hand, in the case of the metal dependent yields of Woosley & Weaver (1995), the results differ substantially from the reference model of François et al. (2004) and do not fit the observations.

Finally, we also investigated how different hypotheses about Type Ia SN progenitors can affect the chemical evolution model for the Galaxy. We found out that the adoption of the single degenerate progenitor model, which we have adopted throughout all this thesis is fully justified by the fact that it is one of the best progenitor models to reproduce the main features of the Milky Way.

Appendix A

Abundances of O and Fe in the supershell

In the following tables we summarize all our results concerning the abundances of oxygen and iron calculated with our model for the initial throwing radial coordinates $R_0 = 4, 8, 12$ kpc and for metallicities: $Z_\odot$, $0.1 \times Z_\odot$, $0.01 \times Z_\odot$, $10^{-4} \times Z_\odot$.

Table A.1: $Z = Z_{\odot}$ 8 kpc

Number of SNe	$M_{*Fe_{56}}$	$M_{*O_{16}}$	M_{*ej}	$M_{ShellFe_{56}}$	$M_{ShellO_{16}}$	M_{tot}	$X_{*Fe_{56}}$	$X_{*O_{16}}$	$[O/Fe]$
10	0.95	10.28	1.16×10^2	678.40	5.56×10^3	57.91×10^4	1.17×10^{-3}	9.60×10^{-3}	1.97×10^{-4}
50	3.95	49.89	4.77×10^2	681.40	5.60×10^3	57.94×10^4	1.17×10^{-3}	9.67×10^{-3}	1.36×10^{-3}
100	6.99	97.55	8.52×10^2	684.44	5.69×10^3	57.98×10^4	1.18×10^{-3}	9.75×10^{-3}	3.11×10^{-3}
500	24.69	437.46	3.18×10^3	702.14	5.99×10^3	58.22×10^4	1.21×10^{-3}	1.03×10^{-2}	1.74×10^{-2}

Table A.2: $Z = 0.1 \times Z_{\odot}$ 8 kpc

Number of SNe	$M_{*Fe_{56}}$	$M_{*O_{16}}$	M_{*ej}	$M_{ShellFe_{56}}$	$M_{ShellO_{16}}$	M_{tot}	$X_{*Fe_{56}}$	$X_{*O_{16}}$	$[O/Fe]$
10	0.95	9.33	1.14×10^2	68.70	5.64×10^2	57.91×10^4	1.19×10^{-4}	9.75×10^{-4}	1.17×10^{-3}
50	3.95	45.48	4.81×10^2	71.70	6.01×10^2	57.95×10^4	1.24×10^{-4}	1.04×10^{-3}	9.55×10^{-3}
100	6.99	88.97	8.59×10^2	75.57	6.44×10^2	57.99×10^4	1.30×10^{-4}	1.11×10^{-3}	1.71×10^{-2}
500	24.69	401.60	3.21×10^3	92.43	9.57×10^2	58.22×10^4	1.59×10^{-4}	1.64×10^{-3}	1.01×10^{-1}

Table A.3: $Z = 0.01 \times Z_{\odot}$ 8 kpc

Number of SNe	$M_{*Fe_{56}}$	$M_{*O_{16}}$	M_{*ej}	$M_{ShellFe_{56}}$	$M_{ShellO_{16}}$	M_{tot}	$X_{*Fe_{56}}$	$X_{*O_{16}}$	$[O/Fe]$
10	0.95	8.96	1.14×10^2	7.72	64.50	57.91×10^4	1.33×10^{-5}	1.11×10^{-4}	8.29×10^{-3}
50	3.95	43.67	4.82×10^2	10.73	99.20	57.95×10^4	1.85×10^{-5}	1.71×10^{-4}	5.23×10^{-2}
100	6.99	85.72	8.61×10^2	13.77	1.41×10^2	57.99×10^4	2.37×10^{-5}	2.43×10^{-4}	9.74×10^{-2}
500	24.69	394.21	3.23×10^3	31.46	4.50×10^2	58.22×10^4	5.40×10^{-5}	7.72×10^{-4}	2.41×10^{-1}

Table A.4: $Z = 10^{-4} \times Z_{\odot}$ 8 kpc

Number of SNe	$M_{*Fe_{56}}$	$M_{*O_{16}}$	M_{*ej}	$M_{ShellFe_{56}}$	$M_{ShellO_{16}}$	M_{tot}	$X_{*Fe_{56}}$	$X_{*O_{16}}$	$[O/Fe]$
10	0.95	8.55	1.14×10^2	1.02	9.10	57.91×10^4	2.09×10^{-6}	1.57×10^{-5}	3.68×10^{-2}
50	3.95	41.54	4.81×10^2	4.02	42.10	57.95×10^4	7.26×10^{-6}	7.26×10^{-5}	1.06×10^{-1}
100	6.99	81.58	8.60×10^2	7.06	82.14	57.99×10^4	1.22×10^{-5}	1.42×10^{-4}	1.52×10^{-1}
500	24.69	377.66	3.23×10^3	24.75	3.78×10^2	58.22×10^4	4.25×10^{-5}	6.52×10^{-4}	2.70×10^{-1}

Table A.5: $Z = Z_{\odot}$ 12 kpc

Number of SNe	$M_{*Fe_{56}}$	$M_{*O_{16}}$	M_{*ej}	$M_{ShellFe_{56}}$	$M_{ShellO_{16}}$	M_{tot}	$X_{*Fe_{56}}$	$X_{*O_{16}}$	$[O/Fe]$
10	0.92	10.23	1.13×10^2	456.70	3.75×10^3	38.97×10^4	1.17×10^{-3}	9.61×10^{-3}	3.13×10^{-4}
50	3.74	49.28	4.47×10^2	459.52	3.78×10^3	39.00×10^4	1.18×10^{-3}	9.70×10^{-3}	2.14×10^{-3}
100	6.35	95.73	7.95×10^2	462.13	3.83×10^3	39.03×10^4	1.18×10^{-3}	9.81×10^{-3}	4.98×10^{-3}
500	23.27	421.95	2.95×10^3	479.05	4.16×10^3	39.25×10^4	1.22×10^{-3}	1.06×10^{-2}	2.48×10^{-2}

Table A.6: $Z = 0.1 \times Z_{\odot}$ 12 kpc

Number of SNe	$M_{*Fe_{56}}$	$M_{*O_{16}}$	M_{*ej}	$M_{ShellFe_{56}}$	$M_{ShellO_{16}}$	M_{tot}	$X_{*Fe_{56}}$	$X_{*O_{16}}$	$[O/Fe]$
10	0.92	9.29	1.11×10^2	46.50	3.83×10^2	38.97×10^4	1.19×10^{-4}	9.82×10^{-4}	1.98×10^{-3}
50	3.74	45.00	4.51×10^2	49.32	4.18×10^2	39.00×10^4	1.26×10^{-4}	1.07×10^{-3}	1.51×10^{-2}
100	6.35	87.27	8.02×10^2	51.92	4.61×10^2	39.03×10^4	1.33×10^{-4}	1.18×10^{-3}	3.46×10^{-2}
500	23.27	388.11	2.97×10^3	68.85	7.62×10^2	39.25×10^4	1.75×10^{-4}	1.94×10^{-3}	1.30×10^{-1}

Table A.7: $Z = 0.01 \times Z_{\odot}$ 12 kpc

Number of SNe	$M_{*Fe_{56}}$	$M_{*O_{16}}$	M_{*ej}	$M_{ShellFe_{56}}$	$M_{ShellO_{16}}$	M_{tot}	$X_{*Fe_{56}}$	$X_{*O_{16}}$	$[O/Fe]$
10	0.92	8.93	1.11×10^2	5.48	46.29	38.97×10^4	1.41×10^{-5}	1.19×10^{-4}	1.31×10^{-2}
50	3.74	43.24	4.52×10^2	8.30	80.60	39.00×10^4	2.13×10^{-5}	2.07×10^{-4}	7.36×10^{-2}
100	6.35	84.64	8.06×10^2	10.90	121.82	39.04×10^4	2.79×10^{-5}	3.12×10^{-4}	1.35×10^{-1}
500	23.27	381.99	3.00×10^3	27.83	419.35	39.25×10^4	7.09×10^{-5}	1.07×10^{-3}	2.64×10^{-1}

Table A.8: $Z = 10^{-4} \times Z_{\odot}$ 12 kpc

Number of SNe	$M_{*Fe_{56}}$	$M_{*O_{16}}$	M_{*ej}	$M_{ShellFe_{56}}$	$M_{ShellO_{16}}$	M_{tot}	$X_{*Fe_{56}}$	$X_{*O_{16}}$	$[O/Fe]$
10	0.92	8.51	1.11×10^2	0.97	8.88	38.97×10^4	2.49×10^{-6}	2.28×10^{-5}	4.80×10^{-2}
50	3.74	41.13	4.52×10^2	3.79	41.5	39.00×10^4	9.72×10^{-6}	1.06×10^{-4}	1.26×10^{-1}
100	6.35	80.47	8.05×10^2	6.39	80.84	39.04×10^4	1.64×10^{-5}	2.07×10^{-4}	1.88×10^{-1}
500	23.27	367.43	2.99×10^3	23.31	367.81	39.25×10^4	5.94×10^{-5}	9.37×10^{-4}	2.84×10^{-1}

Table A.9: $Z = Z_{\odot}$ 4 kpc

Number of SNe	$M_{*Fe_{56}}$	$M_{*O_{16}}$	M_{*ej}	$M_{ShellFe_{56}}$	$M_{ShellO_{16}}$	M_{tot}	$X_{*Fe_{56}}$	$X_{*O_{16}}$	$[O/Fe]$
10	0.97	10.32	1.19×10^2	1179.14	9.67×10^3	100.71×10^4	1.17×10^{-3}	9.60×10^{-3}	1.04×10^{-4}
50	4.26	50.57	5.20×10^2	1182.42	9.71×10^3	100.75×10^4	1.17×10^{-3}	9.63×10^{-3}	7.02×10^{-4}
100	7.79	99.37	9.33×10^2	1185.95	9.76×10^3	100.79×10^4	1.18×10^{-3}	9.69×10^{-3}	1.58×10^{-3}
500	27.36	457.84	3.53×10^3	1205.52	10.11×10^3	101.05×10^4	1.19×10^{-3}	1.00×10^{-2}	1.01×10^{-2}

Table A.10: $Z = 0.1 \times Z_{\odot}$ 4 kpc

Number of SNe	$M_{*Fe_{56}}$	$M_{*O_{16}}$	M_{*ej}	$M_{ShellFe_{56}}$	$M_{ShellO_{16}}$	M_{tot}	$X_{*Fe_{56}}$	$X_{*O_{16}}$	$[O/Fe]$
10	0.97	9.36	1.16×10^2	118.79	9.75×10^2	100.71×10^4	1.18×10^{-4}	9.68×10^{-4}	6.17×10^{-4}
50	4.26	45.99	5.19×10^2	122.08	10.11×10^2	100.75×10^4	1.21×10^{-4}	1.00×10^{-3}	4.77×10^{-3}
100	7.79	90.67	9.41×10^2	125.61	10.56×10^2	100.79×10^4	1.25×10^{-4}	1.05×10^{-3}	1.11×10^{-2}
500	27.36	418.89	3.56×10^3	145.17	13.84×10^2	101.05×10^4	1.44×10^{-4}	1.37×10^{-3}	6.58×10^{-2}

Table A.11: $Z = 0.01 \times Z_{\odot}$ 4 kpc

Number of SNe	$M_{*Fe_{56}}$	$M_{*O_{16}}$	M_{*ej}	$M_{ShellFe_{56}}$	$M_{ShellO_{16}}$	M_{tot}	$X_{*Fe_{56}}$	$X_{*O_{16}}$	$[O/Fe]$
10	0.97	9.00	1.16×10^2	12.76	1.05×10^2	100.71×10^4	1.27×10^{-5}	1.05×10^{-4}	4.06×10^{-3}
50	4.26	44.18	5.20×10^2	16.04	1.41×10^2	100.75×10^4	1.59×10^{-5}	1.40×10^{-4}	2.96×10^{-2}
100	7.79	87.06	9.43×10^2	19.57	1.84×10^2	100.79×10^4	1.94×10^{-5}	1.82×10^{-4}	5.87×10^{-2}
500	27.36	408.93	3.58×10^3	39.14	5.05×10^2	101.06×10^4	3.87×10^{-5}	5.00×10^{-4}	1.97×10^{-1}

Table A.12: $Z = 10^{-4} \times Z_{\odot}$ 4 kpc

Number of SNe	$M_{*Fe_{56}}$	$M_{*O_{16}}$	M_{*ej}	$M_{ShellFe_{56}}$	$M_{ShellO_{16}}$	M_{tot}	$X_{*Fe_{56}}$	$X_{*O_{16}}$	$[O/Fe]$
10	0.97	8.58	1.16×10^2	1.09	9.55	100.71×10^4	1.08×10^{-6}	9.48×10^{-6}	2.89×10^{-2}
50	4.26	42.06	5.20×10^2	4.38	43.03	100.75×10^4	4.35×10^{-6}	4.27×10^{-5}	7.86×10^{-2}
100	7.79	82.80	9.42×10^2	7.91	83.77	100.79×10^4	7.85×10^{-6}	8.31×10^{-5}	1.11×10^{-1}
500	27.36	390.33	3.58×10^3	27.47	391.30	101.05×10^4	2.71×10^{-5}	3.87×10^{-4}	2.40×10^{-1}

Bibliography

[1] Alibés A., Labay J., & Canal R., 2001, A&A, 370, 1103

[2] Anders, E., Grevesse, N. 1989, Geochim. Cosmochim. Acta 53, 197

[3] Andrievsky S.M., Bersier D., Kovtyukh V. V. et al 2002a, A&A 384, 140

[4] Andrievsky S.M., Kovtyukh V. V., Luck R.E. et al 2002b, A&A 381, 32

[5] Andrievsky S. M., Kovtyukh V. V., Luck R.E. et al 2002c, A&A 392, 491

[6] Andrievsky S. M., Luck R. E., Martin P. et al 2004, A&A 413, 159

[7] Asplund, M., Grevesse, N., Sauval, A. J. 2005, in "Cosmic Abundances as Records of Stellar Evolution and Nucleosynthesis", eds T. G. Barnes III, F. N., Bash, ASP Conf. Ser. 336, 25

[8] Aubourg, E., Tojeiro, R., Jimenez, R., Heavens, A., Strauss, M. A., Spergel, D. N.,2008, A&A, 492, 631

[9] Avesidova, V., S., 1971, Astron. Zh., 48, 894 [Sov. Astron. 15, 708 (1972)]

[10] Barbon, R., Buondì, V., Cappellaro, E., Turatto, M., 1999, A&ASS, 139, 531

[11] Barbon, R., Benetti, S., Cappellaro, E., Patat, F., Turatto, M., Iijima, T., 1995, :A&ASS, 110 513

[12] Barnabè, M., Ciotti, L., Fraternali, F., Sancisi, R., 2006, A&A, 446, 61

[13] Baron, E., 1992, MNRAS, 255, 267

[14] Baron, E., A., Burrows, A., Lattimer, J., M., Yahil, A., 1982 BAAS,14R,936

[15] Basu, S., Johnstone, D., Martin, P. G., 1999, ApJ, 516, 843

[16] Bensby, T., Feltzing, S., Lundstrom, I., 2004, A&A, 415, 155

[17] Bertola, F., 1964, Annals. Ap., 27 319

[18] Bisnovatyi-Kogan, G., S., Silich, S. A. 1995, RvMP, 67, 661

[19] Bisnovatyi-Kogan, G., S., Blinnikov, S., I., Silich, S. A. 1989, Astrophys. Space. Sci. 154, 229

[20] Blaauw, A., 1991, in *The Physics of Star Formation and Early Stellar Evolution*, eds C.J. Lada & N.D. Kylafis, NATO ASI Ser. C, Vol. 342 (Dordrecht: Kluwer), 125

[21] Blitz, L., Spergel, D. N., Teuben, P. J., Hartmann, D., Burton, W. B. 1999, ApJ 514, 818

[22] Bluhm, H., de Boer, K., Marggraf, O., Richter, P. 2001, A&A, 367, 299

[23] Boomsma, R., Oosterloo, T., A., Fraternali, F., van der Hulst, J., M., Sancisi, R., 2005, A&A, 431, 65

[24] Boomsma, R., Oosterloo, T., Fraternali, F., van der Hulst, T., Sancisi, R. 2005, in "Extra-planar Gas"Conference, ASP Conf. Series, ed. R. Braun, vol. 331, p. 247

[25] Booth, C. M., Theuns, T. 2007, MNRAS, 381, 89

[26] Bregman, J. N. 1980, ApJ, 365, 544

[27] Brown, A.G.A., Hartmann, D., Burton, W.B., 1995, A&A, 300, 903

[28] Brown, A., G., A., 2001, RMxAC, 11, 89

[29] Brown, A.G.A., de Geus E.J., de Zeeuw P.T., 1994, A&A, 289, 101

[30] Burrows, D.N., Singh, K.P., Nousek, J.A., Garmire, G.P., Good, J., 1993, ApJ, 406, 97

[31] Calura, F.; Pipino, A.; Matteucci, F., 2008, A&A, 479, 669

[32] Cappellaro, E., Evans, R., Turatto, M., 1999, A&A, 351, 459

[33] Carney, B.W., Wright, J.S., Sneden, C., Laird, J.B., Aguilar, L.A., & Latham, D.W. 1997, AJ, 114, 363

[34] Carretta, E., Gratton, R.G., Cohen, J.G. et al. 2002, AJ, 124, 481

[35] Castor, J., R., McCray, Weaver, R., 1975, Astrophys. J. Lett, 200,107

[36] Cayrel, R., Depagne, E., Spite, M. et al. 2003, A&A, 416, 1117

[37] Cescutti, G., Matteucci, F., Francois, P., & Chiappini, C. 2007, A&A, 462, 943

[38] Chang R. X., Hou J. L., Shu C. G., Fu C. Q., 1999, A&AS, 141, 491

[39] Charlton, J. C. & Salpeter, E.E. 1989, ApJ, 346,101

[40] Chiano, A., K., R., 1985, ApJ 299, 24

[41] Chiappini C., Matteucci F., & Gratton R., 1997, ApJ, 477, 765

[42] Chiappini C., Matteucci F., & Padoan P., 2000, ApJ, 528, 711

[43] Chiappini C., Matteucci F., & Romano D., 2001, ApJ, 554, 1044

[44] Chiappini C., Matteucci F., & Meynet G., 2003a, A&A, 410, 257

[45] Chiappini C., Romano D., & Matteucci F., 2003b, MNRAS, 339, 63

[46] Cioffi, D., F., McKee, C., F., Bertschinger, E., 1988, ApJ, 334,252

[47] Collins, J., A., Benjamin, R. A., Rand, R. J., 2002, ApJ, 578, 98

[48] Cox, D. P., 2005, Annu. Rev. Astro. Astrophys., 43, 337

[49] Dahlen, T., Strolger, L.G., Riess, A.G. et al. 2004, ApJ, 613, 189

[50] de Avillez, M.,A., 2000, MNRAS, 315, 479

[51] de Geus, E.J., 1992, A&A, 262, 258

[52] Dekel, A., & Silk, J. 1986, ApJ, 303, 39

[53] Della Valle, M., Panagia, N., Padovani, P., Cappellaro, E., Mannucci, F., Turatto, M., 2005, ApJ 629, 750

[54] Dettmar, R.-J., 2005, in Magnetic Fields in the Universe: from Laboratory and Stars to Primordial Structures, E.M. de Gouveia Dal Pino, G. Lugones, A. Lazarian (eds.), AIP Procs., vol. 784, p. 354

[55] de Zeeuw, P. T., Hoogerwerf, R. de Bruijne J.H.J., 1999, ApJ, 117, 354

[56] Dopita, M.,A., Ryder, S., D., 1994, ApJ, 430, 163

[57] Draine, B.T., & Salpeter, E.E. 1979, ApJ, 231, 438

[58] Dyson, J., E., 1973, A&A, 23, 381

[59] Dwek, E., 1998, ApJ, 501, 643

[60] Edmunds, M.G. 1990, MNRAS, 246, 678

[61] Edvardsson, B., Andersen, J., Gustafsson, B. et al. 1993, A&A, 275, 101

[62] Elias,J.,H., Frogel,J., A.,Hackwell, J., A., Persson, S., E., 1981, Astrophys. J. Lett., 251,13

[63] Ferrière, K.,M., 1995, ApJ, 441, 281

[64] Ferrière, K.,M., 1998, ApJ, 497, 759

[65] Filippenko, A., V., : In: *Thermonuclear Supernovae*, ed.by P.Ruiz-Lapuente, R.Canal, J.Isern (Kluwer Academic Publishers, Dordrect 1997) p.795

[66] Filippenko, A., V., W.L.W.Sargent, W.,L.,W., 1985, Nature, 316, 407

[67] François, P., & Matteucci, F., 1993, A&A, 280, 136

[68] François P., Matteucci F., Cayrel R., Spite, M., Spite, F., & Chippini, C., 2004, A&A, 421, 613

[69] Fraternali, F., & Binney, J., 2008, MNRAS, 386, 935

[70] Fraternali, F., Oosterloo, T., Boomsma, R., Swaters, R., Sancisi, R., 2004 IAUS..217..136

[71] Fraternali, F., Oosterloo, T. Sancisi, R. 2004, A&A, 424, 485

[72] Fuhrmann, K., 1999, Ap&SS 338,161

[73] Fulbright, J.P. 2000, AJ 120, 1841

[74] Garnett, D.R. 2002, ApJ, 581, 1019

[75] Gratton, R.G. & Sneden, C. 1988, A&A, 204, 193

[76] Gratton, R., Carretta, E., Matteucci, F., & Sneden, C., 2000, A&A, 358, 671

[77] Greggio, L., Cappellaro, E., 2009, astro-ph/0902.0700

[78] Greggio, L., 2005, A&A 441, 1055 (G05)

[79] Greggio L.,& Renzini A., 1983a, A&A, 118, 217

[80] Greggio L.,& Renzini A., 1983b, in Frascati Workshop on First Stellar Generations, Vulcano, Italy, Societá Astronomica Italiana, vol. 54. no. 1, p. 311-319

[81] Greggio, L.,Renzini, A., Daddi, E., 2008, MNRAS, 388, 829

[82] Grevesse, N., & Sauval, A.J. 1998, Space Sci. Rev., 85, 161

[83] Grevesse, N., & Noels, A. 1993, in Orgin of the Elements, ed. N. Prantzos, E. Vangioni-Flam, & M. Cassé, (Cambridge: Univ. Press), 15

[84] Hachisu, I., Kato, M. & Nomoto, K., 1996, ApJ 470, 97

[85] Hachisu, I., Kato, M. & Nomoto, K.,1999, ApJ 522, 487

[86] Harfst, S., Theis, Ch., & Hensler,G., 2006, A&A, 449, 509

[87] Harkness, R., P., 1987, ApJ 317, 355

[88] Hartwick, F.D.A. 1976, ApJ, 209, 418

[89] Heiles, C., 1979, ApJ, 229, 533

[90] Heiles, C., 1984, ApJSS, 55, 585

[91] Hernquist L.,1990, ApJ, 356, 359

[92] Houck, J. C., & Bregman, J. N. 1990, ApJ, 352, 506

[93] Ibata, R. A., Gilmore, G., Irwin, M. J. 1994, *Nature* 370, 194

[94] Iben, I.Jr., Tutukov, A. 1984, ApJSuppl., 54, 335

[95] Iben, I., Jr., Renzini, A., 1983, ARA&A,21,271I

[96] Imshennik, V., S., Nadezhin, D., K., 1989, Sov. Sci. Rev., Sect. E, Vol. 8, Part 1, p. 1 - 147

[97] Iwamoto, K., Brachwitz, F., Nomoto, K., et al. 1999, ApJ Suppl. Ser. 125, 439

[98] Jones, A.P., Tielens, G.G.M., & Hollenbach, D.J. 1996, ApJ, 469, 740

[99] Jørgensen, B. R., 2000, A&A, 363, 947

[100] Kahn F. D., 1981, in Investigating the Universe, Kahn F. D. (ed.), Ap&SS, vol. 91, p. 1

[101] Kennicutt, R. C., Jr., 1989, ApJ, 344, 685

[102] Kennicutt, R. C., Jr., 1998, ApJ, 498, 541

[103] Kenyon, S.J., Livio, M., Mikolajewska, J., Tout, C. A., 1993, ApJ, 407, L81

[104] Kobayashi, C., Umeda, H., Nomoto, K., Tominaga, N., Ohkubo, T., 2006. ApJ,653, 1145

[105] Kobayashi, C., Tsujimoto, T., Nomoto, K., Hachisu, I. Kato, M., 1998, ApJ, 503, L155

[106] Kompaneets, A. S., 1960, Soviet Phys. Dokl., 5, 46

[107] Koo, B., McKee, C.,F., 1990, ApJ, 354, 513

[108] Koo,B., McKee, C., F., 1992, ApJ, 388, 103

[109] Köppen, J., & Edmunds, M.G. 1999, MNRAS, 306, 317

[110] Korycansky, D., G., 1992, ApJ, 398, 184

[111] Korobeinikov, V., P., 1985, Problems of the Theory of the Point Explosion (Nauka, Moscow)

[112] Kroupa, P., Tout, C.,A., Gilmore, G., 1993, MNRAS, 262, 545

[113] Larson, R.,B., 1998, MNRAS,301, 569

[114] Laumbach, D., D., Probstein, R., F., 1969, J. Fluid Mech. 35, 53

[115] Leibundgut. B., 2000, Astron. Astrophys. Rev

[116] Leitherer,C., Schaerer, D., Goldader, J., D., González D., R. M., Robert, Carmelle; Kune, D., F., de Mello, D., F., Devost, D., Heckman, T., M., 1999, ApJS, 123, 3L

[117] Limongi, M., Tornambé, A., 1991, ApJ, 371, 317

[118] Lu, L., Sargent, W. L. W., Savage, B. D., Wakker, B. P., Sembach, K. R., Oosterloo, T. A. 1998, AJ, 115, 162

[119] Luck R. E., Gieren W. P., Andrievsky S. M. et al. 2003, A&A, 401, 939

[120] Mac Low, M. M., McCray, R., 1988. ApJ, 324, 776

[121] Mac Low, M.M., McCray, R., Norman, M. L., 1989, ApJ, 1989, 337, 141

[122] Maeder, A., 1984, AUS, 1984, 105, 299

[123] Maeder, A., & Maynet, G., 1989, A&A, 210, 155

[124] Malinie, G., Hartmann, D.H., Clayton, D.D.,& Mathews G.J., 1993, ApJ, 413, 633

[125] Mannucci, F., Della Valle, M., Panagia, N., 2006, MNRAS 370, 773 (MVP06)

[126] Mannucci, F ., Della Valle, M., Panagia, N., Cappellaro, E., Cresci, G., Maiolino, R., Petrosian, A., & Turatto, M, 2005, A&A, 433, 807

[127] Martin, C. L., & Kennicutt, R. C., Jr., 2001, ApJ, 555, 301

[128] Matteucci, F., Chiosi, 1983, A&A, 123, 121

[129] Matteucci, F., 2001, The Chemical Evolution Of The Galaxy, Kluwer Academic Publishers.

[130] Matteucci, F., & Francois, P., 1989, MNRAS, 239, 885

[131] Matteucci M.F., 1986, A&A, 305, 81

[132] Matteucci M.F., Greggio L., 1986, A&A, 154, 279

[133] Matteucci, F., Raiteri, C.M., Busson, M., Gallino, R. & Gratton, R. 1993, A&A, 272, 421

[134] Matteucci, F., Recchi, S., 2001, ApJ, 558, 351 (MR01)

[135] Maza, J., van den Bergh, S., 1976, ApJ, 204, 519

[136] McCray, R., 1993, ARA&A, 31, 175

[137] McCray, R., Kafatos, M.,1987, ApJ, 317,190

[138] McKee, C.,F., Williams, J.,P., 1997, ApJ 476, 144

[139] McMillan, R., J., Ciardullo, R., 1996, ApJ, 473, 707

[140] McWilliam, A., Preston, G. W.,Sneden, C., Searle, L. 1995, AJ, 109, 2757

[141] Melioli, C., Brighenti, F., D'Ercole, A., & de Gouveia Dal Pino, E.M., 2008a, MNRAS, 388, 573

[142] Melioli, C., Brighenti, F., D'Ercole, A., & de Gouveia Dal Pino, E.M., 2009, MNRAS, 399, 1089

[143] Melo, V.L.,Munoz-Tunon, C., Maiz-Apellaniz, J., Tenorio-Tagle, G., 2005, ApJ, 619, 700

[144] Meyer, D. M., Jura, M., Cardelli, J. A. 1998, ApJ, 493, 222

[145] Minkowski, R., MNRAS, 1941, 53, 224

[146] Miyamoto, M., & Nagai, R., 1975, Publ. Astron. Soc. Japan, 27, 533

[147] Miyaji, S., Nomoto, K., Yokoi, K., Sugimoto, D., 1980, PASJ, 32,303

[148] Morton, D., C., 1967, ApJ, 159, 535

[149] Munari, U., Renzini, A., 1992, ApJ, 397, L87

[150] Murphy, E. M., Sembach, K. R., Gibson, B. K., Shull, J. M., Savage, B. D., Roth, K. C., Moos, H. W., Green, J. C., York, D. G., Wakker, B. P., 2000, ApJ, 538, L35

[151] Navarro, J. D., Frenk, C. S., White S. D. M., 1996, ApJ, 462, 563

[152] Nissen, P.E., & Schuster, W.J. 1997, A&A, 326, 751

[153] Nissen, P.E., Primas, F., Asplund, M., Lambert, D.L. 2002, A&A, 390, 235

[154] Nomoto, K., 1981, IAUS, 93, 295

[155] Nomoto, K, Thielemann, F.-K., Yokoi, K., 1984, ApJ, 286, 644

[156] Nordström, B., Mayor, M., Andersen, J., Holmberg, J., Pont, F., Jørgensen, B. R., Olsen, E. H., Udry, S., Mowlavi, N., 2004, A&A, 418, 989

[157] Oort, J. H. 1970, A&A 7, 381

[158] Pagel, B.E.J., & Patchett, B.E. 1975, MNRAS, 172, 13

[159] Pagel, B.E.J.,& Tautvaisiene, G., 1995, MNRAS, 276, 505

[160] Panagia, N.,1985 LNP, 224,14

[161] Pikelner, S., B., 1968, Astrophys Lett. 2, 97

[162] Pikelner, S., B., Shcheglov, P., V., 1968, Astron. Zh. 45, 953 [Sov. Astron. 12, 757 (1969)]

[163] Pols, Onno, R., 1997, ASPC, 130, 153

[164] Pols, Onno, R., Tout, C., A., Schroder, K-P, Eggleton, P. P. Manners, J., 1997, MNRAS,.289, 869

[165] Porter, A., C., Filippenko, A., V., 1987, Astron. J., 93, 1372

[166] Prantzos, N., & Aubert, O. 1995, A&A, 302, 69

[167] Prantzos, N., Boisser S., 2000, MNRAS, 313, 338

[168] Pritchet, C. J., Howell, D. A., Sullivan, M., 2008, ApJ, 683, L25 (PHS08)

[169] Ramirez, I., Prieto, C.A., Lambert, D.,L., 2007, A&A, 465, 271

[170] Recchi S., Matteucci, F., D'Ercole, A., 2001, MNRAS, 322, 800

[171] Reid M.J., 1993, ARAA, 31, 345

[172] Richter, P., Sembach, K. R., Wakker, B. P., Savage, B. D., Tripp, T. M., Murphy, E. M., Kalberla, P. M. W., Jenkins, E. B., 2001, ApJ, 559, 318

[173] Rieschick A., & Hensler G., 2000, in Cosmic Evolution and Galaxy Formation: Structure, Interactions and Feedback, ASP Conferences Series, eds. J. Franco, E. Terlevich, O. Lòpez Cruz and I. Aretxaga

[174] Roskar, R., Debattista, V. P., Quinn, T. R., Stinson, G.S., Wadsley, J., 2008, ApJ, 684, L79

[175] Roy, J., & Kunth, D. 1995, A&A, 294, 432

[176] Ryan, S., Norris, J. E. Bessell, M. S.. 1991, AJ, 102, 303

[177] Salpeter, E. E., 1955, ApJ, 121, 161

[178] Savage, B. D., Sembach, K. R. 1991, ApJ, 379, 245

[179] Scalo, J. M., 1986, FCPh, 11, 1

[180] Scalo, J. M., 1998,in "The Stellar Initial Mass function", ASP Conf. Ser. Vol. 142 p.201

[181] Scannapieco, E., Bildsten, L.,2005 ApJ 629, L85

[182] Schiano, A. V. R., 1985, ApJ, 299, 24

[183] Schmidt M., 1959, ApJ, 129, 243

[184] Schmidt M., 1963, ApJ, 137, 758

[185] Searle, L., & Sargent, W.L.W. 1972, ApJ, 173, 25

[186] Sedov, L., I., 1946, Dokl., Akad. Nauk SSSr 42, 17

[187] Sedov, L., I., 1958, Similarity and Dimensional Methods in Mechanics (Academic, New York)

[188] Sembach, K. R., Oosterloo T. A. 1998, AJ, 115, 162

[189] Sembach, K. R., Howk, J. C., Savage, B. D., Shull, J. M. 2001, AJ, 121, 992

[190] Shapiro, P.R., 1979, ApJ 233, 831

[191] Shapiro, P. R., Field, G. B. 1976, ApJ 205, 762

[192] Silk, J. 2003, MNRAS, 343, 249

[193] Skillman, E.D. 1997, Rev. Mex. AC, 6, 36

[194] Snowden, S.L., Burrows, D.N., Sanders, W.T., Aschenbach, A., Pfeffermann, E., 1995, ApJ, 439, 399

[195] Spitoni, E., Recchi, S., & Matteucci, F. 2008, A&A, 484, 743

[196] Stephens, A., 1999, AJ, 117, 1771

[197] Strolger, L.G., Riess, A.G., Dahlen, T. et al., 2004, ApJ 613, 200 (S04)

[198] Talbot, R., J., Jr., Arnett, W., D., 1973, 186, 51

[199] Taylor, G., I., 1950, Proc. R. Soc. London, Ser. A 201, N1065, 159

[200] Tenorio-Tagle G., 1996, AJ, 111, 1641

[201] Tenorio-Tagle, G., Bodenheimer, P., Różyczka, M., 1987, A&A, 182, 120

[202] Tenorio-Tagle, G., Różyczka, M. ,Bodenheimer, P., 1990, A&A, 237, 207

[203] Tenorio-Tagle, G., Silich, S. A., Kunth, D., Terlevich, E., Terlevich, R., 1999, Mon. Not. R. Astron. Soc., 309, 332

[204] Thielemann, F.-K., Nomoto, K., Hashimoto, M., 1996, ApJ, 460, 408

[205] Thomas, D., Greggio, L., & Bender, R., 1998, MNRAS, 296, 119

[206] Timmes, F.X., Woosley, S.E., Weaver, T.A., 1995, ApJS, 98, 617

[207] Tinsley, B.M. 1974, ApJ, 192, 629

[208] Tinsley B.M., 1975, ApJ, 197, 159

[209] Tinsley, B.M. 1980, Fund. Cosmic Phys., 5, 287

[210] Tomisaka, K., 1992, PASJ, 44, 177

[211] Tomisaka, K., 1998, MNRAS, 298, 797

[212] Tomisaka, K., Ikauchi, S., 1986, Publ. Astron. Soc. Jpn., 38, 697

[213] Tornambé, A., Matteucci, F.,1987, ApJ, 318, L25

[214] Tosi, M., 1988, A&A, 197, 338

[215] Totani, T. Morokuma, T., Oda, T., Doi, M., Yasuda, N. 2008, PASJ, 60, 1327

[216] Tremonti, C.A., Heckman, T.M., Kauffmann, G., et al. 2004, ApJ, 613, 898

[217] Trimble, V., 1982,RVMP,54, 1183

[218] Twarog, B. 1980, ApJ, 242, 242

[219] van den Hoek L.B., & Groenewegen M.A.T. 1997, A&A Suppl., 123, 305

[220] Van Dyk, S. D., Peng, C., Y., Barth, A., J., Filippenko A., V., 1999 AJ, 118, 2331

[221] Wakker, B. P., et al. 1999, Nature, 402, 388

[222] Wakker, B. P., York, D. G., Howk, C., Barentine, J.C., Wilheim, R., Peletier, R. F., van Woerden, H., Beers, T. C., Ivezic, Z., Richter, P., Schwarz, U. J., 2007, ApJ, 670, 113

[223] Weaver, R., McCray, R., Castor, J., Shapiro, P., Moore, R., 1977, ApJ, 218, 377

[224] Wheeler, J. C., 1982, sscr.conf..167

[225] Whelan J., Iben I. Jr., 1973, ApJ, 186, 1007

[226] Williams, J.,P., McKee, C.,F., 1997, ApJ, 476, 166

[227] Wolfire, M. G., McKee, C. F., Hollenbach, D. Tielens, A. G. G. M., 2003, ApJ, 587,278

[228] Woosley, S. E., Weaver, T. A., 1986, ARA&A..24..205

[229] Woosley, S. E., Weaver, T. A., 1995, ApJ, 101, 181

Acknowledgments

I am deeply thankful to my supervisor, Prof. Francesca Matteucci, for her encouragement, guidance and support during this PhD period. This thesis would not have been possible without her help. I am very grateful to Simone Recchi for his constant help and great generosity during the time of our collaboration. It has been a grat pleasure for me to work with him.

I also thank Gabriele Cescutti, Francesco Calura, Cristina Chiappini and Antonio Pipino for usefull discussions.

List of Figures

List of Tables